1993

The incongruent melting and melt textured solidification process of Bi2Sr2CaCu2O8

Jack Polonka
Iowa State University

INFORMATION TO USERS

This manuscript has been reproduced from the microfilm master. UMI films the text directly from the original or copy submitted. Thus, some thesis and dissertation copies are in typewriter face, while others may be from any type of computer printer.

The quality of this reproduction is dependent upon the quality of the copy submitted. Broken or indistinct print, colored or poor quality illustrations and photographs, print bleedthrough, substandard margins, and improper alignment can adversely affect reproduction.

In the unlikely event that the author did not send UMI a complete manuscript and there are missing pages, these will be noted. Also, if unauthorized copyright material had to be removed, a note will indicate the deletion.

Oversize materials (e.g., maps, drawings, charts) are reproduced by sectioning the original, beginning at the upper left-hand corner and continuing from left to right in equal sections with small overlaps. Each original is also photographed in one exposure and is included in reduced form at the back of the book.

Photographs included in the original manuscript have been reproduced xerographically in this copy. Higher quality 6" x 9" black and white photographic prints are available for any photographs or illustrations appearing in this copy for an additional charge. Contact UMI directly to order.

U·M·I

University Microfilms International
A Bell & Howell Information Company
300 North Zeeb Road, Ann Arbor, MI 48106-1346 USA
313/761-4700 800/521-0600

Order Number 9414014

The incongruent melting and melt textured solidification process of $Bi_2Sr_2CaCu_2O_8$

Polonka, Jack, Ph.D.

Iowa State University, 1993

U·M·I
300 N. Zeeb Rd.
Ann Arbor, MI 48106

The incongruent melting and melt textured solidification process of $Bi_2Sr_2CaCu_2O_8$

by

Jack Polonka

A Dissertation Submitted to the
Graduate Faculty in Partial Fulfillment of the
Requirements for the Degree of
DOCTOR OF PHILOSOPHY

Department: Chemistry
Major: Physical Chemistry

Approved:

Signature was redacted for privacy.

In Charge of Major Work

Signature was redacted for privacy.

For the Major Department

Signature was redacted for privacy.

For the Graduate College

Iowa State University
Ames, Iowa

1993

TABLE OF CONTENTS

GENERAL INTRODUCTION

The high T_c ceramic superconductors, such as $(La,Sr)_2CuO_4$[1] and $YBa_2Cu_3O_7$[2], have a two dimensional structure containing copper-oxygen planes. The copper atoms are square planar coordinated with oxygen and the Cu $d_{x^2-y^2}$ orbitals mix heavily with the O 2p orbitals to form a major conducting plane in the normal state. Most of these materials have holes in the oxygen 2p band as shown by electron energy loss spectroscopy[3], and these holes are the dominant charge carriers in the materials we investigate here. It is believed that the Cu-O planes play a prominent role in the superconductivity of the material. It is in these planes that phenomena, like electron-phonon coupling, occur giving rise to the material's superconducting properties.

The long range goal of many groups in this field is to process the $YBa_2Cu_3O_7$ and bismuth cuprate[3] superconducting materials into a usable form. Even though the bismuth cuprates have a high T_c above liquid N_2 temperature, they are also charaterized by a very low critical current density of about $10^3 amps/cm^2$. The low critical current is partly due to the misalignment of the Cu-O planes between the randomly

oriented crystals and grain boundries between the crystals in a polycrystalline material. One way to increase the critical current density to about 10^5 amps/cm^2, is to have the material preferentially oriented. In the case of the $Bi_2Sr_2CaCu_2O_8$ superconductor, all of the grains in the material need to have their crystallographic c-axis parallel to each other and perpendicular to the current. The reason for wanting such a preferred orientation is that the Cu-O planes, where the superconducting phenomenon occurs, are perpendicular to the c-axis in this compound. Many groups have processed the $Bi_2Sr_2CaCu_2O_8$ superconductor into tapes, wires and films with this kind of preferred orientation. Almost all of the processes used to obtain textured superconductor material involve melting and resolidification.

Morimoto and Maeda[4,5,6] use a doctor blade casting process to obtain textured tapes. The doctor blade process involves the preparation of a mixture of metal oxides and carbonates in addition to an organic binder. The mixture is applied to a substrate using a doctor blade to a thickness of 50μm to form a ribbon. The ribbon is heated at 500°C for one hour to volatilize the organic binder and then calcined at 820°C for 12 hours. There are two routes one can take for the next step in the procedure. The first is to take the calcined ribbon and cold roll it several times with intermittent sintering at 840°C for 4 hours[4,5,]. The second involves

heating the calcined ribbon to 870^0C-880^0C for five hours followed by an air quench[6]. At these temperatures the ribbon is partially melted and the $Bi_2Sr_2CaCu_2O_8$ solidifies with the c-axis perpendicular to the substrate. To obtain higher phase-purity material, a much longer heat treatment (24-48 hours) is required[7].

Snyder[8] used a different process to obtain thick textured films. The initial calcination step before heat treatment was simplified by forming the initial constituent mixture into a glass. The stoichiometric mixture of metal oxides and carbonates was melted in a crucible at 1100^0C and quenched to room temperature. The glass was heat treated in a similar manner as the doctor blade material except the heat treatment took only one and a half hours. The processed material contained a significant amount of secondary phases.

Kinoshita et al.[9] created a process to obtain textured fibers. This process involved heating a melt-quenched glassy plate of $Bi_2Sr_{1.9}Ca_{2.2}Cu_4O_x$ at 865^0C in a stream of O_2 for 120 hours. In this case the c-axis of the superconductor was perpendicular to the fiber axis.

Ray and Hellstrom[10] obtained wires by packing powdered $Bi_2Sr_2CaCu_2O_8$ into a Ag sheath. The packed material was heated to 905^0C and slowly cooled to 830^0C for annealing. The whole process took 50 hours to complete. The material in the wire had the same orientation as the fibers. For all of the

processes described above, one can see that long time periods were required for processing.

A major problem in the processing of $Bi_2Sr_2CaCu_2O_8$ is the fact that the compound melts incongruently. A series of Sr-Ca-Cu-O phases form in the Bi-rich liquid during melting and solidification. This complicates the solidification process by introducing second phases, which in turn change the composition of the liquid. With the composition of the melt changed, the sought after compound cannot be solidified. The long heat treatments are required to remove any second phase that might have formed during solidification.

The presence of a second phase in the material does have some benefits. Small amounts of a second phase in the superconductor material are useful for pinning flux vortices. As the current in the superconductor approaches the critical current density, magnetic flux lines (or vortices) are created even in the absence of an external magnetic field. These vortices are able to move through the material under the influence (Lorentz force) of the current and change the superconducting state to normal state. As the current is increased, more of the superconducting state is converted to the normal state until the material does not superconduct. By introducing pinning sites, the vortices can be pinned and prevented from causing dissipation. Thus the material can

operate at higher current densities.

By studying the high-temperature chemistry in-situ during the melting and melt textured solidification of $Bi_2Sr_2CaCu_2O_8$, one can hopefully improve the formation process in two ways. The first is to reduce the time required for processing. Finding a new processing procedure will decrease the heat treatment time and lower costs of industrial manufacturing. The second is to find ways of manipulating the formation of second phases so that they can be used as pinning sites for flux vortices.

Many groups have done high temperature studies of the Bi-Sr-Ca-Cu-O system, but the results seem to be ambiguous. Maeda et al.[11-14], using $Bi_2Sr_2CaCu_2O_8$ as the starting composition, observed the formation of $Bi_2Sr_2Cu_1O_6$, $(Sr,Ca)CuO_2$ and $Bi_3(Sr_4Ca_3)O_x$ phases when the sample was air quenched from 890^0C and 880^0C. Only when the material was cooled from 870^0C was the textured $Bi_2Sr_2CaCu_2O_8$, instead of $Bi_2Sr_2Cu_1O_6$, observed along with the $Bi_3(Sr_4Ca_3)O_x$ phase. In contrast, Oka et al.[15,16] using high temperature X-ray diffraction found that on cooling from 920^0C Bi-2212 formed between 890^0C and 850^0C whereas Bi-2201 formed at 730^0C. Ray and Hellstrom[17], using oil quenching, observed that $(Sr,Ca)CuO_2$, $(Sr,Ca)_2CuO_3$ and $(Sr,Ca)_{14}Cu_{24}O_{41}$ formed at 890^0C. Samples quenched from 870^0C showed textured Bi-2212

and (Sr,Ca)CuO_2. All of the mentioned studies were done in air. Note that in none of the studies mentioned above observed any (Sr,Ca)O phases in the melt.

Hettich and Petzow[18] generated a phase diagram for the Bi-Sr-Ca-Cu-O system by heating and air quenching samples. The phase identification was carried out by using SEM. The phase diagram, though useful, is limited by the fact that it does not go above 850^0C. Hettich[19] also found that the Bi-2212 phase is not a line compound but has a homogeneity range of $2.1 \leq Bi \leq 2.3$ and $2.05/.95 \geq Sr/Ca \geq 1.6/1.4$. A possible reason why many groups observe different phases during the incongruent melting and solidification is that their starting $Bi_2Sr_2CaCu_2O_8$ compositions are different.

The specific goals of this project are divided into two steps. The first step in the study is to find what phases form and in what sequence, in the incongruent melting process. It is also important to understand how the occurrence of these phases affects the textured solidification. The second step is to determine what effects partial O_2 pressure has on the formation of melt textured $Bi_2Sr_2CaCu_2O_8$ and impurity phases.

One of the best methods to use in studying the melting and solidification of any solid is high temperature X-ray diffraction. When using X-ray diffraction, caution must be

exercised when studing quenched samples. In some cases high-temperature phases cannot be retained upon quenching because they decompose during cooling. The reason why the technique of quenching samples for study has been used for so long is that it is a simple procedure. The only equipment needed is a furnace and a room-temperature X-ray diffraction unit. To determine what phases exist at high temperature, the sample must be studied in-situ.

Explanation of Dissertation Format

This dissertation presents the results in three sections. Section one describes the high-temperature X-ray powder diffractometer used in the study. Sections two and three present the results of the melting and solidification respectively, of $Bi_2Sr_2CaCu_2O_8$ as a function of partial O_2 pressures.. The experimental techniques used in the last three sections are described at the beginning of this dissertation. All references cited in the dissertation are presented in the reference section.

EXPERIMENTAL

Sample Preparation

The $Bi_2Sr_2CaCu_2O_8$ starting powder was prepared by reactions of mixed metal oxides and carbonates. The metal oxides used were CuO and Bi_2O_3 with chemical purities of 99.999% and 99.99% respectively. The metal carbonates used were $SrCO_3$ and $CaCO_3$ with chemical purities of 98+% and 99.995% respectively. Stoichiometric amounts of the reagents were weighed on an analytical balance and ground together using a mortar and pestle. The mixture was placed in an Al_2O_3 boat (an elongated crucible) and heated in air to 800°C. After 12 hours of heating, the mixture was removed from the tube furnace and ground again. The second heat treatment lasted 12 hours at 820°C. The reason for the low temperatures in the two initial heat treatments is to prevent any bismuth oxide compounds that might have formed from melting. Such compounds have melting points above 812°C. At this stage, the mixture was pressed into a pellet. The pellet was subjected to two heat treatments at 865°C and 860°C for 12 hours each. In between all of the heat treatments, the sample was always

reground before it went to the next heating step. After the last heat treatment the pellet was quenched by cooling and ground into a powder for future use.

Sample Characterization

Room Temperature X-ray Diffraction

The phase purity of the synthesized sample was determined using a Phillips θ - 2θX-ray diffractometer. Nickel filtered Cu $K\alpha$ ($\lambda_{avg.}$= 1.542 Å) radiation was used to obtain the diffraction pattern. The diffraction data were collected on a θ - 2θ stepscan mode with a step size of 0.05° in 2θ. The counting time used was 60 seconds per degree. The phase fraction of various phases in the sample was determined by comparing the most intense peak of $Bi_2Sr_2CaCu_2O_8$ with those of other phases. No external standard was used.

ICP Analysis

Before and after the samples were studied in the high temperature powder X-ray diffractometer, they were analyzed by the Ames Lab analytical division using induction coupled plasma (ICP). The samples to be analyzed were first dissolved

in a acid solution. The solution was then converted to an aerosol and injected into a RF field. Once in the RF field, all of the constituent atoms are ionized. Quantitative analysis is done by the ICP using the emission spectra of the ions. The ICP presents the composition analysis in the form of elemental ratios.

High Temperature X-ray Powder Diffractometer

The melting and textured solidification of $Bi_2Sr_2CaCu_2O_8$ were primarily studied using high-temperature powder diffraction. With this diffractometer, the X-rays were generated by a copper rotating anode at a power of 40kV X 130mA. The X-ray beam was monochromated to Cu K_α using a flat graphite crystal by diffraction from the (002) planes at an angle of 26.5° in 2θ. The monochromatic X-rays enter an Edmund Buhler high-temperature chamber. The chamber consisted of a cylindrical double wall and water cooled stainless steel pot with a beryllium window. The sample was placed on a gold coated platinum strip sample holder. The sample holder was heated by passing an AC current through the sample holder via connecting electrodes. The sample temperature and electrode current were regulated by a thermal controller. A chromel-alumel thermocouple was used by the thermal controller to monitor the sample temperature. The chamber was connected to

a turbo-molecular pump, capable of generating a chamber vacuum of 10^{-7} torr, and a rough pump. Using the vacuum system, the $Bi_2Sr_2CaCu_2O_8$ samples were studied under different partial O_2 pressures. This was done by evacuating the chamber and refilling it with premixed gas of O_2 and N_2 from a cylinder. The scattered X-rays were detected by a position sensitive detector. The detector was fixed in place when collecting data. The data collecting time was three minutes. The signals from the detector electronics were collected by an MCA and used to generate a diffraction pattern.

Scanning Electron Microscope

The samples, after being run on the high-temperature powder X-ray diffractometer, were studied using a scanning electron microscope (SEM). The specific SEM used in this project was a Cambridge S-200 equipped with a Tracor-Northern energy dispersive spectrometer (EDS) and operated at 15kV. The SEM was used to determine the textured micro structure of $Bi_2Sr_2CaCu_2O_8$ and the dispersal of secondary phases. Chemical analysis of the secondary phases was carried out using the EDS to an accuracy of 20%. The analysis was satisfactory for secondary phase identification but the accuracy was not high. Most samples were studied as solidified, without being polished.

SECTION 1: HIGH TEMPERATURE POWDER DIFFRACTOMETER

INTRODUCTION

The high temperature powder diffractometer (HTPD) is designed to perform in situ studies on phase transformations, transformation kinetics and solid state chemistry at high temperatures using X-rays. The HTPD used in studying the melting and solidification of $Bi_2Sr_2CaCu_2O_8$ is composed of three parts: the rotating anode X-ray generator, the high temperature chamber and the position sensitive detector (see Fig. 1.1).

By combining all three parts mentioned above into the HTPD, one gains capabilities which are not inherent in a standard powder diffractometer. With the combination of a rotating anode (operating at 40kVx130mA) and a position sensitive detector, a diffraction pattern can be obtained in a fraction of the time that it would normally take. Using a standard diffractometer, the time required to acquire a diffraction pattern with good counting statistics is eight hours. With the HTPD, the diffraction pattern can be obtained in three minutes. The data collection time is thus cut by a factor of a 100.

Adding a high temperature chamber, one gains the capability of doing time vs temperature studies in pseudo real time. Because of the rapid data acquisition, the HTPD

can perform DTA like scans. Unlike the DTA, which monitors the heat exchange of a sample, the HTPD allows the study of the structural changes that occur when the sample is heated. With these new capabilities, the operator gains the ability to study melting, solidification, thermal expansion, high-temperature chemistry, phase transformations and transformation kinetics in ways that did not exist before.

X - X-ray beam path

M - monochromator

S - sample holder

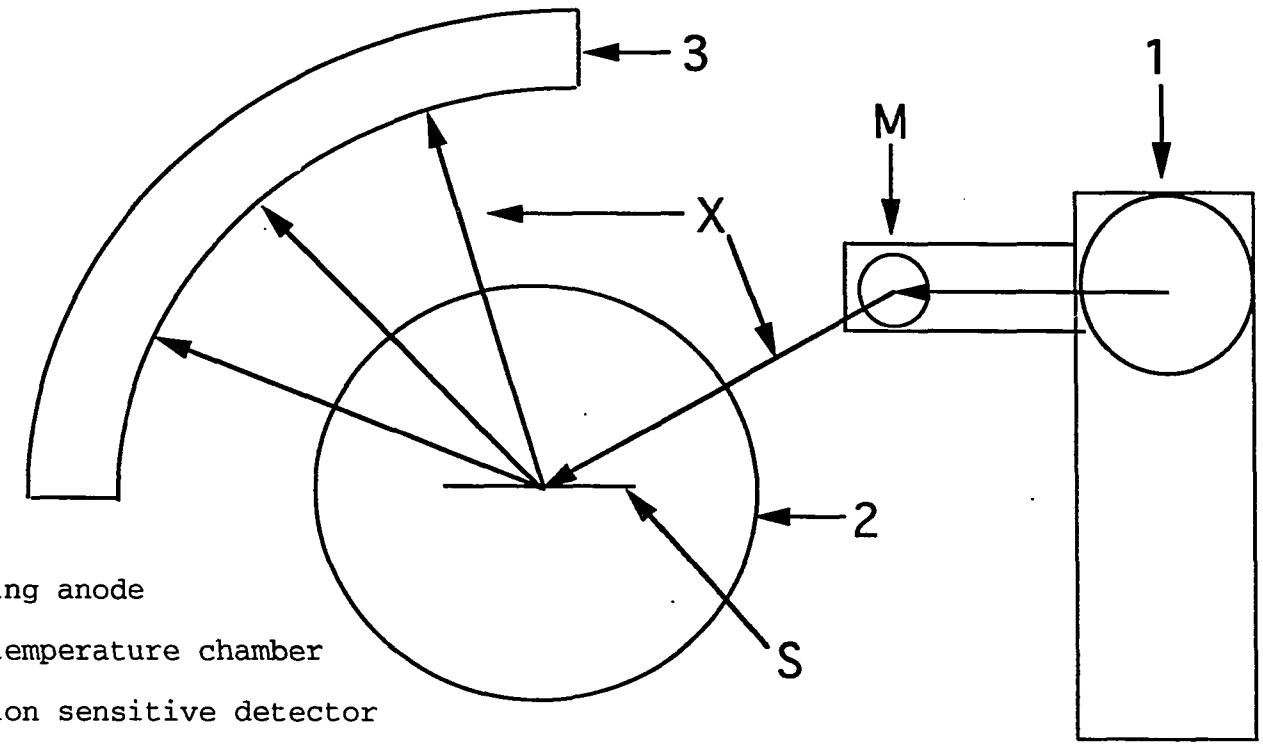

1.- rotating anode

2.- high temperature chamber

3.- position sensitive detector

Fig. 1.1 - Components of the HTPD

MAJOR COMPONENTS OF THE HTPD

Rotating Anode

The HTPD uses an Elliot GX-21 rotating anode as a X-ray source. When using the rotating anode, the normal operating power to generate X-rays is 40kVx130mA. A normal X-ray tube has a maximum power limit of 40kVx25mA. By comparing the two power settings, one notices that the rotating anode generates an X-ray beam of 6X the intensity of a normal X-ray tube. The Elliot GX-21 used in this project had a copper anode target. The X-rays generated by the copper rotating anode are monochromated to Cu $K\alpha$ and diffracted by a flat graphite monochromater into a high temperature chamber.

High Temperature Chamber

An Edmund Buhler chamber is used to contain the sample in a high temperature enviroment with a controlled atmosphere. There is a beryllium window soldered to the chamber allowing the Cu $K\alpha$ X-rays to pass through with 75% of the beam intensity transmitted. The temperature is controlled by a thermal controller connected to the chamber. To prevent any heat damage to the chamber while operating at high

temperatures a water cooling system is used.

Normal operating temperatures of the chamber are between 25°C to 2000°C. The powdered sample is placed on a metal strip sample holder which is connected to two electrodes(see Fig. 1.2). The sample is heated resistivly by passing an A.C. current through the sample holder. A metal strip radiator, connected to two other electrodes, is also used to heat the sample. The radiator, once it is mounted, nearly surrounds both the sample and sample holder. The primary purpose of the radiator is to minimize any thermal gradients in the sample. The most commonly used materials for the sample holder and radiator are platinum and molybdenum. Choosing which material to use for the heating elements depends on the atmospheric composition inside the chamber and the highest temperature to be studied in the experiment.

The thermal controller is connected to the chamber by high-current cables going into the electrodes and a thermocouple link. A pair of thermocouple wires are connected to the link by two metal posts. The thermocouple junction is spot welded onto the bottom of the sample holder. As with the heating elements, the decision on what kind of thermocouple is used depends on the atmospheric composition and temperature range of interest.

The thermal controller can be programmed to follow any temperature profile by specifying the heating rate,

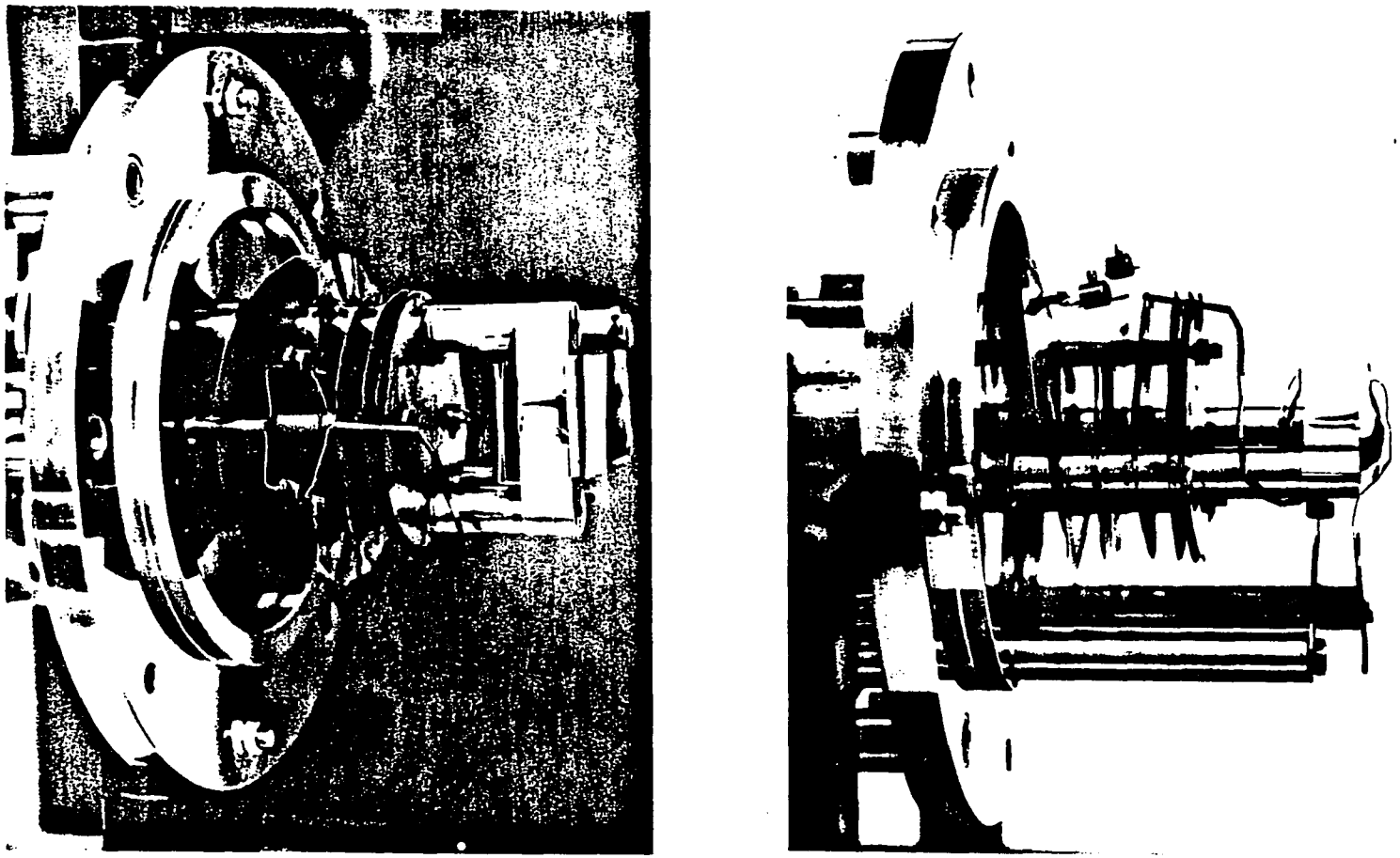

(a) (b)

Fig. 1.2 Top (a) and side (b) view of the HTPD sample holder and heating elements

temperature of an isotherm and how long an isotherm is to be held. Using the potentiometers on the controller, one can set the current output ratio between the sample holder and radiator. By controlling the amount of current going through the sample holder (0-100 amps) and radiator (0-250 amps), the thermal controller is able to follow the programmed temperature profile. The controller determines the temperature by comparing the programmed thermocouple voltage to the actual voltage at the junction. Any difference in the two voltage readings is displayed on a deviation indicator. The controller compensates for any voltage deviation by changing the amount of current going to the electrodes. One also has the option to switch to manual control and heat the samples by using the potentiometers and observing the deviation indicator.

The high temperature chamber can operate at pressures ranging from 760 torr to 10^{-7} torr. Vacuum is obtained using a turbomolecular pump directly attached to the chamber (see Fig. 1.3). An ion gauge monitors the vacuum pressure. Almost any atmospheric composition can be used in the chamber. The only limitation on the composition is the reactivity of the gas to the inner chamber wall and electrodes. There are two ways to fill an evacuated chamber with a gas mixture. The first is to use a cylinder containing the gas mixture. The

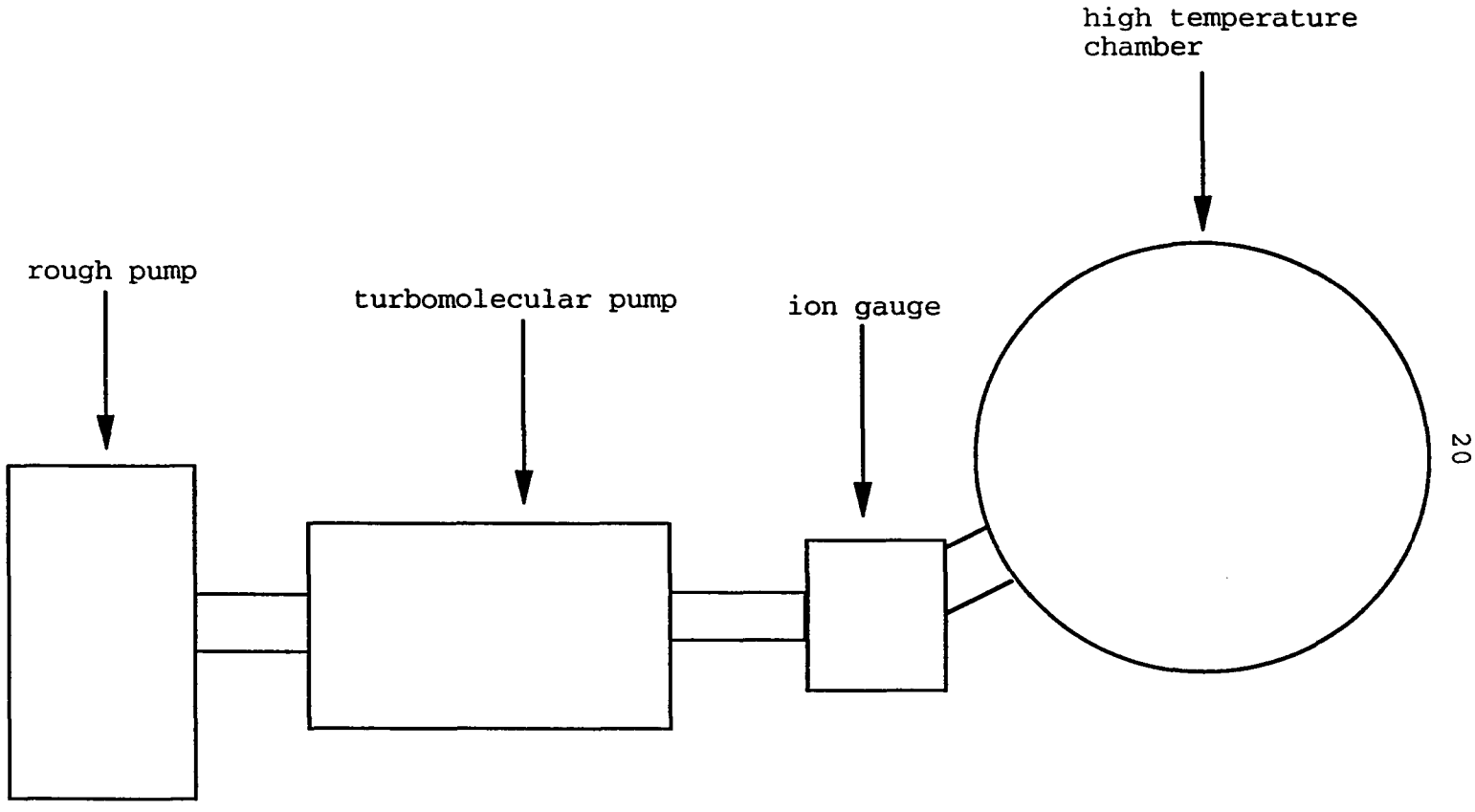

Fig. 1.3 Vacuum system of the HTPD

second is to use flow meters and let the pure gases mix inside the chamber.

The high temperature chamber, in its present configuration, has some problems in operation. One of these problems is due to the mechanical properties of the sample holder. At high temperatures, the metal sample holder becomes soft and begins to sag or distort. The sample is therefore not always centered in the diffractometer. This shift in sample position causes errors in the peak positions in the diffraction pattern. A partial solution to this problem is to constantly tighten the sample holder by rotating the electrodes.

Another problem is the location of the thermocouple junction. The junction, being spot welded to the underside of the sample holder, does not measure the sample temperature directly. The assumption is that the sample and sample holder are at thermal equilibrium with each other. This assumption is not quite correct because there are large thermal gradients between the sample holder and sample. A major part of the thermal gradient is caused by ineffective heating of the sample surface at low temperatures. The sample is heated primarily from the sample holder via thermal conductivity below 700^{o}C. In the temperature range of 25^{o}C to 1000^{o}C, the theral conductivity is relativly constant, while the radiated power increases as T^4, where T is the temperature. Below

T^4, where T is the temperature. Below 700°C, the Pt radiator makes a marginal contribution to the heating of the sample surface.Only above 700°C is the radiating power of Pt sufficiently large to make a significant contribution to the heating of the sample. The error in the thermocouple readings is $\pm 5^0$C as determined by thermal calibration.

Position Sensitive Detector

Once the X-rays scatter from the sample and exit the chamber through the beryllium window, they enter the position sensitive detector. The HTPD uses a position sensitive detector (PSD) to obtain a diffraction pattern. A PSD operates basically as a modified proportional counter (see Fig. 1.4). As the X-rays enter the PSD, they ionize the gas inside the detector. The electrons that are formed from the gas ionization move toward an anode wire. The generated signal, when the ionized electrons strike the anode wire, is collected to generate a diffraction pattern.

The signal from the anode wire travels to the opposite ends of the detectors. The position at which the signal was generated on the anode wire is determined by the difference in the rise time of the signal, at each end, due to the

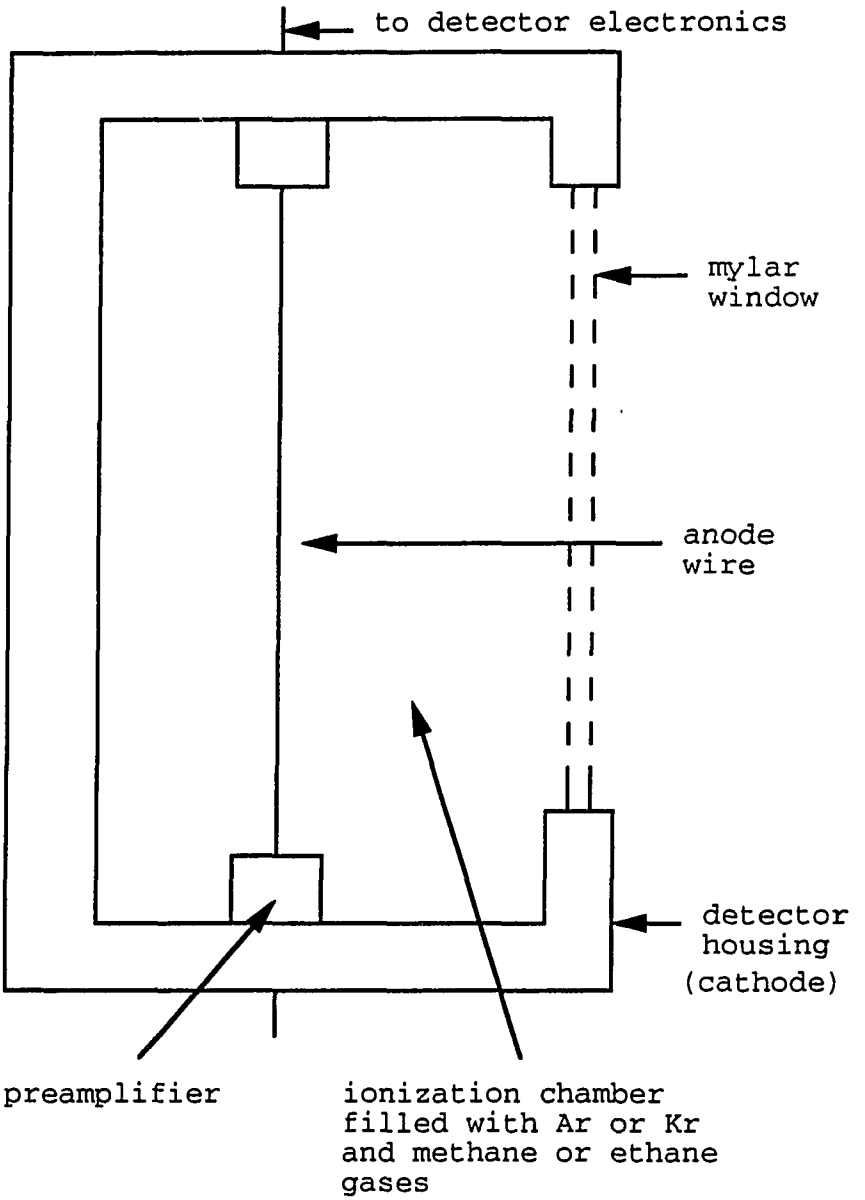

Fig. 1.4 Position sensitive detector

capacitance of the anode wire. The electronics (see Fig. 1.5) convert the difference into a signal pulse of some specified height, with the height of the pulse being proportional to the time difference. The pulse signal is sent from the detector electronics to the multichannel analyzer(MCA).

The MCA sorts the pulse signal into specific channels according to pulse height. At this stage, each channel corresponds to a specific position on the anode wire. Over a period of time signal pulses are collected by the MCA to generate a diffraction pattern. Using a powdered standard (i.e. Si or SiO_2), one can calibrate the channel numbers.

The detector electronics also contain a single channel analyzer. The single channel analyzer discriminates any X-ray radiation outside of the wavelength (or energy) band of interest. The main cause of background radiation is sample fluorescence. By blocking the background radiation, the peak/background ratio of the diffraction pattern is improved.

The PSD uses argon for the detection gas in the ionization chamber. This particular gas is used because of the high absorption coefficent for Cu $K\alpha$ radiation. Ethane is mixed with the ionization gas at a concentration of 15% by volume. The alkane is used in the electron transfer process to assist in reducing the noble gas ions. By doing so, the maximum count rate is increased by a factor of two (normal

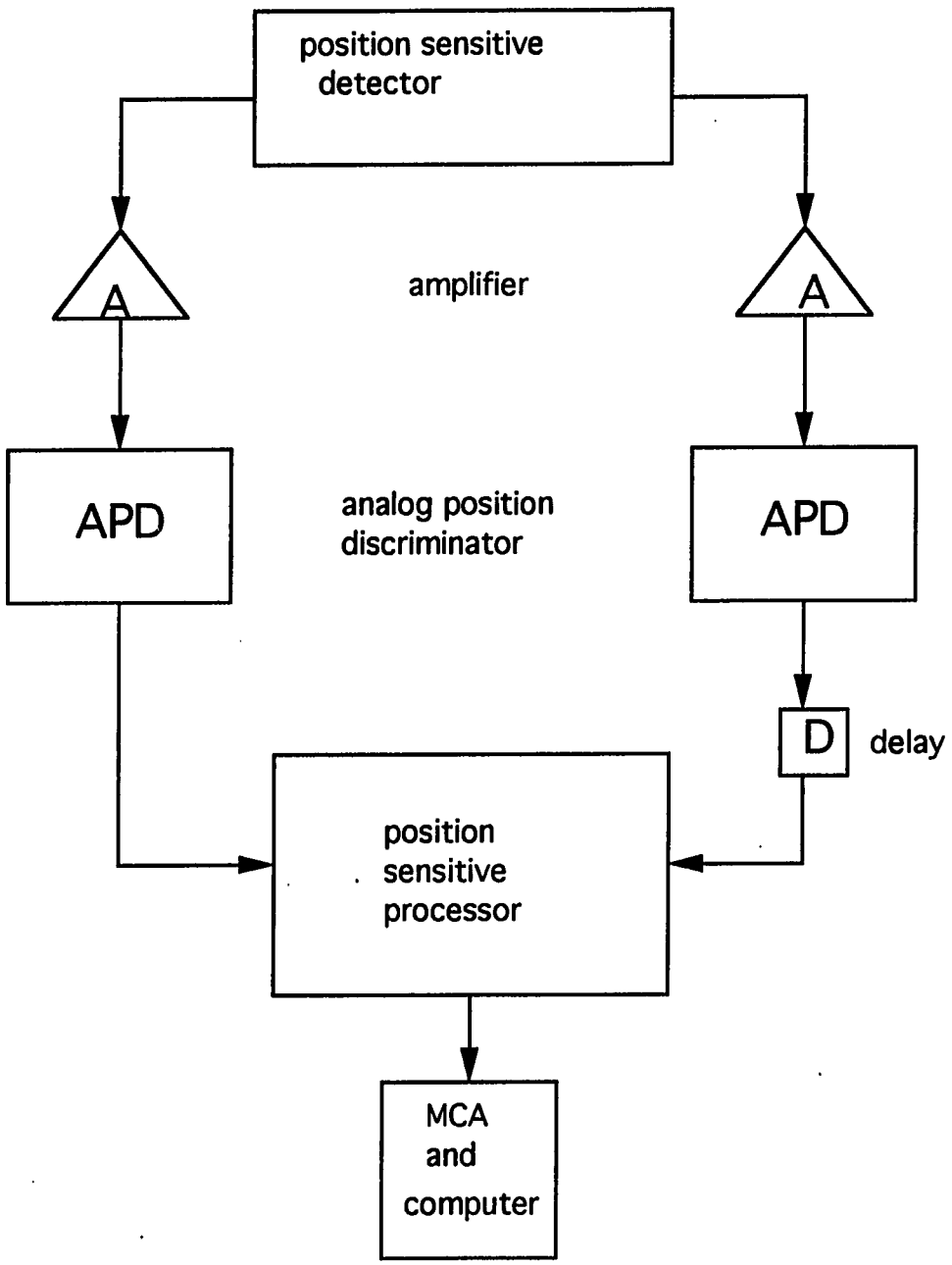

Fig. 1.5 PSD electronics

maximum count rates for a proportional counter are on the order of 10,000 cps).

LINEAR AND CURVED PSD

In studying the melting and solidification of $Bi_2Sr_2CaCu_2O_8$, two different PSD's were used on the HTPD. The first detector used was a linear TEC detector. The second detector was an Inel curved detector. The linear TEC detector has a few characteristic problems which were rectified by using the Inel detector

For the linear detector the problem lies in the fact that the detector is flat. The TEC linear detector has an infinite radius of curvature, while the Inel curved detector has a radius of curvature of 250mm. For the linear detector, the distances between the sample and the anode wire are not all equal (see Fig. 1.6). The relationship between the diffraction angle (2θ) and the position on the anode wire is therefore nonlinear. This nonlinear relationship causes a distortion in the diffraction pattern generated by the MCA. The nonlinearity affects the pattern by shifting the peak position away from the center of the pattern.

There is another distortion that occurs when using the linear detector. This distortion arises because the beam path from the sample to the linear detector does not intersect

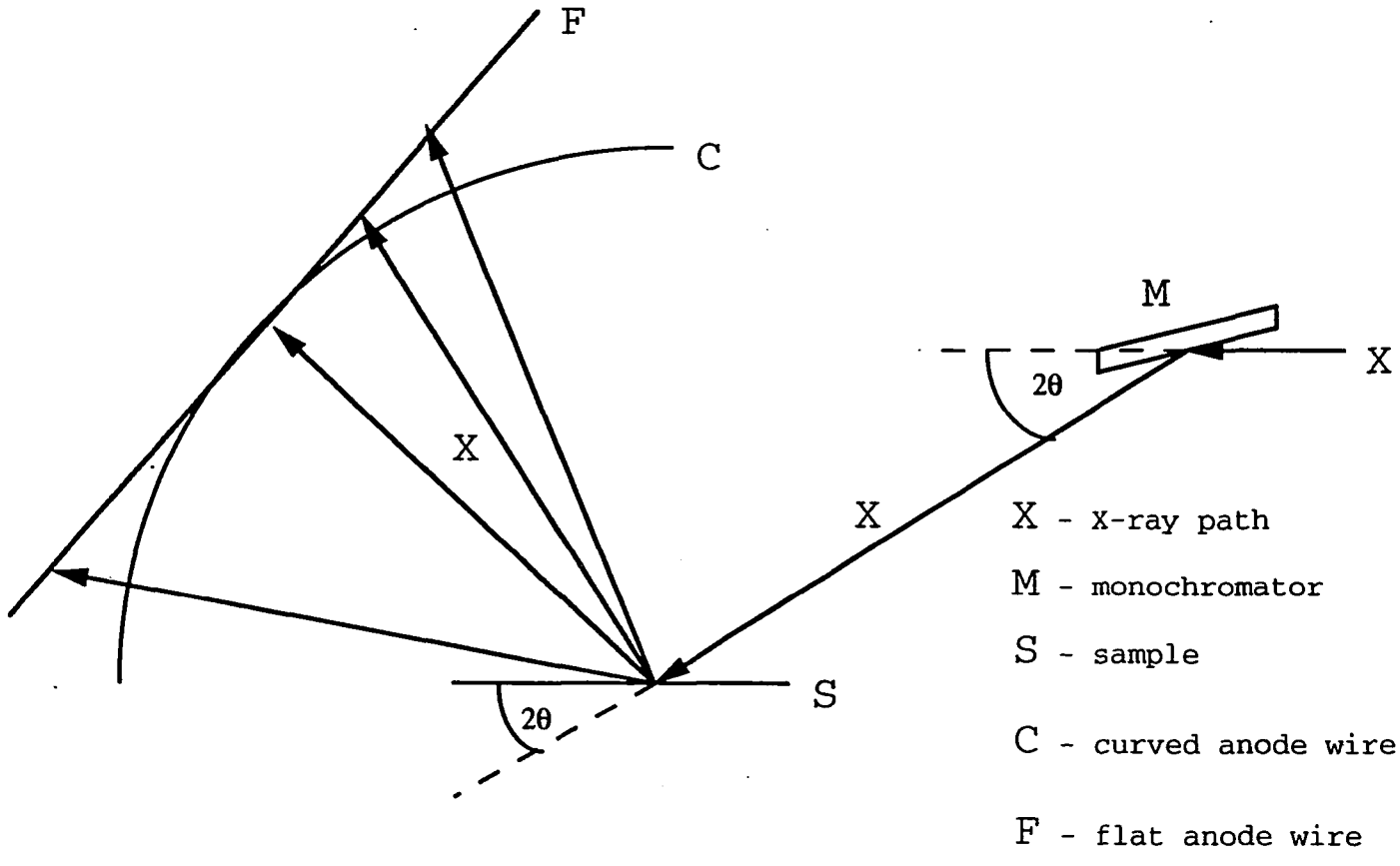

Fig. 1.6 Position error between a flat and curved anode wire

the anode wire perpendicularly. This causes an asymmetric distortion and broadening to any diffraction peak not located at the center of the detector. The distortion is caused by the electric field in the detector, which causes some of the generated electrons to deviate from the beam path. Both of these distortions become more pronounced as the length of the linear detector is increased. Because of the distortions, the useful length and detection region of a linear detector is limited. The TEC detector used in this work has a detection range of 30^0 (2θ). The curved Inel detector does not suffer from these problems and has a much larger (120^o) detection range.

DIFFRACTION CHARATERISTICS OF THE HIGH TEMPERATURE POWDER DIFFACTOMETER

The diffraction characteristics of the HTPD, using the Inel curved detector, were determined by running an NBS standard Si powder sample at 25°C. The data collection time was set at three minutes. The Cu K_α line, generated by the rotating anode at a power of 40kVx130mA, was used. Fig. 1.7 shows the Si diffraction pattern generated by the MCA. The (220) and (422) Si peaks were used to calibrate the 2θ range of the MCA. The slope of the calibration (2θ vs channel number) curve was determined to be 0.01569 deg(2θ)/channel From the diffraction pattern the positions, FWHM, area and count intensities were determined (see Table 1.1).

From Fig. 1.7 and Table 1.1, one notices that the (111) peak at 28.44° is ,relative to (220), weaker than expected. The relative peak intensity is attenuated by 88%. The intensity discrepancy can be accounted for by the fact that the X-rays are attenuated by the absorption of the sample. The extent of the attenuation by absorption as a function of 2θ follows the equation (1):

$$\frac{I_D}{I_O} = \frac{1}{\mu(1 + \sin\alpha/\sin\beta)} \qquad (1)$$

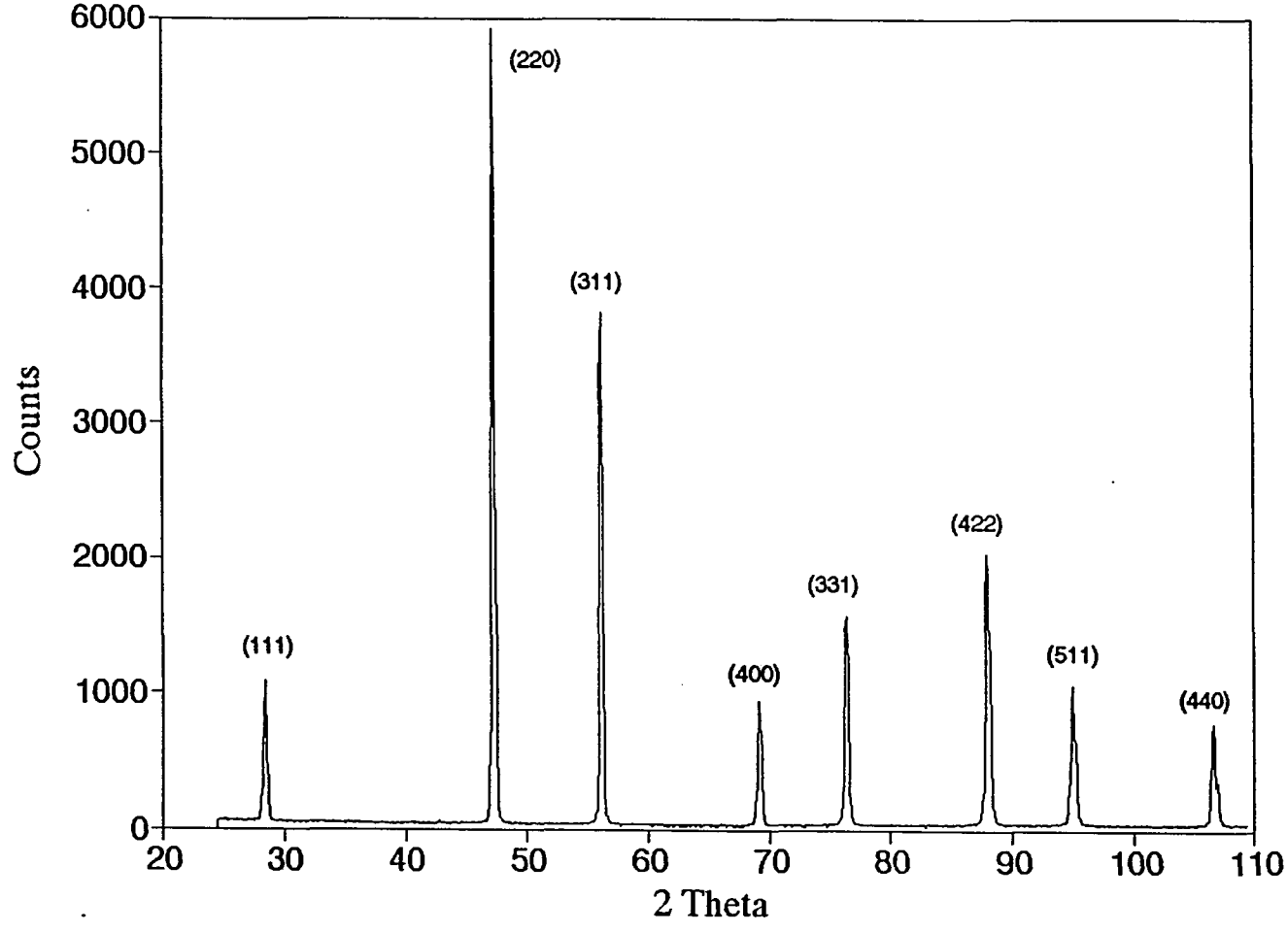

Fig. 1.7 diffraction pattern of Si powder taken with the HTPD

Table 1.1 Diffraction characteristics of the HTPD using NBS silicon powder

hkl	$2\theta_{cal}$	$2\theta_{obs}$	$\Delta 2\theta$	FWHM	I_{cal} ratio	I_{area}	I_{area} corr	I_{obs} ratio
111	28.44	28.46	+.02	.30	100	41556 ±513	615920	100
220	47.30	X	0	.22	55	143909 ±677	324733	53
311	56.12	56.15	+.02	.26	30	84205 ±602	160224	27
400	69.12	69.15	+.02	.38	8	28088 ±457	46597	7
331	76.38	76.39	+.01	.36	13	45156 ±620	71496	12
422	88.03	X	0	.44	17	67056 ±636	101100	16
511	94.95	94.95	0	.15	9	37183 ±548	55024	8
440	106.71	106.68	-.03	.17	5	23628 ±420	34015	5

X - peak used as a calibration point

$\alpha = 26.5^{o}$ $\beta = 2\theta - 26.5^{o}$

μ = absortion coefficient of the sample for a specific X-ray wavelength.

I_D and I_O are the intensities of the diffracted and incident X-ray beam, respectively. This specific equation was derived for the geometry of the HTPD (see Fig.1.8). From equation (1), the attenuation of the diffracted beam increases as the value of the 2θ approaches 26.5^{o}. 26.5^{o} is the angle at which the X-rays are diffracted from the graphite monochromator. The increase in attenuation occurs because the diffracted beam is transmitted through more material at lower 2θ values.

The FWHM of the diffraction peaks in the pattern get larger at higher angles (see Table 1.1). The peak broadening is partly due to the divergent nature of the X-ray beam and geometrical aberrations caused by misaligments in the diffractometer. These reasons are insignificant compared to the inability to resolve the $k\alpha 1$ and $k\alpha 2$ diffraction peaks. The sharp drop in the FWHM's of the (511) and (440) peaks are caused by the complete resolution of the $k\alpha 1$and $k\alpha 2$ components. In the case of the (511) and (440) peaks, the $k\alpha 1$ component was used for the FWHM.

Peak intensity ratios were determined by using area

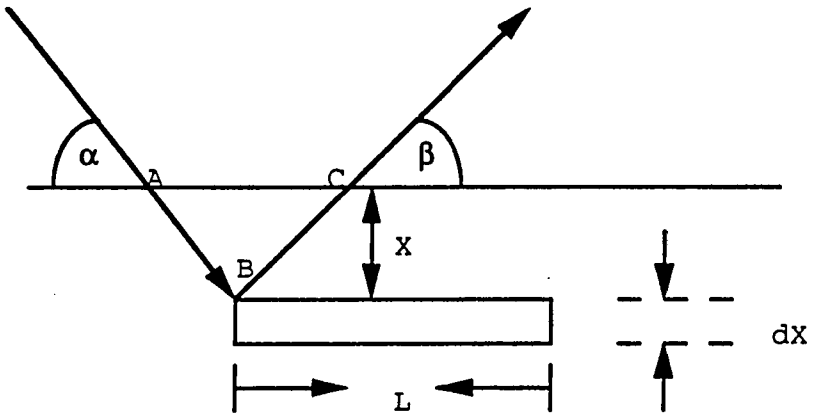

The figure above shows X-rays been diffracted from a sample volume, LdX, which is at a depth, X, from the surface of the sample. For the X-ray path ABC, the absorption of the diffracted X-rays by the sample can be represented by equation 2:

$$dI_D = I_O e^{-\mu(AB+BC)} dX \qquad (2)$$

but

$$L = 1/\sin\alpha \qquad AB = X/\sin\alpha \qquad BC = X/\sin\beta$$

therefore,

$$dI_D = (dI_O/\sin\alpha) e^{-\mu X(1/\sin\alpha + 1/\sin\beta)} dX \qquad (3)$$

The diffracted intensity of the X-ray beam is obtained by integrating over an infinitely thick sample:

$$I_D = \int_0^{\infty} dI_D = \frac{1}{\mu(1 + \sin\alpha/\sin\beta)}$$

where α is the incident angle and β is the diffracted angle.

Fig. 1.8 Derivation of the absorption factor for the HTPD

intensity. The (111) peak was used as the base peak with the intensity of 100%. In the case where the diffraction peak was split into the $K\alpha 1$ and $K\alpha 2$ components, the sum of the areas of the two components was used. The area intensity was determined through the use of the MCA and corrected for absorption. All of the calculated intensity ratios are listed in Table 1.1.

The HTPD has a major limitation in that the sample holder does not rotate. The sample holder remains horizontal throughout the experiment so that liquids will not run out of the sample holder. The lack of movement in the sample holder, also of the detector and X-ray source for that matter, causes difficulties in two ways. First the detection range is cut off at low angles. The low angle limit is dependent on the Bragg angle (2θ) of the monochromater,which in the present configuration is 26.5^{o} (see Fig. 1.6). The diffracted x-rays from the monochromater and sample are not able to transmit through the sample holder. The lowest diffraction angle X-rays that can be detected graze the surface of the sample holder. The cut off angle for the detection range is equal to the diffraction angle of the monochromater. The second difficulty occurs when the sample has a very high degree of preferred orientation (almost a single crystal). The incident angle of the X-ray beam on the sample may not satisfy the

Bragg condition for any of the Bragg planes in the preferred oriented sample. In such a case, no diffraction occurs.

TEMPERATURE CALIBRATION OF THE HTPD

A K_2SO_4 sample (NBS) was used as a standard to determine the accuracy of the thermal controller in determining the sample temperature. K_2SO_4 has a crystallographic first order phase transiton at 586°C which is detectable by the HTPD. The sample was heated from 570°C to 595°C in 5°C steps.During the time when the sample was held isothermally, a diffraction pattern was taken with the detection time set at three minutes. The transition was observed at a thermocouple reading corresponding to 590°C (see Fig.1.9). The $\beta \rightarrow \alpha$ transition can be noticed by the shift in peak position of the (222) peak at 42.12°(2θ) of the orthorhombic βphase. The new peak position, at 41.80°(2θ), corresponds to the (202) peak of the hexagonal αphase. Also the (212) and (141) peaks of the β phase, at 39.11° and 40.15°(2θ) respectivly, disappear. The HTPD was also calibrated with the melting point of 2212. In a standared furnace, the 2212 compound melted at 875°C. The HTPD indicated that 2212 melted at 870°C. these results show that the controller has a ±5°C error in determining the temperature.

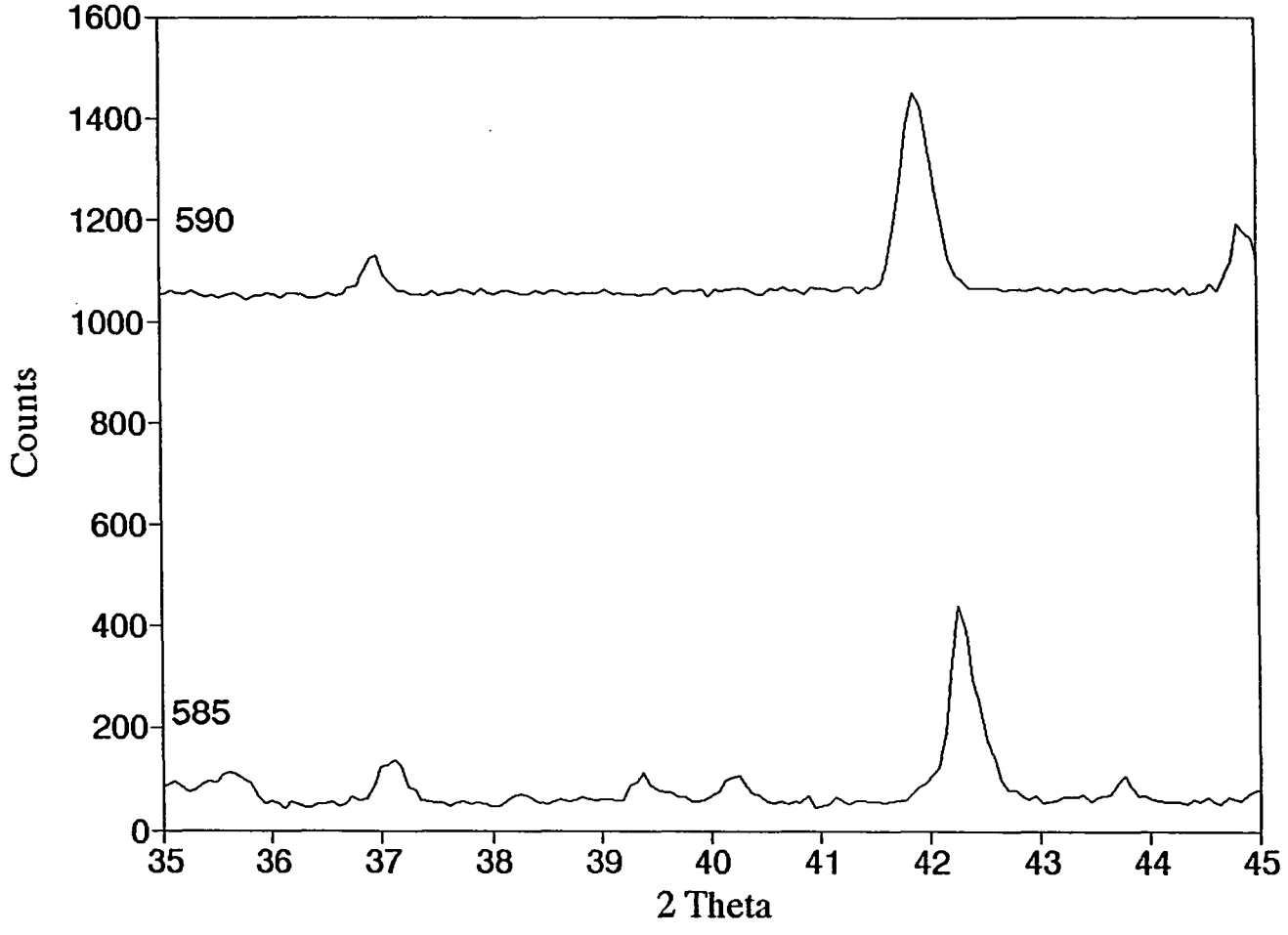

Fig. 1.9 X-ray diffraction patterns of K_2SO_4 powder at 585°C and 590°C

SECTION 2: THE INCONGRUENT MELTING OF $Bi_2Sr_2CaCu_2O_8$

NOMENCLATURE

The high Tc ceramic superconductor field has developed a nomenclature of its own for the composition of the superconductor and common side phases. Listed below is a glossary of terms used for the Bi-Sr-Ca-Cu-O system.

2212 ---- $Bi_2Sr_2CaCu_2O_8$

2201 ---- $Bi_2Sr_2Cu_1O_6$

21 ---- $(Sr,Ca)_2CuO_3$

11 ---- $(Sr,Ca)CuO_2$

10 ---- (Sr,Ca)O

24X ---- $Bi_2(Sr_x,Ca_{1-x})_4O_7$

23X---- $Bi_2(Sr_X,Ca_{1-X})_3O_6$

EXPERIMENT

The 2212 sample used in the experiment was analyzed for phase purity and composition. Room temperature X-ray diffraction, using a θ-2θ diffractometer, showed that the 2212 was single phase (no second phase above 5% by weight). The stoichiometric composition was determined by ICP and found to be $Bi_{1.9}Sr_{1.7}Ca_{0.96}Cu_2O_8$ (see Table 2.1).

The incongruent melting of 2212 was studied at four different partial oxygen pressures: 0.2, 0.1, 0.02 atm and pure N_2. The partial oxygen pressures were obtained by mixing N_2 and O_2 gas into a cylinder, which was later used to fill the high temperature chamber. The high temperature chamber was evacuated, using a rough pump, and flushed three times with the cylinder gas to remove all the air in the chamber. After the flushes, the chamber was filled with the cylinder gas to the pressure of 1 atm. It is important to note that the partial O_2 pressure for the pure N_2 run is not zero. At high temperatures, the 2212 sample evolves O_2 into the pure N_2 atmosphere.

The temperature range of the incongruent melting study was from 800^{o}C to 900^{o}C for all partial O_2 pressures, except for the pure N_2 study. In the case of the pure N_2 study, the highest temperature was set at 890^{o}C. The sample was heated

Table 2.1 Stoichiometry of 2212 form ICP results

Element	Bi	Sr	Ca	Cu
Wt %	47.6	17.6	4.49	15.2
Relative moles	0.2278	0.2008	0.1120	0.2342

Mole ratios

Bi/Ca	Sr/Ca	Ca/Cu	Bi/Sr	Sr/Cu	Bi/Cu
2.034	1.793	0.4682	1.174	0.8396	0.9520

By setting the stoichiometric sbscripts for Cu as 2, the stoichiometric composition of the sample is:

$Bi_{1.9}Sr_{1.7}Ca_{.96}Cu_2O_x$ where x = 8

from room temperature at a rate of 900°C/hr. From 800°C to the melting point, the temperature was raised by 10°C steps and held for three minutes to take a diffraction pattern. Above the melting point, two 3 minute scans were taken at each 10°C step.

The sample was placed on a gold-plated platinum sample holder. The platinum was coated with gold to a thickness of 3 microns by vapor deposition. The gold was used to prevent any reaction between platinum and the 2212 sample. The gold coating was not a complete solution to the problem. The platinum forms an alloy with gold (30 atom % Pt) at high temperature, but the reactivity of the platinum was lowered sufficiently to allow the experiment to be carried out. With such a sample holder, the 2212 material could be held at high temperatures for 3-5 hours without platinum contamination.

Two different detectors were used in this series of runs. For partial O_2 pressure of 0.1 and 0.02 atm, the Inel curved detector was used. In the 0.2 atm of partial O_2 pressure and pure N_2 cases, the TEC linear detector was used. The reason for using two different detectors was that the latter two studies were done before the Inel detector was installed.

RESULTS

The series of diffraction patterns for each experiment at 0.2, 0.1, 0.02 atm of oxygen and pure N_2 are presented in figures 2.1, 2.2, 2.3, and 2.4 respectively. A brief outline and description of the results is given below. The interpretation of the results is given in the discussion section.

0.2 atm Po_2 Study

In the 0.2 atm experiment, 2212 melts at 870°C (see Fig. 2.1). Below this temperature, at 850°C, the diffraction pattern indicates that the sample is sintering. As the sintering occurs, the sample begins to collapse into the sample holder depression and lower angle diffraction peaks decrease in intensity. This effect becomes more pronounced as the temperature is raised toward 870°C. At 870°C, the diffraction pattern shows the liquid melt, with some 2212 still present, and two other phases. These two phases have been identified as 11 and 21. The 11 phase has two peaks corresponding to the (080) and (200) Bragg planes at 44.0° and 51.4° 2θ, respectivly. The 21 phase has one peak at 54.0° corresponding to (002).

As the temperature is raised to 880°, the amount (phase

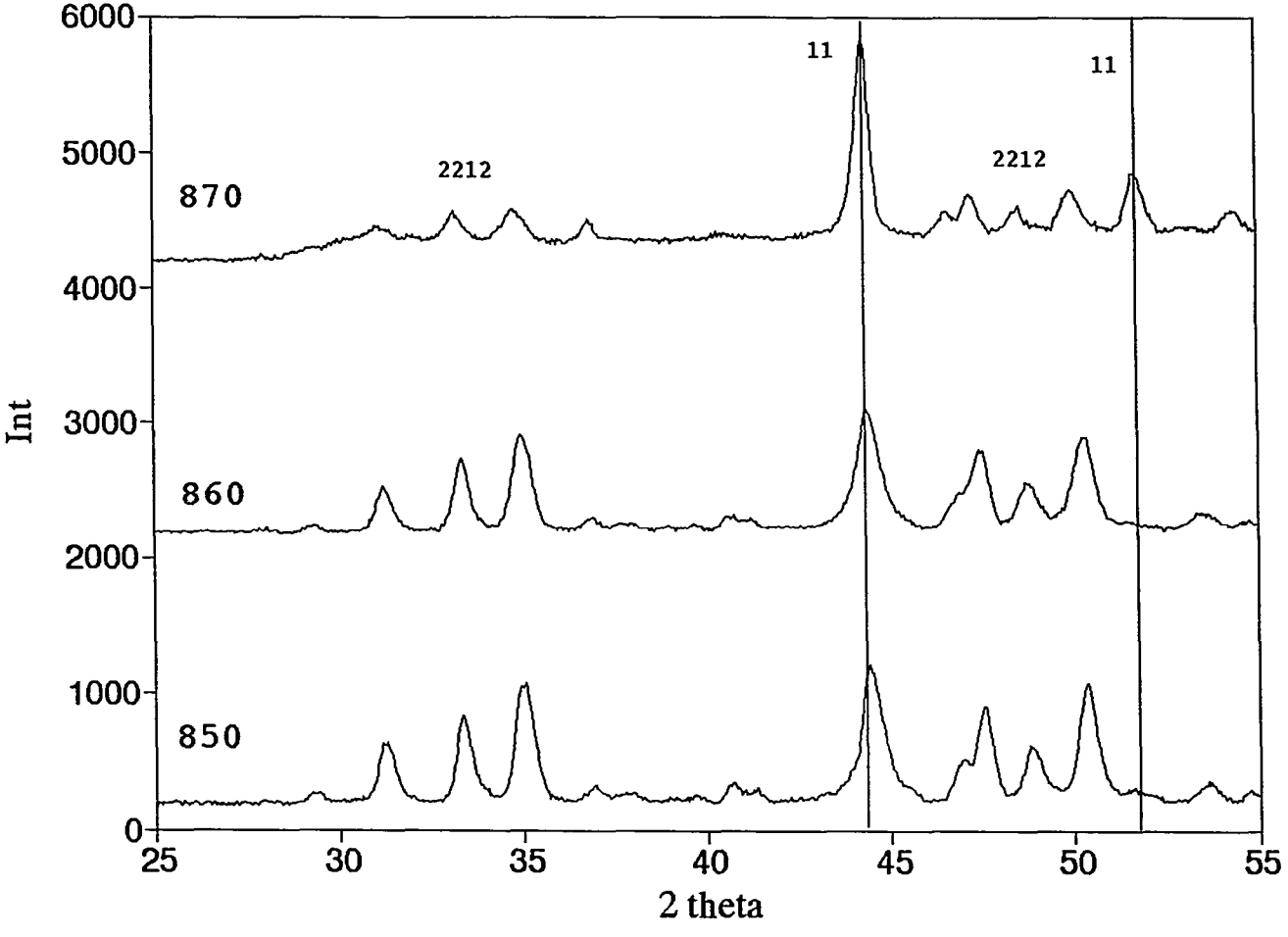

Fig. 2.1 Melting of 2212 in 0.2 atm PO2

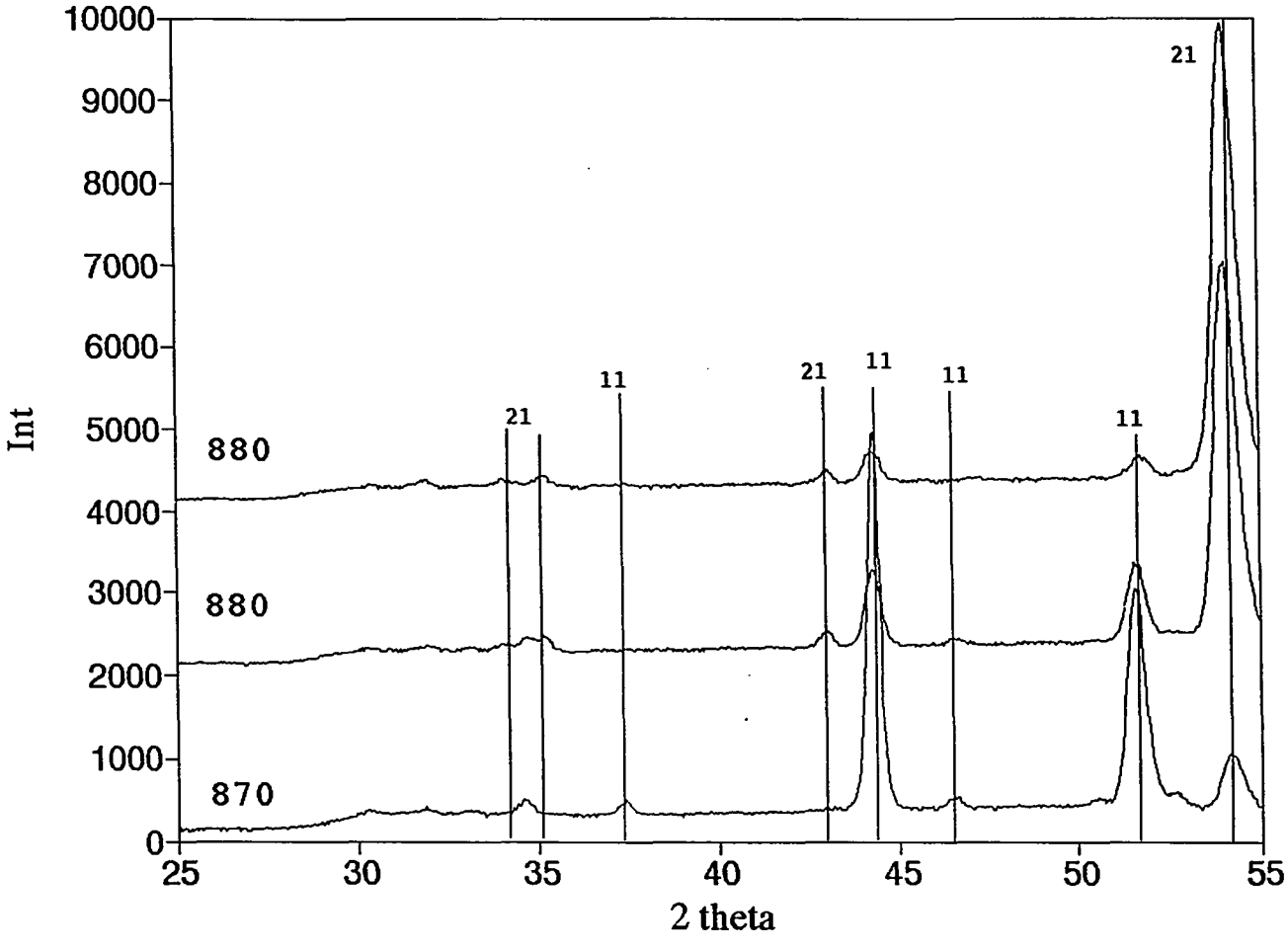
10000
9000
8000
7000
6000
5000
4000
3000
2000
1000
0
Int
880
880
870
21
11
21
11
11
11
21
25
30
35
40
45
50
55
2 theta

Fig. 2.1 Cont

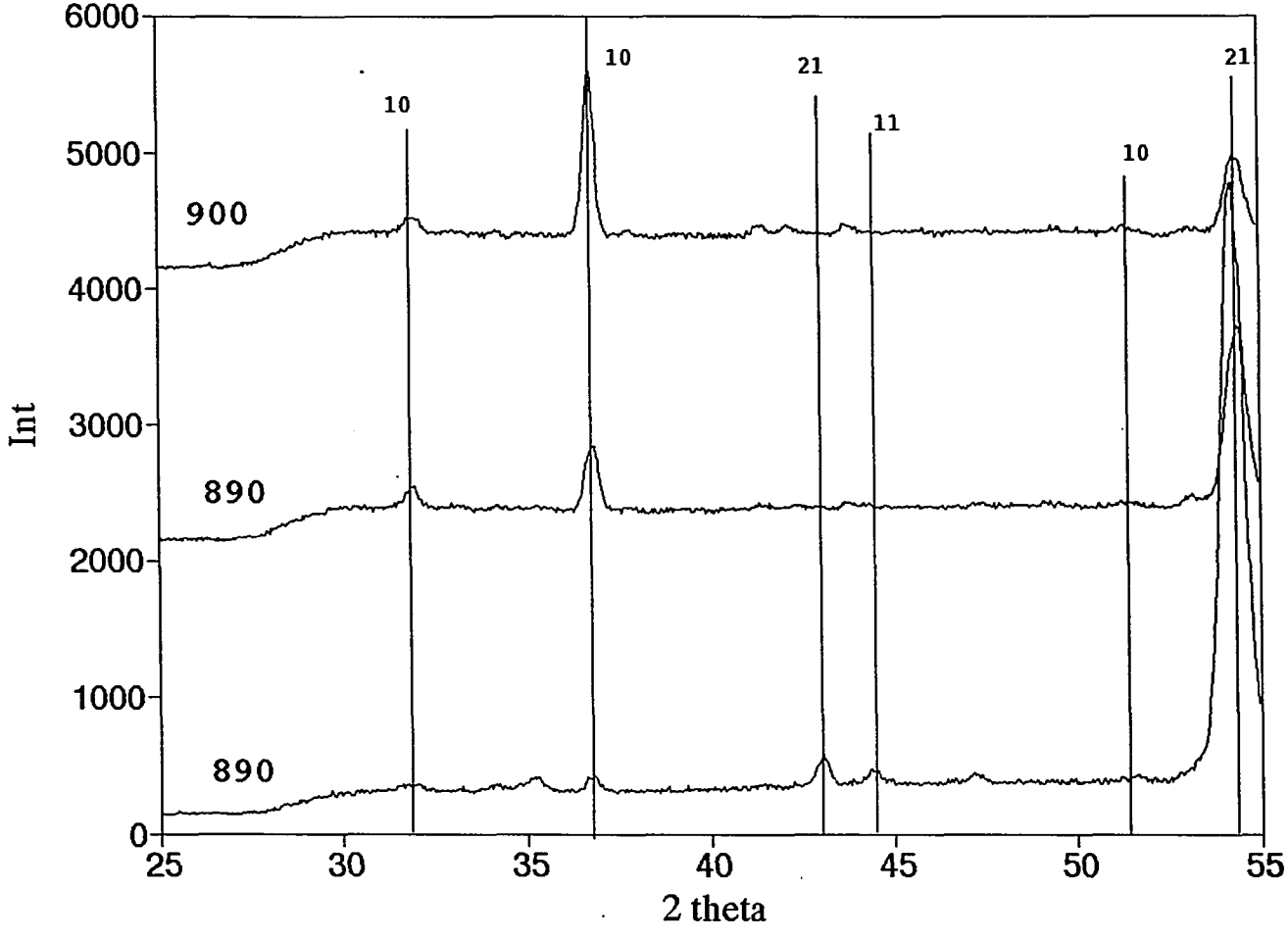
6000
5000
4000
3000
2000
1000
0
Int
900
890
890
10
10
21
11
10
21
25
30
35
40
45
50
55
2 theta

Fig. 2.1 Cont

fraction)of 11 phase decreases (the peak intensity decreases) while the phase fraction of 21 increases. At this temperature, the (600) peak of the 21 phase at 42.6°C is observed. At 890°C, nearly all of the 11 phase has gone. The phase fraction of 21 has also decreased. When the temperature was raised to 900°C, almost all of the 21 phase dissolved back into the melt. Between 890°C and 900°C, the 10 phase begins to grow out of the melt. At 900°C, the (111), (200) and (220) peaks of the 10 phase are located at 31.8°, 36.7° and 52.5°, respectively.

0.1 atm Po_2 Study

The diffraction patterns of the incongruent melting of 2212 in 0.1 atm of oxygen (Fig. 2.2) is similar to the 0.2 atm case. At 870°C, the sample melts with 11 and 21 phases forming out of the liquid. The 11 phase has peaks at 44.0°,51.4° and 52.6° corresponding to the (080),(200) and (171) planes.Only by raising the temperature to 890°C, will 11 phase dissolve back into the melt. The 21 phase has the (002), (600), (011) and (301) peaks at 54.1°, 43.0°, 35.3° and 34.1°, respectively. When the temperature is raised to 880°C, the 21 phase grows out of the liquid (as can be seen by the increase in intensity of the (002) peak), but dissolves back again at 890°C. Only a small amount of 21 is

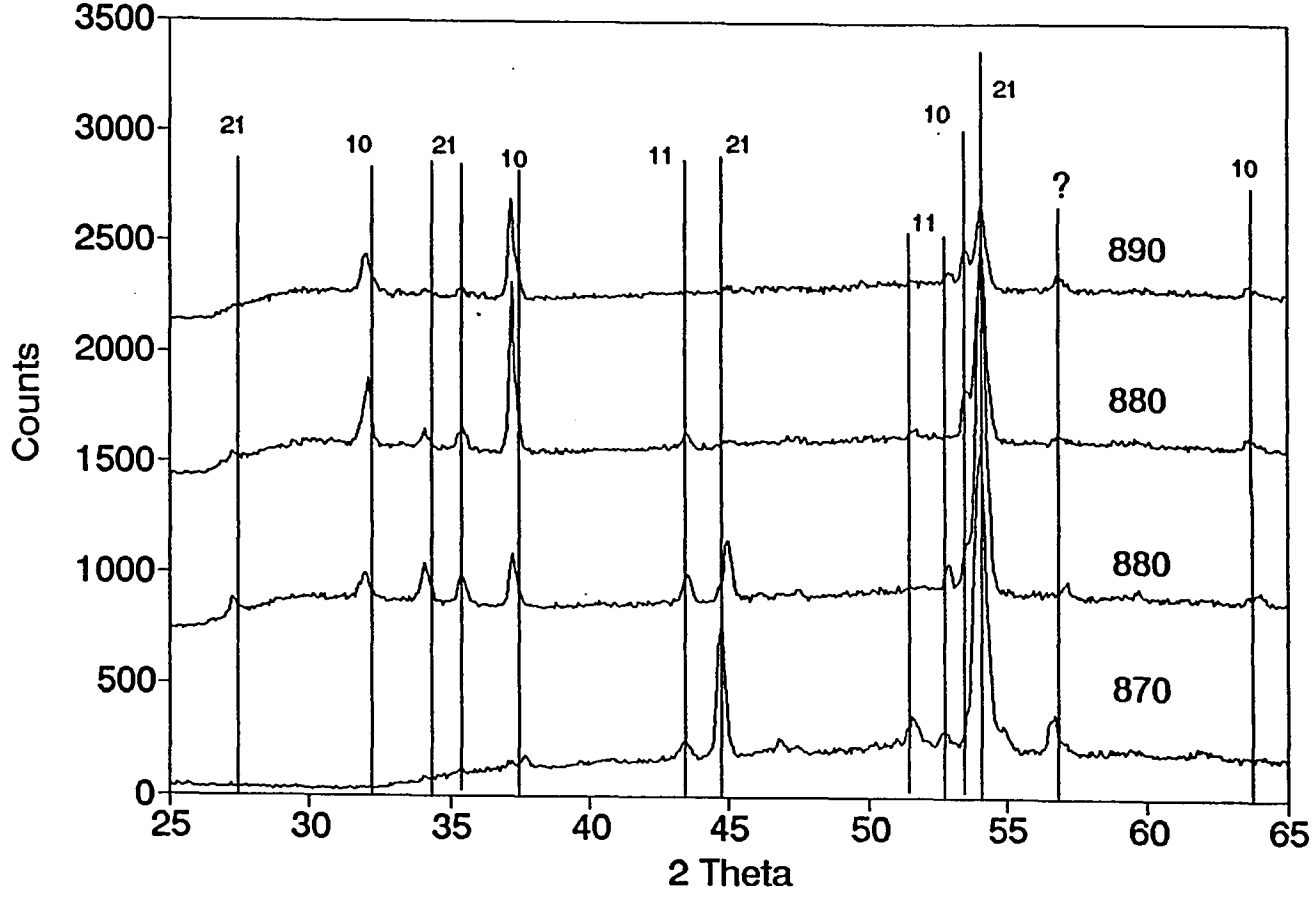

Fig. 2.2 Melting of 2212 in 0.1 atm PO2

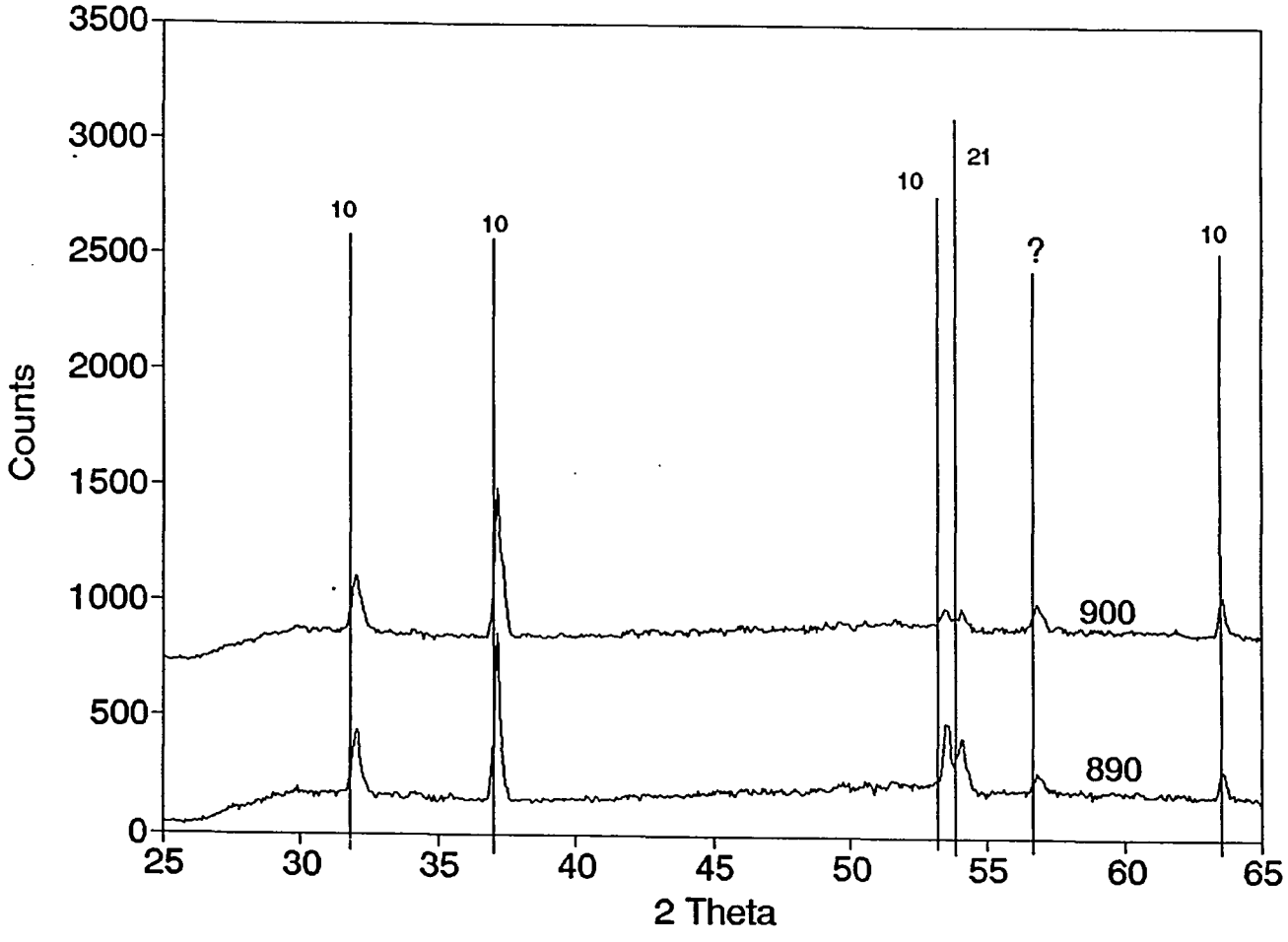
3500
3000
2500
2000
1500
1000
500
0
Counts
10
10
10
21
?
10
900
890
25
30
35
40
45
50
55
60
65
2 Theta

Fig. 2.2 Cont.

left in the melt at 900°C. The major difference between the 0.2 atm and 0.1 atm studies is that the 10 phase forms at a much lower temperature, 880°C. The peaks corresponding to the 10 phase are (111),(200),(220) and (311) located at 32.0°, 37.1°, 53.4° and 63.5°. At 900°C, the 10 phase is still present in the melt.

0.02 atm Po_2 Study

In the 0.02 atm of oxygen case (Fig. 2.3), the incongruent melting has changed significantly. First of all, the melting point of 2212 is lowered to 860°C. At 860°C, a new phase,24X, begins to form. The 24X phase has peaks at 29.3°, 29.8°, 30.0°, 41.4° and 43.0°. This phase exists in the melt up to the temperature of 870°C. The 10 phase also begins to form at 860°C, and exists in the melt to 890°C. Both the 11 and 21 phases form at 860°C and dissolve back into the liquid at 880°C. At 900°C, the only solid phases that exist in the melt are the 10 and a phase with a peak at 56.6°. The 56.6° phase could not be identified and remains unknown. This specific phase exists in the presence of the melt at temperature of 880°C to 900°C for partial O_2 pressure of 0.2,0.1 and 0.02 atm.

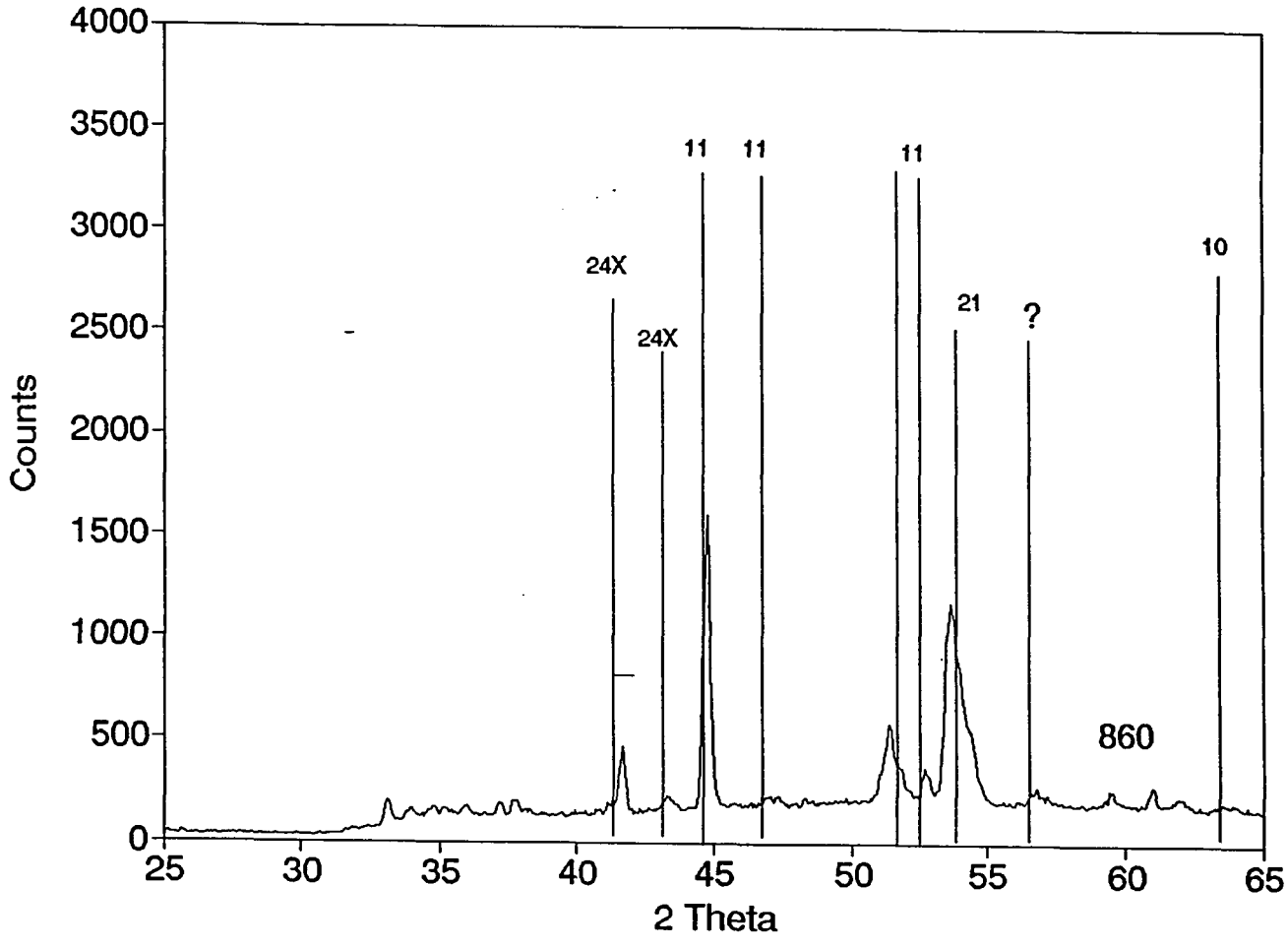

Fig. 2.3 Melting of 2212 in 0.02 atm PO2

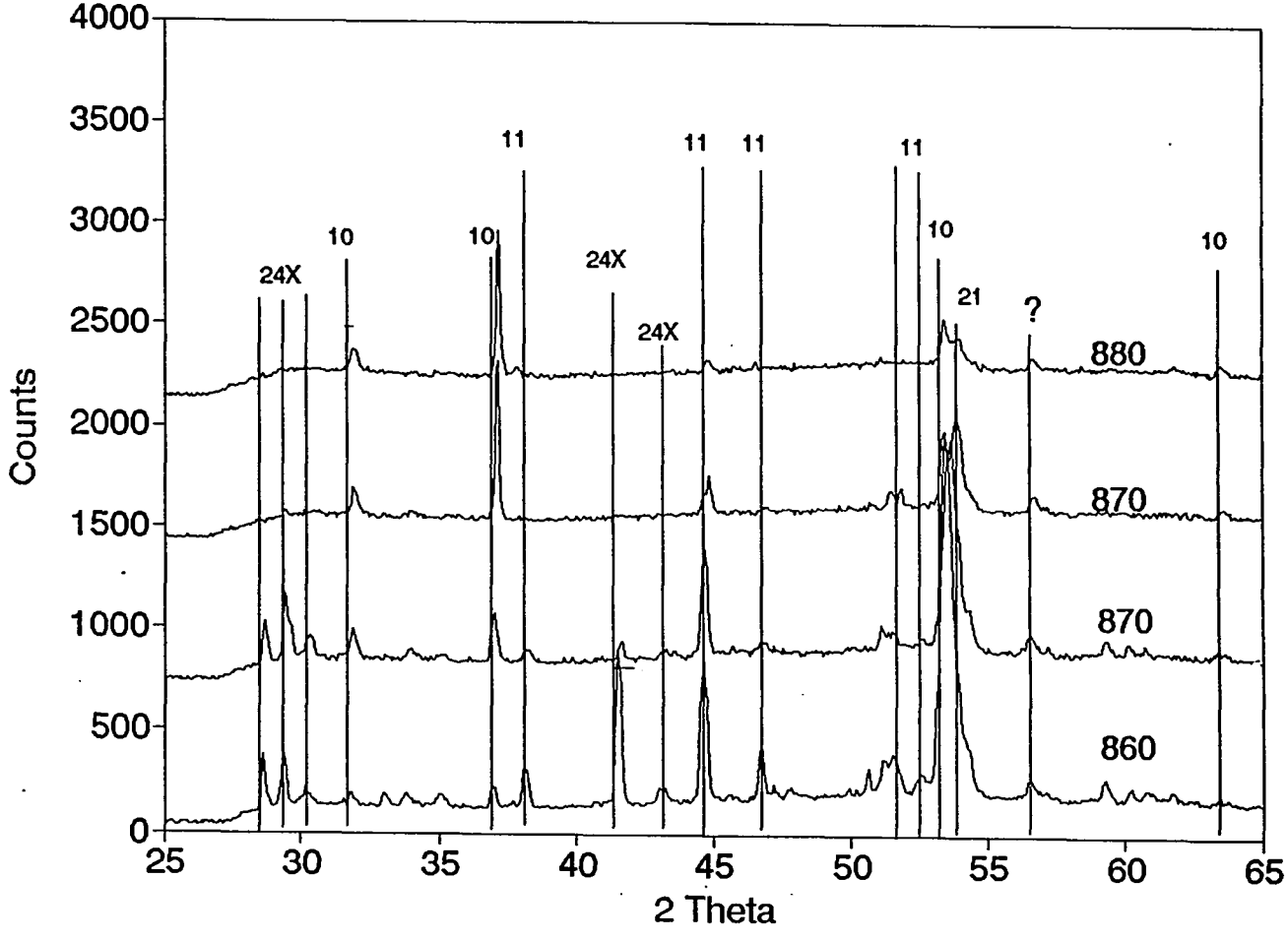
4000
3500
3000
2500
2000
1500
1000
500
0
Counts
25
30
35
40
45
50
55
60
65
2 Theta
24X
10
10
11
24X
24X
11
11
11
10
21
?
10
880
870
870
860

Fig. 2.3 Cont.

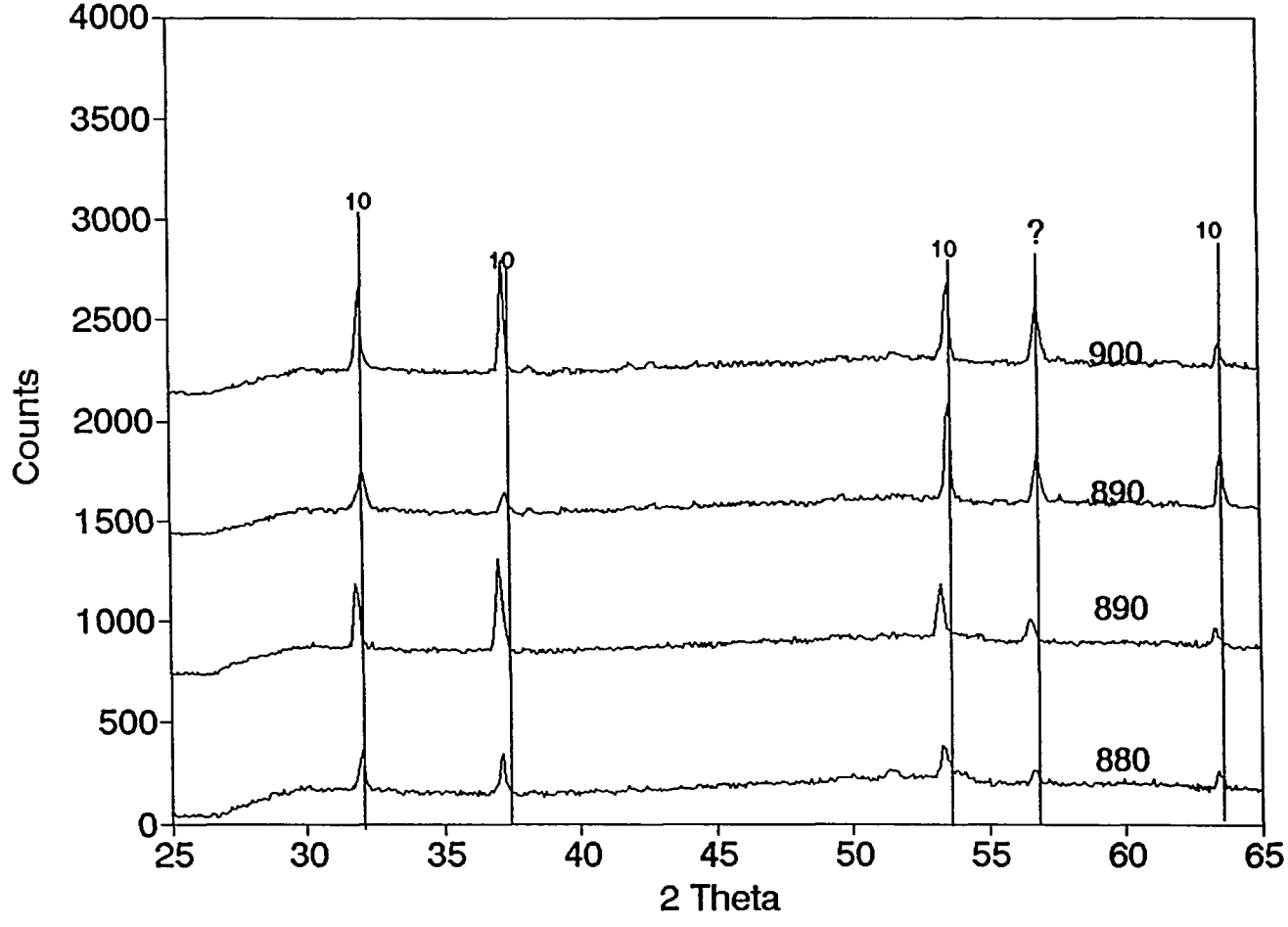
4000
3500
3000
2500
2000
1500
1000
500
0
Counts
25
30
35
40
45
50
55
60
65
2 Theta
10
10
10
?
10
900
890
890
880

Fig. 2.3 Cont.

N_2 Atmosphere Study

In the study with starting atmosphere of pure N_2 (Fig. 2.4), the melting point of 2212 was lowered to 830°C. The 11,21 10 and 24X phases form at the melting temperature. In the pure N_2 atmosphere study, the temperature ranges in which phases exist have changed dramatically (see Table 2.2). The 12X phase can exist up to 880°C. The 21 phase has a smaller phase fraction than the 11 phase when initially formed. Another change in the relative coexistence of these two phases is that the 21 phase dissolves back into the liquid at 850°C. In the case of 11, the phase dissolves at 890°C. Basically in pure N_2, the last Ca-Sr-Cu-O phase to dissolve into the melt switches from 21 to 11. When the temperature is raised from 840°C to 850°C, the (080) peak of the 11 phase disappears. This is due to the low partial O_2 pressure in the run. The 56.6° peak that has been observed in the previous runs is not observed here.

The diffraction patterns at the melting temperatures are distorted in that the low angle region is eliminated. This is due to the sample beading up when it melts. To alleviate this problem, the sample holder was tightened. By tightening the sample holder, the melted sample would spread out on the surface.

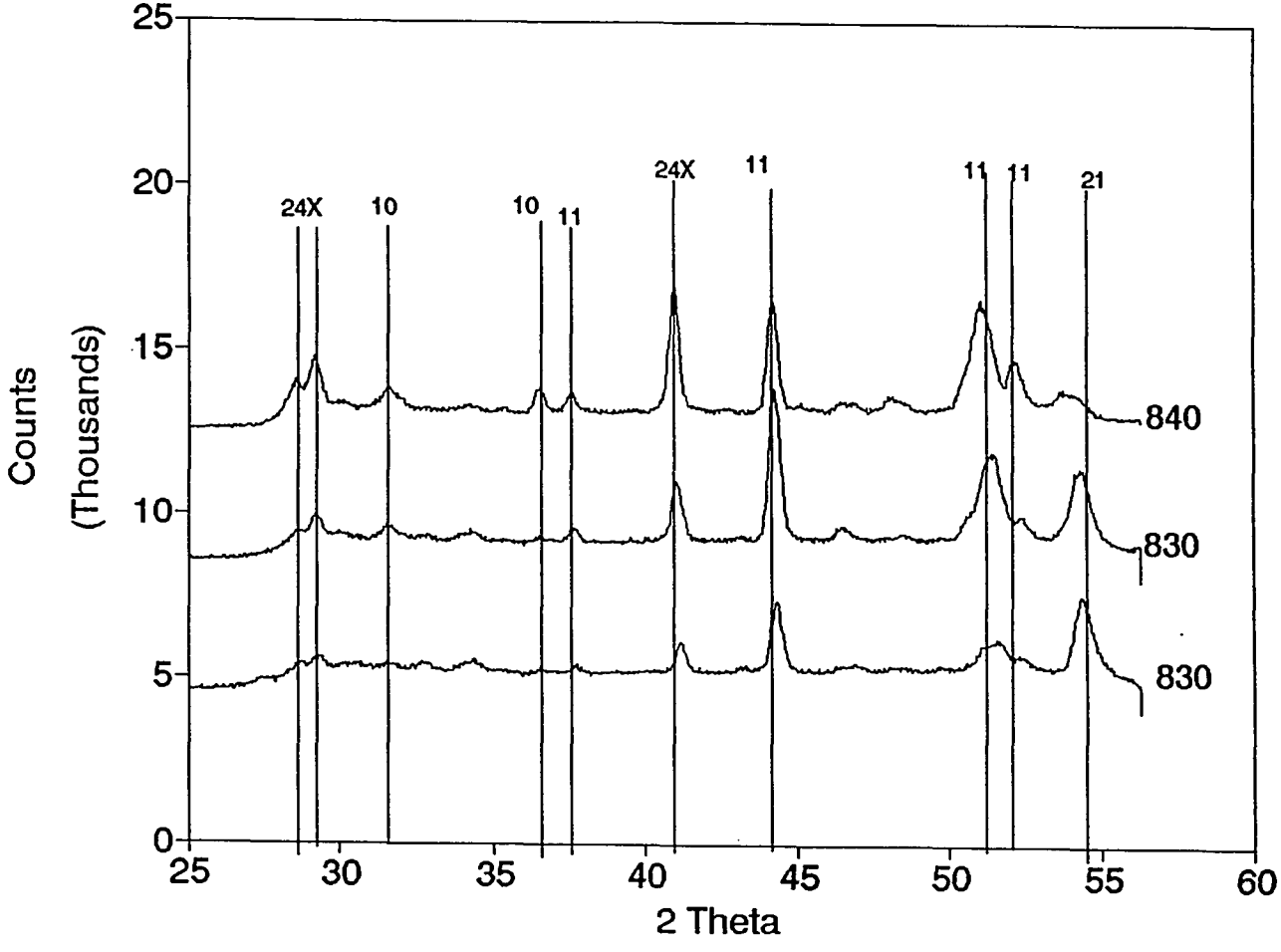

Fig. 2.4 Melting of 2212 in N2

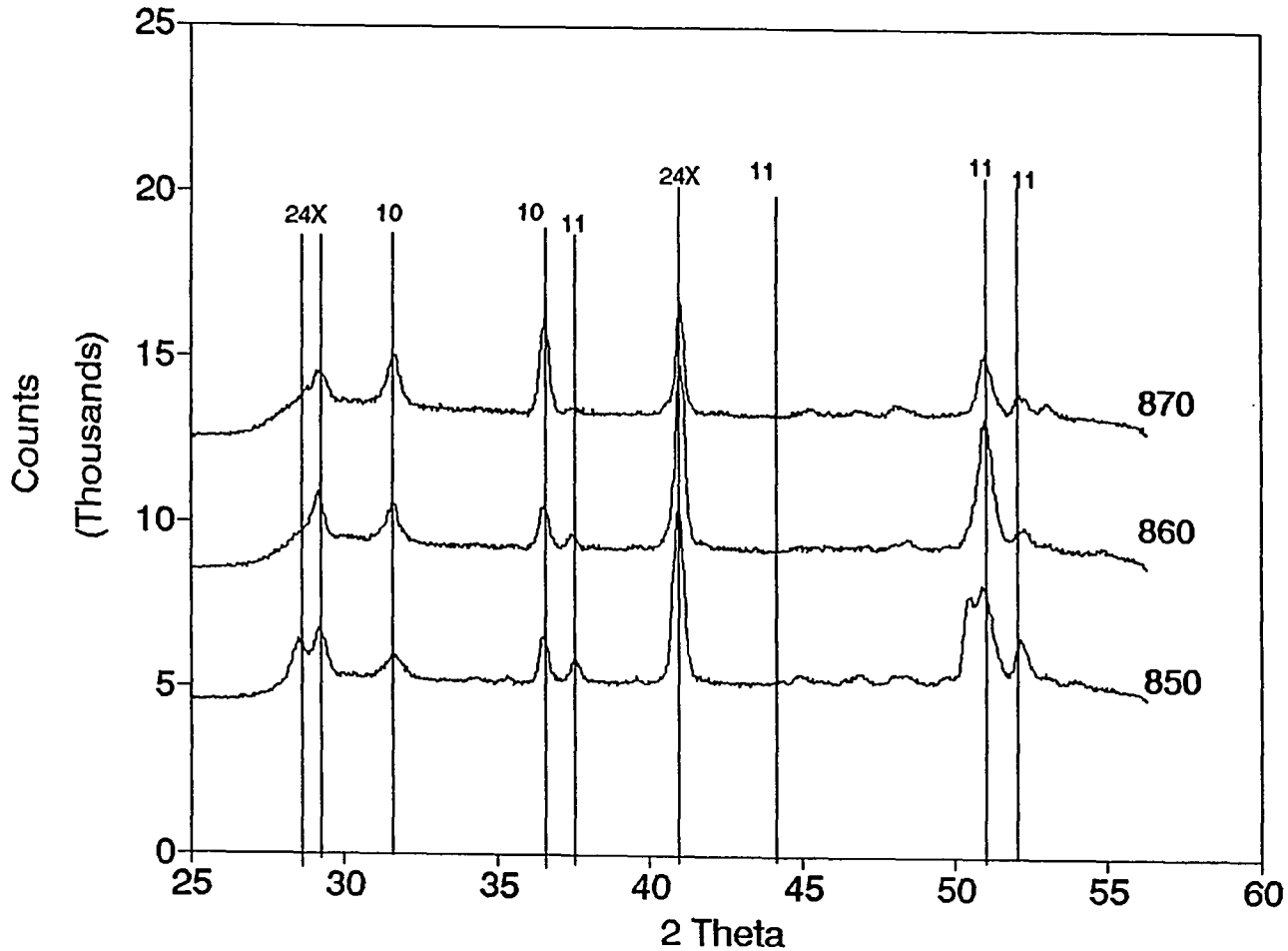
25
20
15
10
5
0
Counts
(Thousands)
24X
10
10
11
24X
11
11
11
870
860
850
25
30
35
40
45
50
55
60
2 Theta

Fig. 2.4 Cont.

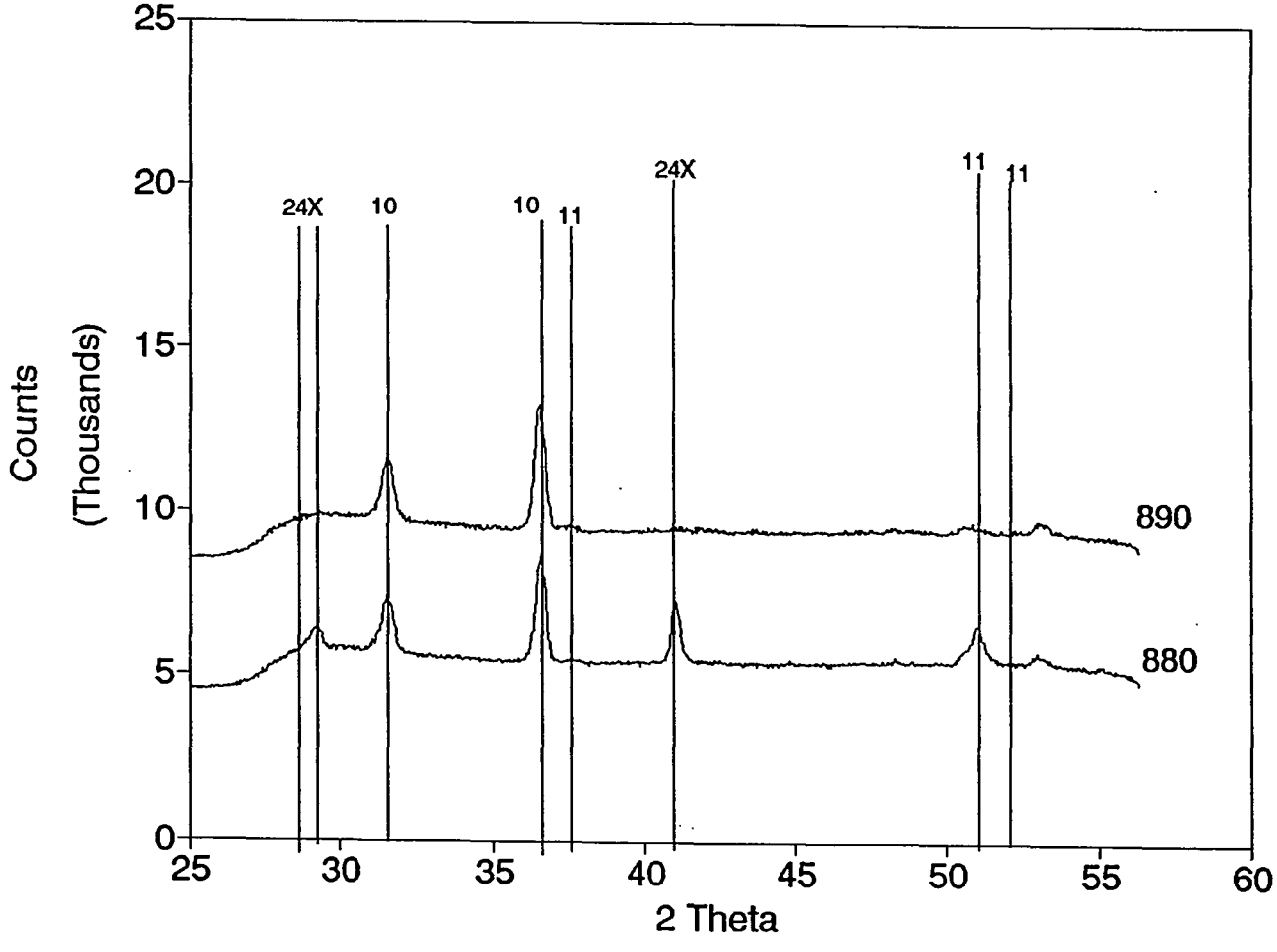
25
20
15
10
5
0
Counts
(Thousands)
24X
10
10
11
24X
11
11
890
880
25
30
35
40
45
50
55
60
2 Theta

Fig. 2.4 Cont.

Table 2.2 Temperature range of crystalline phase existance in the incongruent melting of 2212

Temp /P_{O_2}	0.2 atm	0.1 atm	0.02 atm	N_2
900°C	10	10	10	X
890°C	10,21	21,10	10	11,10
880°C	11,21	11,21,10	11,10	11,10,24X
870°C	(mp)11,21	(mp)11,21	11,21,10	11,10, 24X
860°C	2212	2212	(mp)11,21, 10,24X	11,10, 24X
850°C	2212	2212	2212	11,10, 24X
840°C	2212	2212	2212	11,21,10, 24X
830°C	2212	2212	2212	(mp)11,21, 10,24X
820°C	2212	2212	2212	2212

(mp) - melting point X - scan not taken

DISCUSSION

The incongruent melting of 2212 follows a specific formation sequence of Sr-Ca-Cu-O phases. In general, the Sr-Ca-Cu-O phase formation sequence is 11→21→10 as the temperature is increased. General structural information of these Sr-Ca-Cu-O phases are listed in Table 2.3. In all three phases, there is a homogeneity region of Sr and Ca on the alkaline earth metal sites. For the 10 and 21 phases[1], there is complete solubility of Ca on the Sr sites. The 11 phase has a 70% Ca solubility limit on the Sr sites[2]. In the case of the incongruent melting of 2212, the fraction of Ca substituted in the Sr sites for 11, 21, and 10 are 10%, 50% and 75%, respectively.The fractional occupancy of Ca on the Sr sites is determined by Vegard's law. These fractions vary slightly with different partial O_2 pressures.

The melting of 2212 and the formation of the Sr-Ca-Cu-O phases can be described as following an elemental depletion sequence. When the 2212 phases melts, all the bismuth is removed to form the melt. A large portion of the Sr, Ca and Cu goes to the formation of the bismuth free phases. As the different phases begin to form in sequence, the melt becomes more copper rich. Once the temperature is reached when the only solid phase (besides the unidentified 56.6^{o} phase) is

Table 2.3 Crystallographic parameters of 2212

and certain second phases

Phases	2212	11 (100% Sr)	11 (70% Ca)	21 (100% Sr)	21 (100% Ca)	10 (100% Sr)	10 (100% Ca)
Crystal class	Ortho	Ortho	Ortho	Ortho	Ortho	Cubic	Cubic
Space group	Pnnn	Cmcm	Cmcm	Immm	Immm	Fm3m	Fm3m
Lattice parameters (Å)							
a	5.4287	3.571	3.381	12.684	12.234	5.160	4.8106
b	5.4465	16.329	15.845	3.9064	3.7764	5.160	4.8106
c	30.8632	3.912	3.813	3.4957	3.2573	5.160	4.8106

Ortho - Orthorhombic

10, all of the copper in the system is in the melt.

To understand the phase sequence better, it is helpful to compare the crystal structures of the 2212, 11, 21 and 10 compounds. As can be seen in Fig. 2.5, 2212 unit cell is basically a layered structure. After melting, BiO and Ca layers may be immediately rejected to the Bi-rich melt. Fig. 2.5 does not represent a physical process, but rather an illustration of the intermediate process route to help in understanding of the phase transformation. It is clear from Fig. 2.5 that the CuO_2 layers lose O and are changed to CuO chains. There is also some rearrangement in the Sr and O sites for the SrO layers. One must keep in mind that the Sr sites can also contain Ca. After the unit cell is compressed, the 11 phase is formed. It can be noted that there exists a layered feature for SrO layers, in contrast to CuO chains.

In Fig. 2.6, the plot illustrates the transformation from 11 to 21 phase. It is apparent that the transformation happens if more CuO chains are rejected from 11 phase and the sites of Sr and O in SrO layers are rearranged. Fig. 2.7 shows the transformation from 21 to 10 phase. In this last transformation, the remaining CuO chains are ejected into the melt. Also, the Sr and O positions in the structure need to be rearranged and the unit cell compressed into a cube to obtain the final structure.

It is interesting to note that the longest lattice

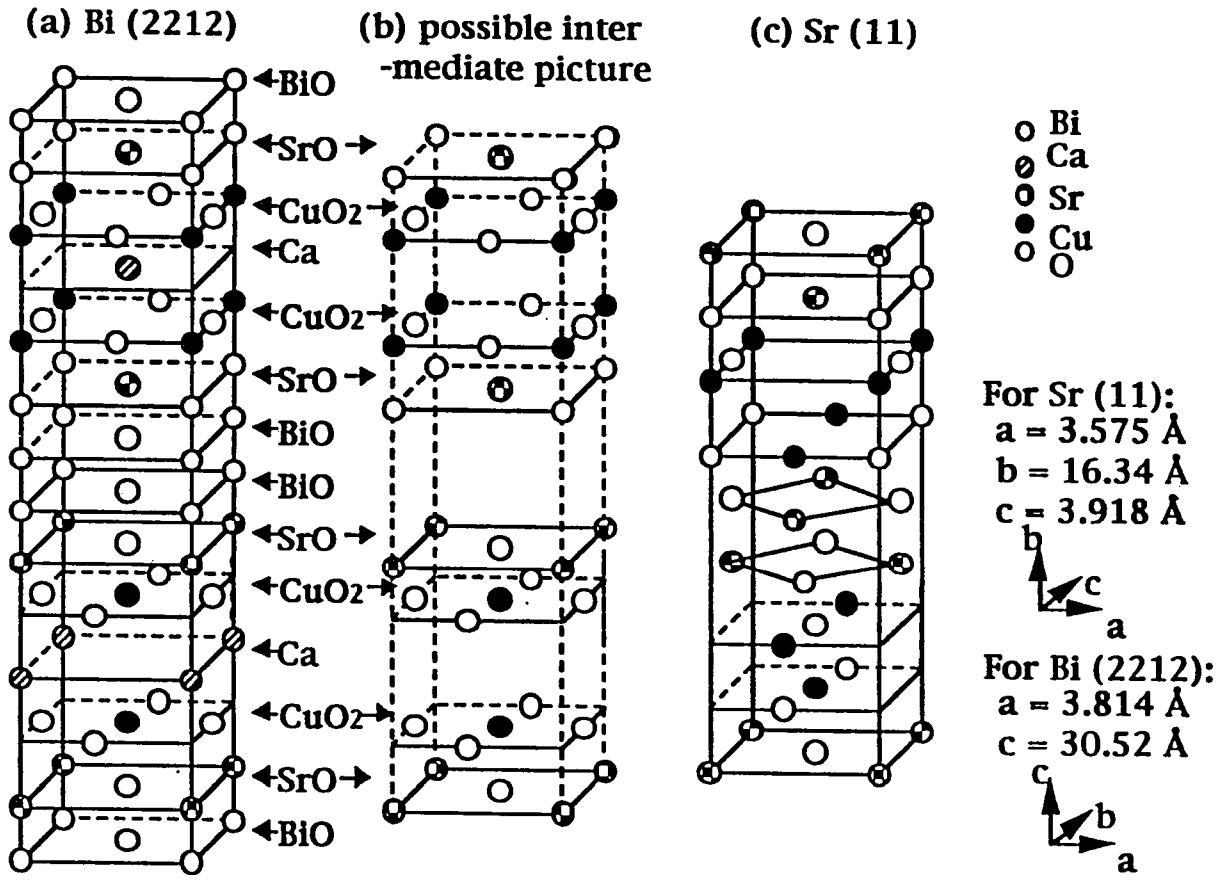

Fig.2.5 Structural comparison of the 2212 and 11 phases

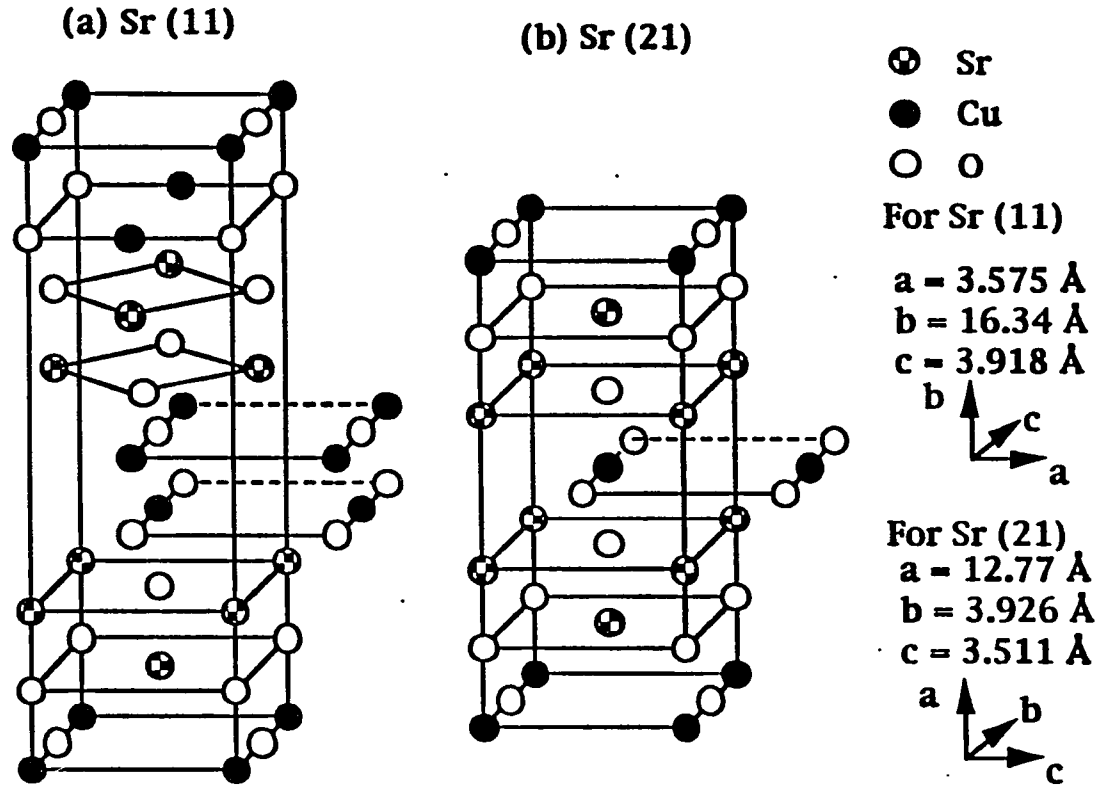

Fig. 2.6 Structural comparison of the 11 and 21 phases

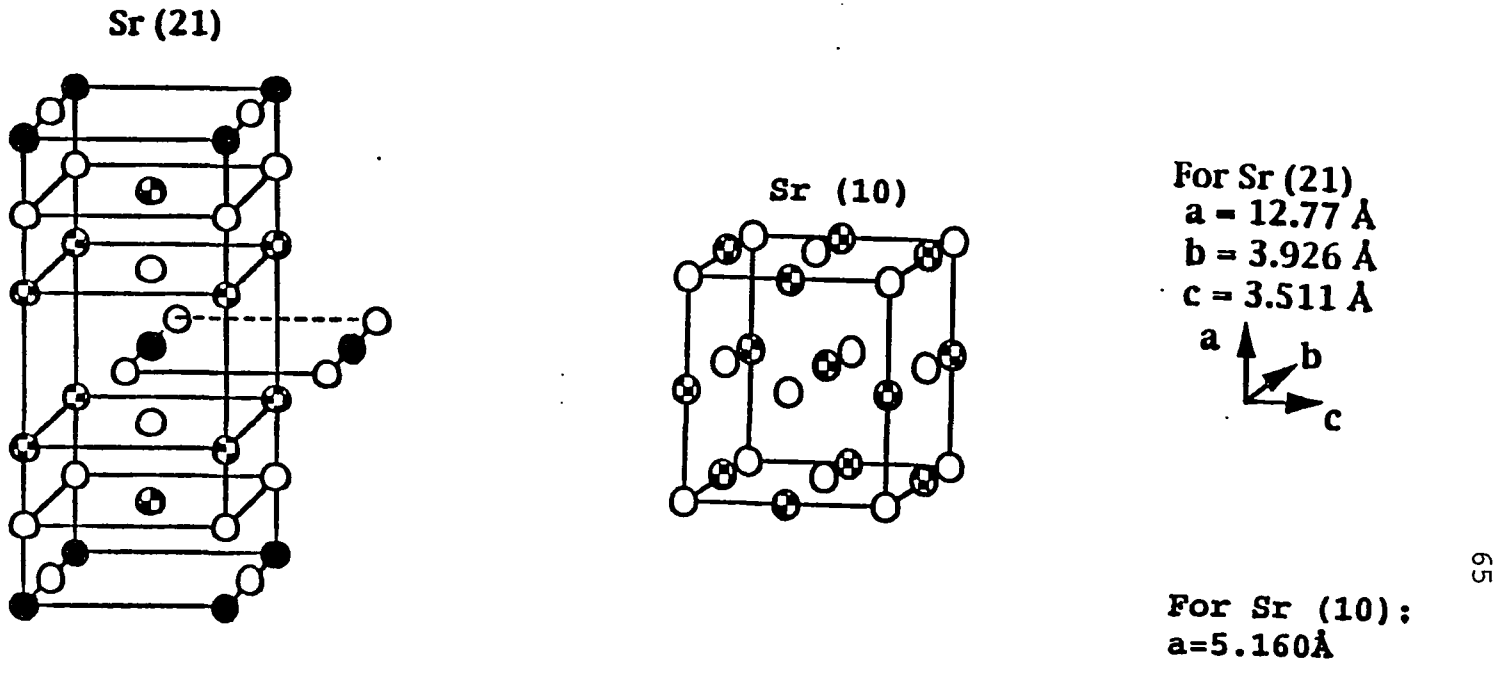

Fig. 2.7 Structural comparison of the 21 and 10 phases

parameter for 2212 is about 30.5Å. The longest lattice parameters for the 11 and 21 phases are 16.3Å and 12.8Å, respectively. There are fourteen layers including BiO, SrO, Ca and CuO_2 layers in the unit cell of 2212 phase. The inter-layer distance is about 2.3Å for 2212. Since there are nine layers and seven layers in one unit cell for the 11 and 21 phases, respectively, the inter-layer distances for both phases (~ 2.2-2.4 Å) are basically the same as for the 2212 phase. Therefore, the picture of rejecting whole layers during the phase transformation could be acceptable, at least in helping to understand the melting process of 2212.

Almost all the crystalline phases that form in the incongruent melting process grow with a preferred orientation having a specific crystallographic axis perpendicular to the sample holder. The exception is the 10 phase which has a random orientation. The preferred orientation can be noticed in the X-ray diffraction patterns by the lack of a significant number of peaks. The diffraction peaks that are observed belong to Bragg planes that are parallel to the sample holder.

Using an SEM, the preferred orientation of the microstructure can be observed (see Fig. 2.8). To obtain the 11, 21 and 10 phases in the melt, three samples of 2212 where heated to 870^{o}C, 880^{o}C and 890^{o}C receptively in air using the HTPD and rapidly cooled (at a rate of 900^{o}C to 100^{o}C in 30

(a)

(b)

Fig. 2.8 SEM photo of (a) 11 phase, (b) 21 phase and (c) 10 phase

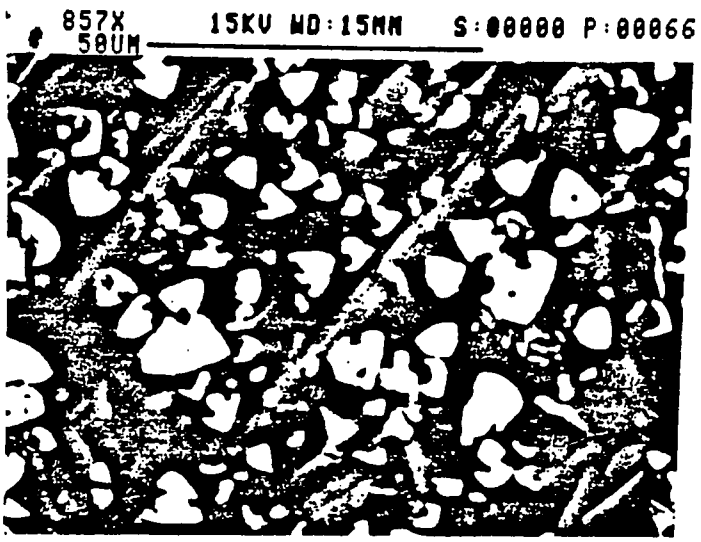

(c)

Fig. 2.8 Cont.

seconds) to room temperature. At 870°C, the SEM shows the 11 phase with its plank like morphology (see Fig. 2.8). These plank like crystals were oriented with their c or a axis perpendicular to the sample holder. From the 880°C sample, needle like crystals of 21 were seen. Almost all of these crystals had their c-axis perpendicular to the sample holder. The 10 phase was observed in the 890°C sample, having a equiaxed crystal habit.

When the oxygen partial pressure is lowered, the incongruent melting of 2212 is significantly affected. As the partial O_2 pressure is lowered so is the melting point of 2212. At 0.2 and 0.1 atm of O_2, the melting point is not affected and the sample melts at 870°C. In the case of 0.02 atm of O_2 and pure N_2 atmosphere, the melting points were lowered to 860°C and 830°C, respectively.

Another effect of lowering the partial oxygen pressure was the formation of a new phase, 24X, when 2212 melts. This phase formed in 0.02 atm of O_2 and pure N_2 at the melting point. The 24X phase existed in the melt up to the temperature of 870°C to 880°C (in 0.02 atm of O_2 and pure N_2, respectively), when it dissolved back into the melt. The reason why this phase was not observed in the 0.2 and 0.1 atm O_2 partial pressure case was that the melting point of 2212 is much higher than the temperature at which 24X would dissolve back into the melt. In such a case, 24X cannot form

in the incongruent melt. When the partial O_2 pressure is lowered and the melting point of 2212 falls below the temperature were 24X is stable in the melt, 24X forms in the incongruent melting process. The existence of this phase in the melt was confirmed by Hellstrom[1].

The effects of oxygen partial pressure on the melting point of 2212 and the formation of the copper free phase were confirmed by a study done by Vander Sande[1]. Vander Sande used a solid state ionic cell with a yttria stabilized zirconia solid electrolyte tube to monitor and control the partial O_2 pressure while heating 2212 in a quartz chamber. Using this apparatus, the melting points of 2212 were determined at partial O_2 pressures down to 10^{-6} atm.

The melting points, as determined by HTPD, in 0.2, 0.1, 0.02 atm of O_2 agree with those observed by Vander Sande. The observed melting point in pure N_2 (at 830°C) would indicate that the partial O_2 pressure, near the vicinity of the sample, was on the order of 10^{-3} atm when the sample melted.

Vander Sande also observed that below $6X10^{-4}$ atm of O_2 2212 underwent a solid state decomposition forming Cu_2O and 23X phases with no liquid present. This agrees with the HTPD observations, except that Cu_2O was not observed (assumed to have dissolved into the melt) and the copper free phase had the composition of 24X. Vander Sande does not report on the formation of the Sr-Ca-Cu-O phases.

Lowering the partial oxygen pressure also affects the formation sequence of the Sr-Ca-Cu-O phases. The phase formation becomes less sequential. Most of the Sr-Ca-Cu-O phases begin to form at about the same temperature and coexist over a large temperature range. This modification to the phase sequence can be noticed by the formation of the 10 phase at lower temperatures. Also the 11 phase exists at higher temperatures in lower partial O_2 pressures. In the pure nitrogen atmosphere case, the 11 phase exists at higher temperatures than the 21 phase, which is the complete opposite from the 0.2 atm O_2 partial pressure case. Also, the 21 phase exists in a much narrower temperature range and has a much lower phase fraction. The reason why the phase sequence changed is that following the formation of the 24X phase the melt becomes more copper rich. In a copper rich melt the formation of the 11 phase is favored over the 21 phase.

It is interesting to point out that in the pure N_2 atmosphere, the diffraction pattern shows only the (002) peak of the 11 phase. In all of the other atmospheres, the 11 phase also has a (080) peak. The loss of the (080) preferred orientation for some of the crystals is due to the change in crystal habit. The way a crystal grows (habit) depends on the environmental conditions. By lowering the partial oxygen pressure, the relative growth rates in a specific

crystallographic directions are changed. They may be changed to such an extent that a phase may switch from one preferred orientation to another.

The best way to rationalize the phase formation sequence in the incongruent melting of 2212 is to compare the experimental HTPD results to a phase diagram of the system. One such phase diagram was constructed by Hettich[1] (see Fig. 2.9). Hettich generated a pseudo-ternary phase diagram for 850°C in air. The reason why the phase diagram is "pseudo" ternary is because one of the components represented in the diagram is actually a fixed ratio of two oxide components. This is one way to simplify a presentation of a quarternary oxide system. Even though the phase diagram is 20°C below the melting point of 2212 (there are no isothermal cuts phase diagrams for this system at or above 870°C), a correlation between the observed phase sequence and an equilibrium phase diagram can still be made.

The incongruent melting of 2212 involves a process of bismuth depletion of the starting material and of a copper depletion process in the Sr-Ca-Cu-O phases. This process can be represented by a straight line path from the 2212 composition point to the (Sr,Ca)O vertex. Notice the sequence of phase regions entered along this path. The 11 phase region is entered before the 21 region and ending in the 10 region.

Fig. 2.9 Phase diagram of the Bi_2O_3 - CuO - (Ca,Sr)O system in air at 850°C by Hettich

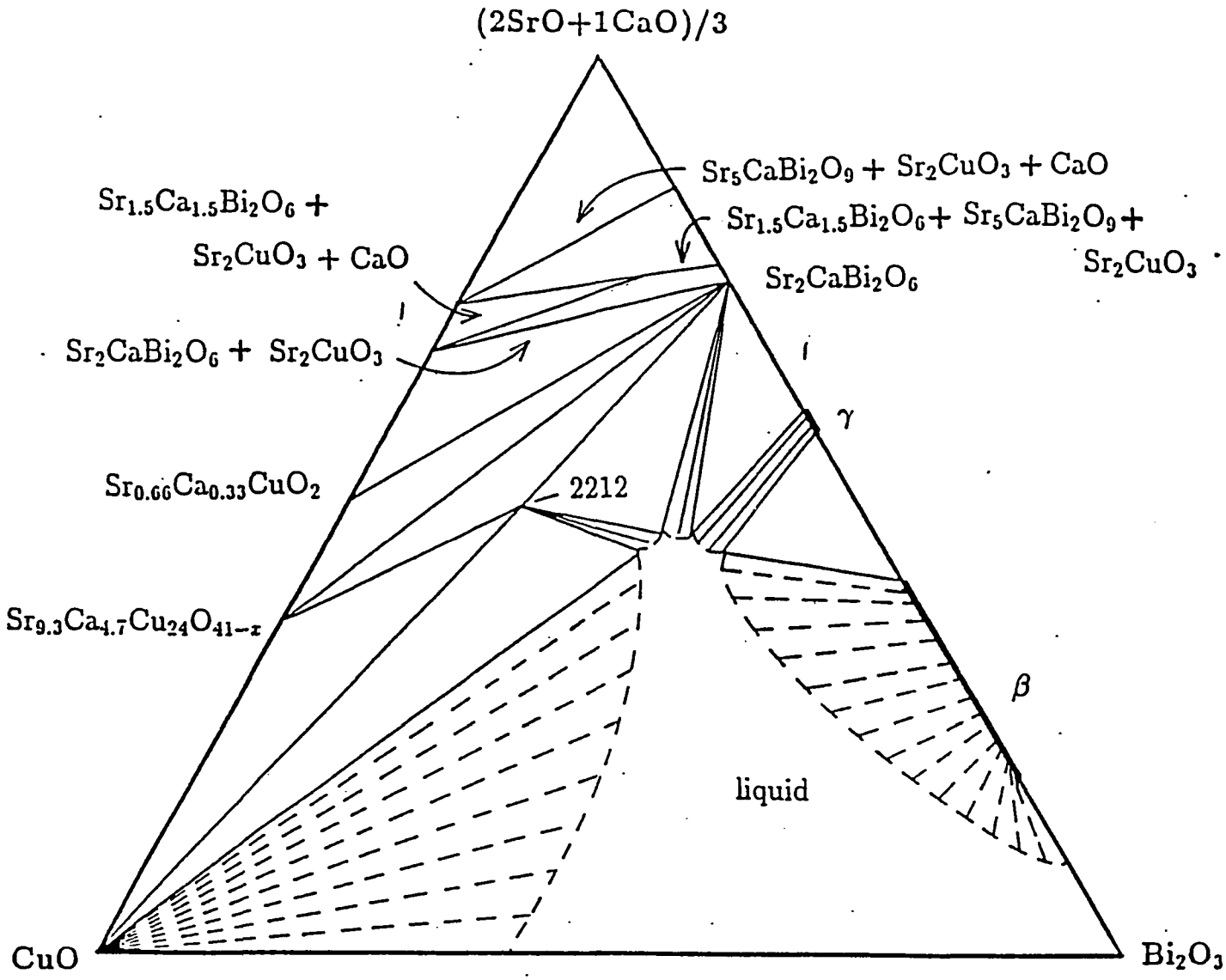
(2SrO+1CaO)/3
$Sr_5CaBi_2O_9 + Sr_2CuO_3 + CaO$
$Sr_{1.5}Ca_{1.5}Bi_2O_6 +$
$Sr_2CuO_3 + CaO$
$Sr_{1.5}Ca_{1.5}Bi_2O_6 + Sr_5CaBi_2O_9 +$
Sr_2CuO_3
$Sr_2CaBi_2O_6$
$Sr_2CaBi_2O_6 + Sr_2CuO_3$
γ
$Sr_{0.66}Ca_{0.33}CuO_2$
2212
$Sr_{9.3}Ca_{4.7}Cu_{24}O_{41-x}$
β
liquid
CuO
Bi_2O_3

This corresponds directly with the experimental observation.

A collection of copper free phases is also noticed along the phase diagram path. The reason why no copper free phases are observed in the 0.2 (and 0.1) atm O_2 partial pressure studies is that they do not exist in the melt above 870°C at these partial oxygen pressures. Only when the O_2 partial pressure and the melting point are lowered can the copper free phase (24X) form out of the melt.

The 14,24 phase was not observed in any of the atmospheres studied using the HTPD. Other groups, eg. Hellstrom[3], have observed the 14,24 phase when melting 2212. The contradiction in observations can possibly be explained by the fact that 2212 has a large homogeneity region. Hettich[4] reports that 2212 has a significant amount of flexibility in the Ca/Sr ratio and in the Bi content. With a 2212 sample that is copper rich with respect to Ca and/or Sr, the 14,24 phase can form out of the melt. Hellstrom may have 2212 which is more copper rich than the samples used in this study.

By taking the two observations into account, the 850°C phase diagram can be modified to represent the system at 870°C in air. A sketch of such a phase diagram presented in Fig. 2.10. The liquidus line is extended to cover the regions were the copper free phases existed. 2212 is given a homogeneity region on the phase diagram to represent the

possible compositions before the material melts. The 14,24 phase region is restricted to the copper rich region of 2212.

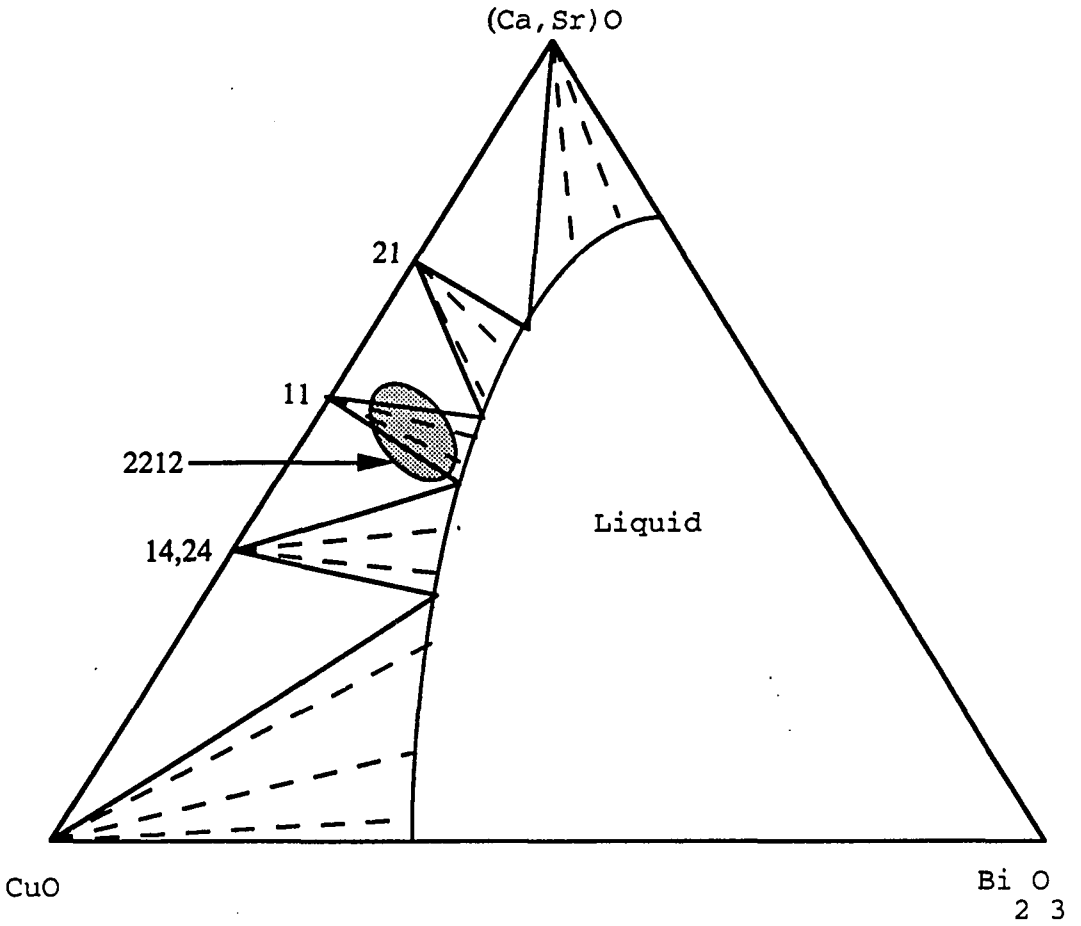

Fig. 2.10 A sketch of a Bi_2O_3 - (Ca,Sr)O - CuO phase diagram at 870°C, in air

SECTION 3: THE SOLIDIFICATION OF $Bi_2Sr_2CaCu_2O_8$

EXPERIMENT

This section continues with the results and discussion of the high temperature phase chemistry of the 2212 system. The solidification studies of the 2212 melt begin where the incongruent melting studies left off, using the same sample and chamber environment. The 2212 melt was solidified in 0.2, 0.1, 0.02 atm of partial O_2 pressure and pure N_2. The procedure for preparing the chamber atmosphere and melting the 2212 samples were discussed in the previous section (section 2).

The temperature range of the solidification studies was from 900°C to 760°C for all partial O_2 pressure except for the pure N_2 study. In the case of the pure N_2 study, the starting temperature of the solidification was 890°C. At the start of the solidification studies in 0.2, 0.1, 0.02 atm of partial O_2 pressure, the sample was cooled rapidly (2°C/sec) from 900°C to 890°C. This was done to limit the amount of platinum contamination due to the sample reacting with the sample holder at higher temperatures (above 890°C). From 890°C to 10°C below the melting point (see section 2), the sample cooled slowly at a rate of 900°C/hr. Once the temperature of 10° below the melting point was reached, the sample was cooled by 20°C steps and held at each temperature for six minutes to take two diffraction patterns. The samples

were cooled in this manner down to 760°C. From this temperature, the sample was cooled to room temperature.

RESULT

The series of diffraction pattern for each experiment at 0.2, 0.1, 0.02 atm partial O_2 pressure and pure N_2 are presented in Figures 3.1, 3.2, 3.3, and 3.4 respectivly. A brief description of the results is given below. The interpretation of the results is given in the discussion section. The results and discussion of the 900°C scans at the start of the solidification studies for the four partial oxygen pressure are presented in the previous section.

0.2 Atm Po_2 Study

The solidification study of the melt in 0.2 atm of partial O_2 pressure started at 860°C (see Fig. 2.1). The 21 phase was present in the first diffraction pattern taken. Because of the high intensity of the (002) peak at 54.6°, the 21 phase must have started to grow above 860°C. Other peaks of the 21 phase were present in the diffraction pattern at 35.5° and 34.0° corresponding to (011) and (301), respectivly. The 11 phase was also present at 860°C, but in smaller quantity. The peaks associated with the 11 phase were (131), (080), (002), (200), (171) with positions of 37.7°, 44.3°, 46.3°, 51.5° and 52.8° in 2θ, respectivly.

When the temperature was lowered to 840°C, the intensities of the 11 phase peaks decreased. As the

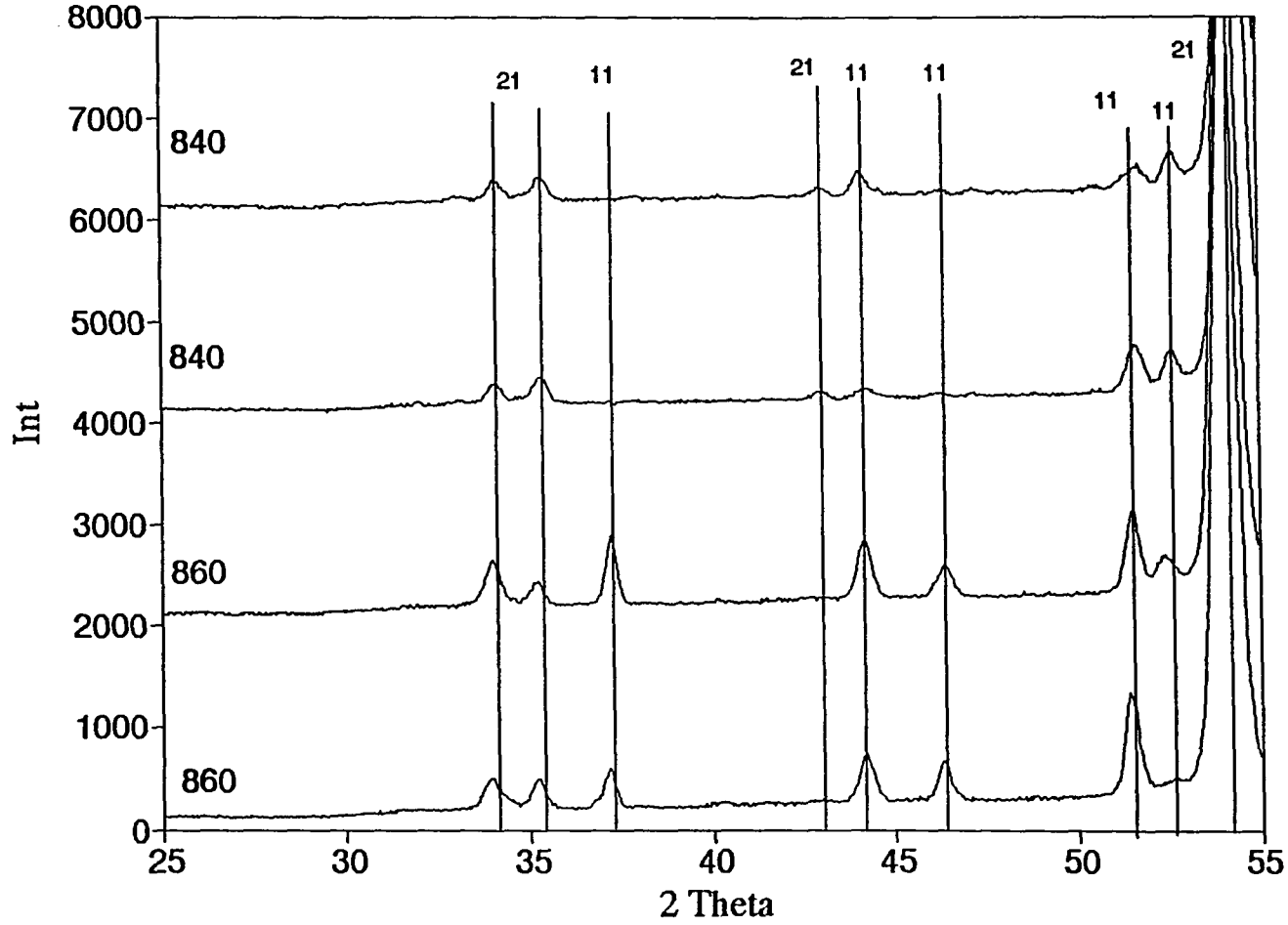

Fig. 3.1 Solidification of 2212 in 0.2 atm PO2

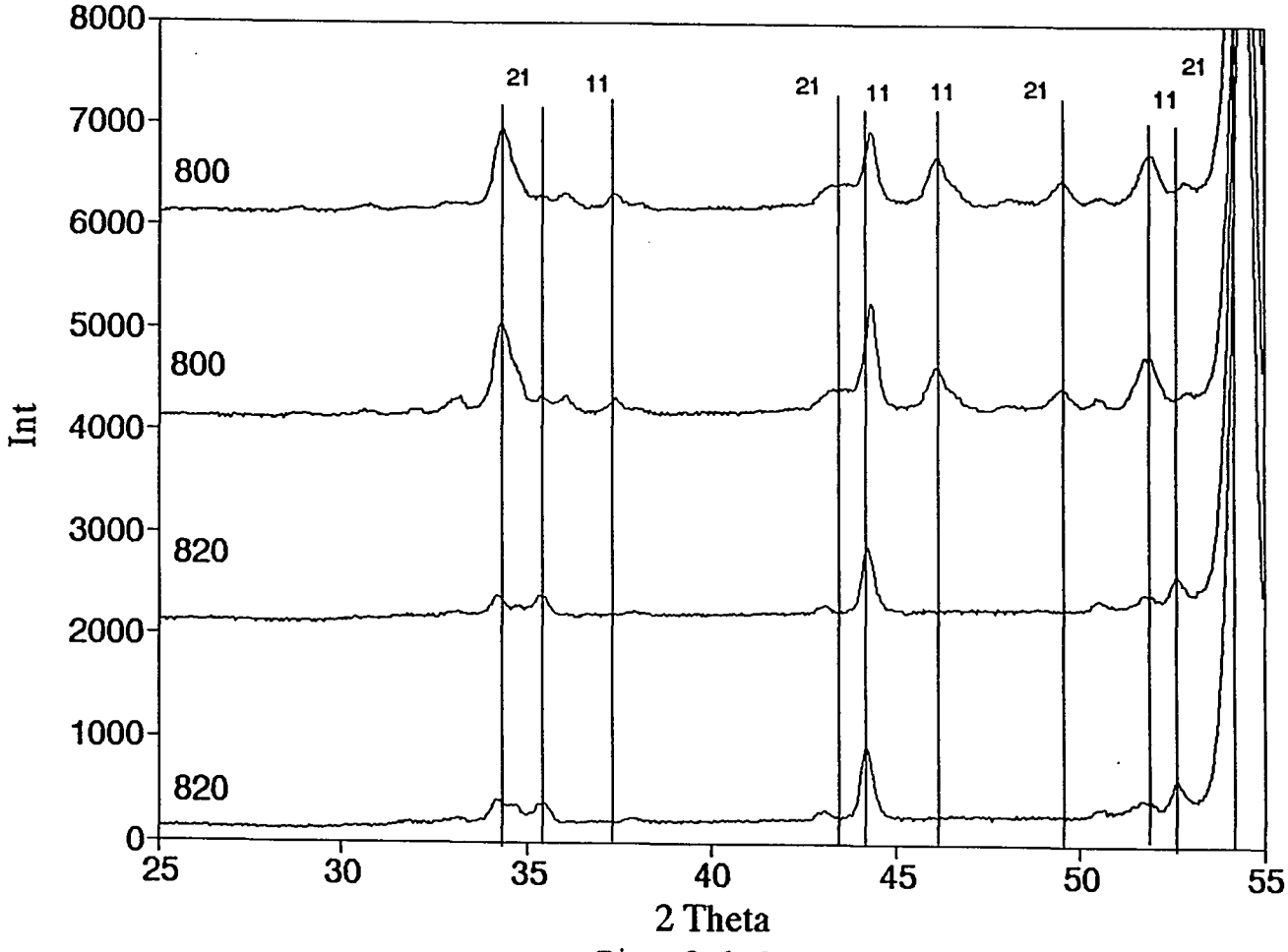
8000
7000
6000
5000
4000
3000
2000
1000
0
Int
800
800
820
820
21
11
21
11
11
21
11
21
25
30
35
40
45
50
55
2 Theta

Fig. 3.1 Cont.

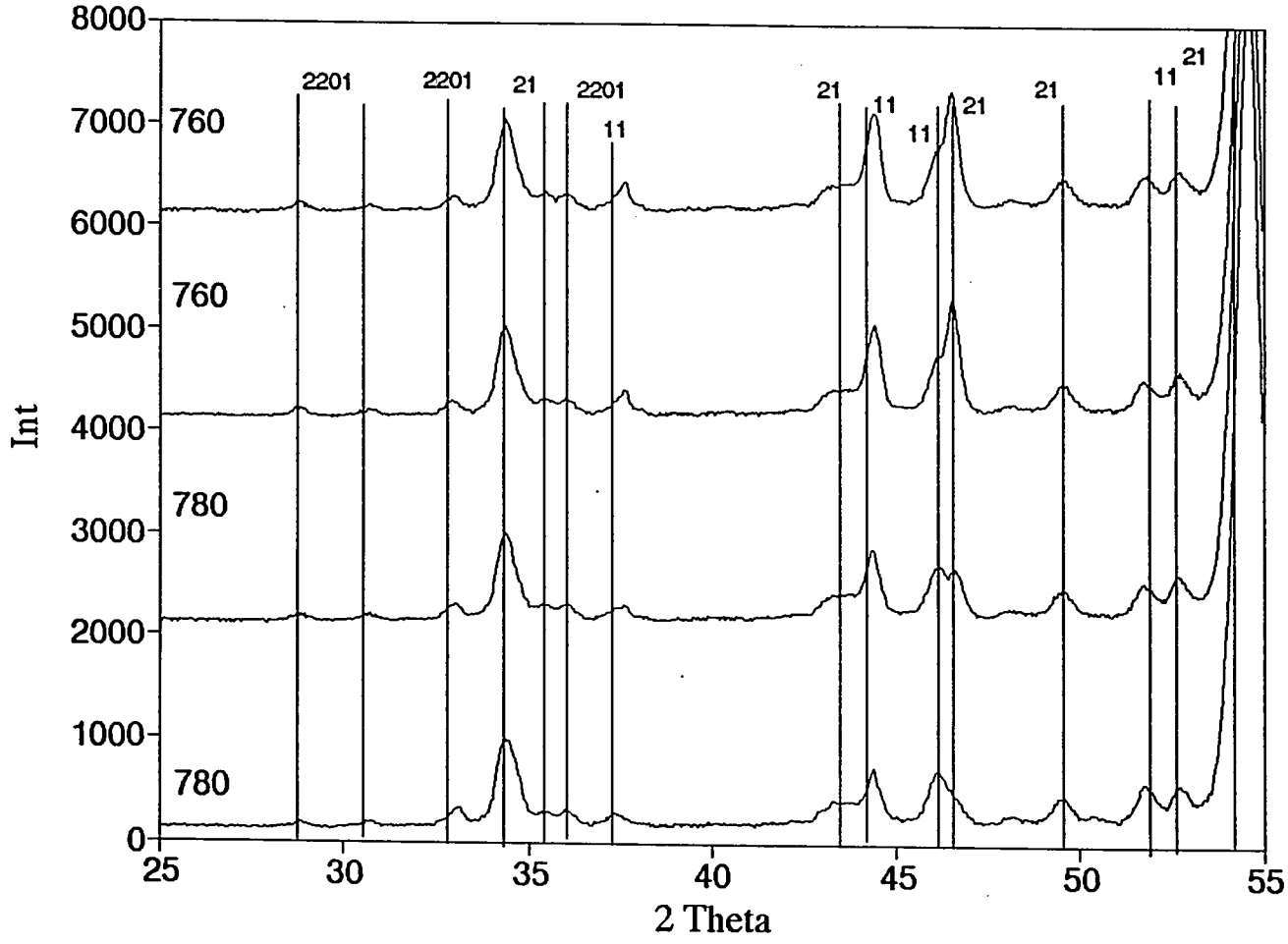
8000
7000
6000
5000
4000
3000
2000
1000
0
Int
760
760
780
780
2201
2201
21
2201
11
21
11
11
21
21
11
21
25
30
35
40
45
50
55
2 Theta

Fig. 3.1 Cont.

temperature was lowered further, the same peaks reappeared. At 820°C, the (080) peak reappeared. At 800°C, the (131) and (002) peak also reappeared. New peaks of 21 phase were observed at lower temperatures. The (600) peak at 43.5° was first observed at 840°C. The (501) and (200) peaks, located at 49.4° and 46.5°, occur at 800°C and 780°C, respectivly. At 800°C, the (301) peak of 21 increases in intensity.

The bismuth rich melt begins to solidify at 800°C. This can be determined by the decrease in the background intensity as the temperature is lowered. By 780°C, weak peaks can be noticed at 29.0°, 30.6°, 33.5° and 36.4°. These peaks correspond to (008), (017), (020) and (0010) planes of the 2201 phase. The 2201 peaks have a small increase in intensity when the temperature is lowered to 760°C.

After the study, the sample surface was noticed to be encrusted (visible to the naked eye) with 21 phase. This layer of 21 covered the 2201 phase that grew out of the melt at lower temperatures. It also inhibited the X-rays from scattering off the 2201 phase.

0.1 Atm Po_2 Study

In the 0.1 atm study, the first diffraction patterns were obtained at 860°C (see Fig. 3.2). At this temperature the only major phases present were 10 and the unknown phase

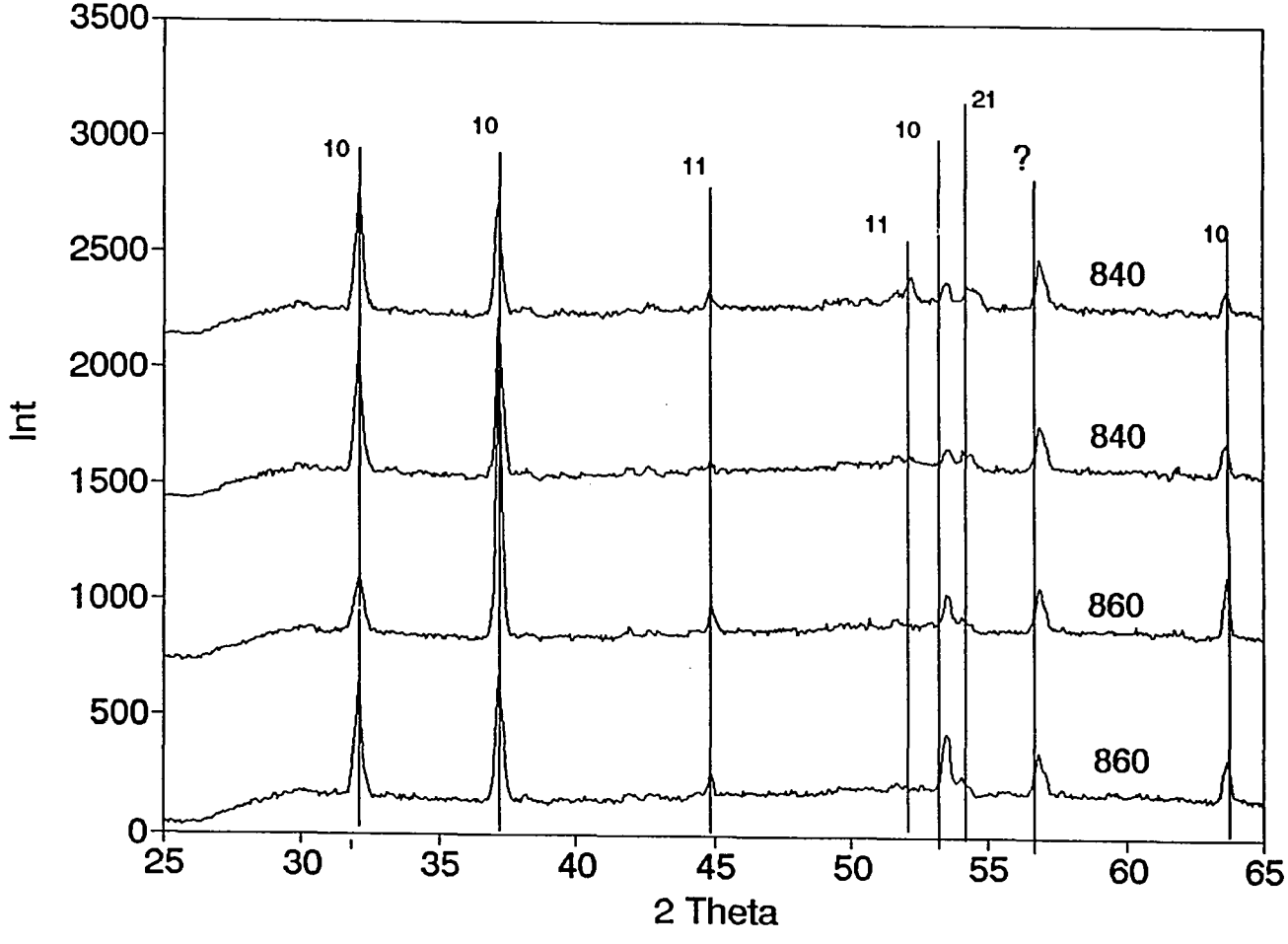

Fig. 3.2 Solidification of 2212 in 0.1 atm PO2

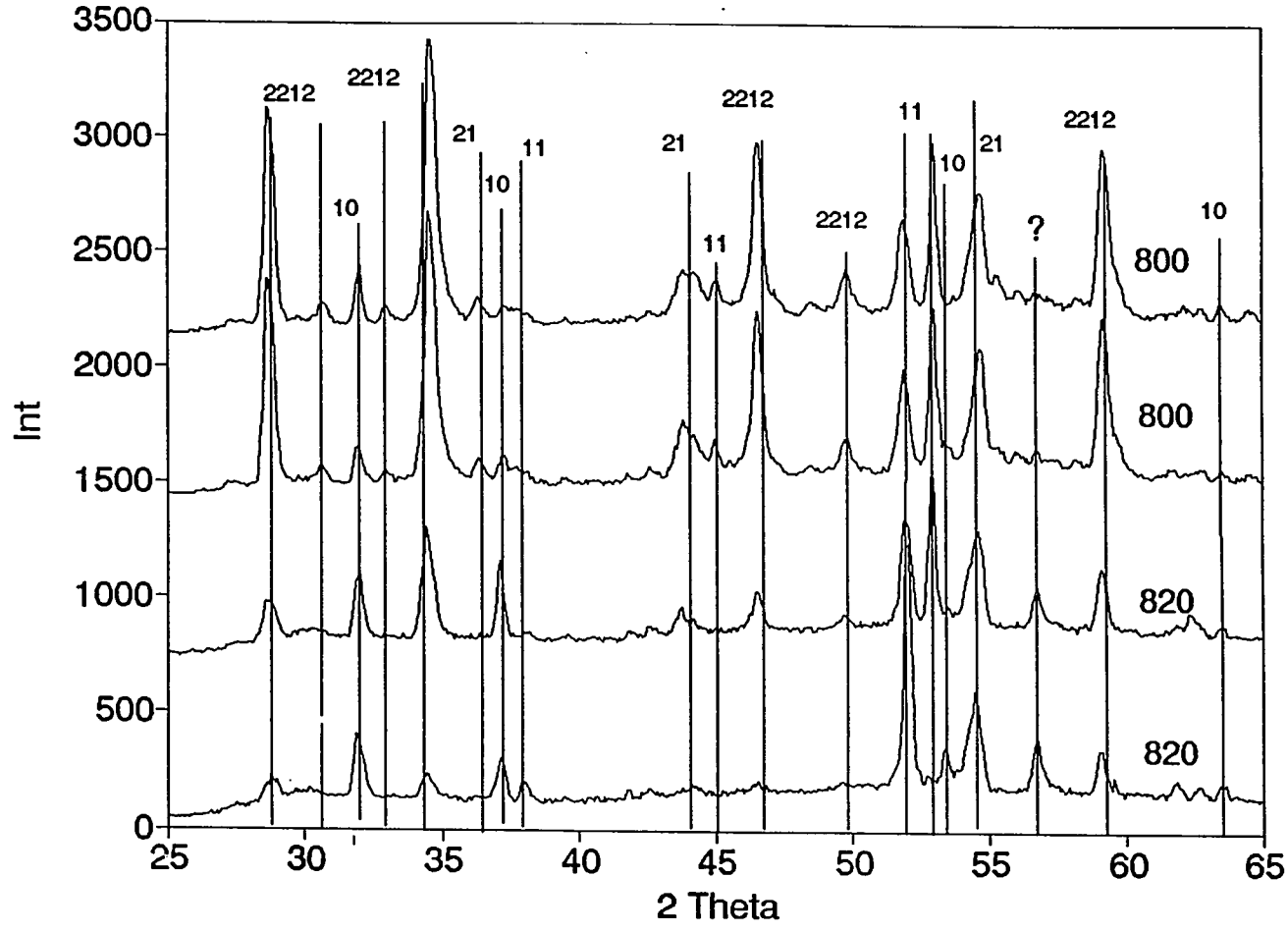
3500
3000
2500
2000
1500
1000
500
0
Int
25
30
35
40
45
50
55
60
65
2 Theta
2212
2212
10
21
10
11
21
11
2212
2212
11
10
21
?
2212
10
800
800
820
820

Fig. 3.2 Cont.

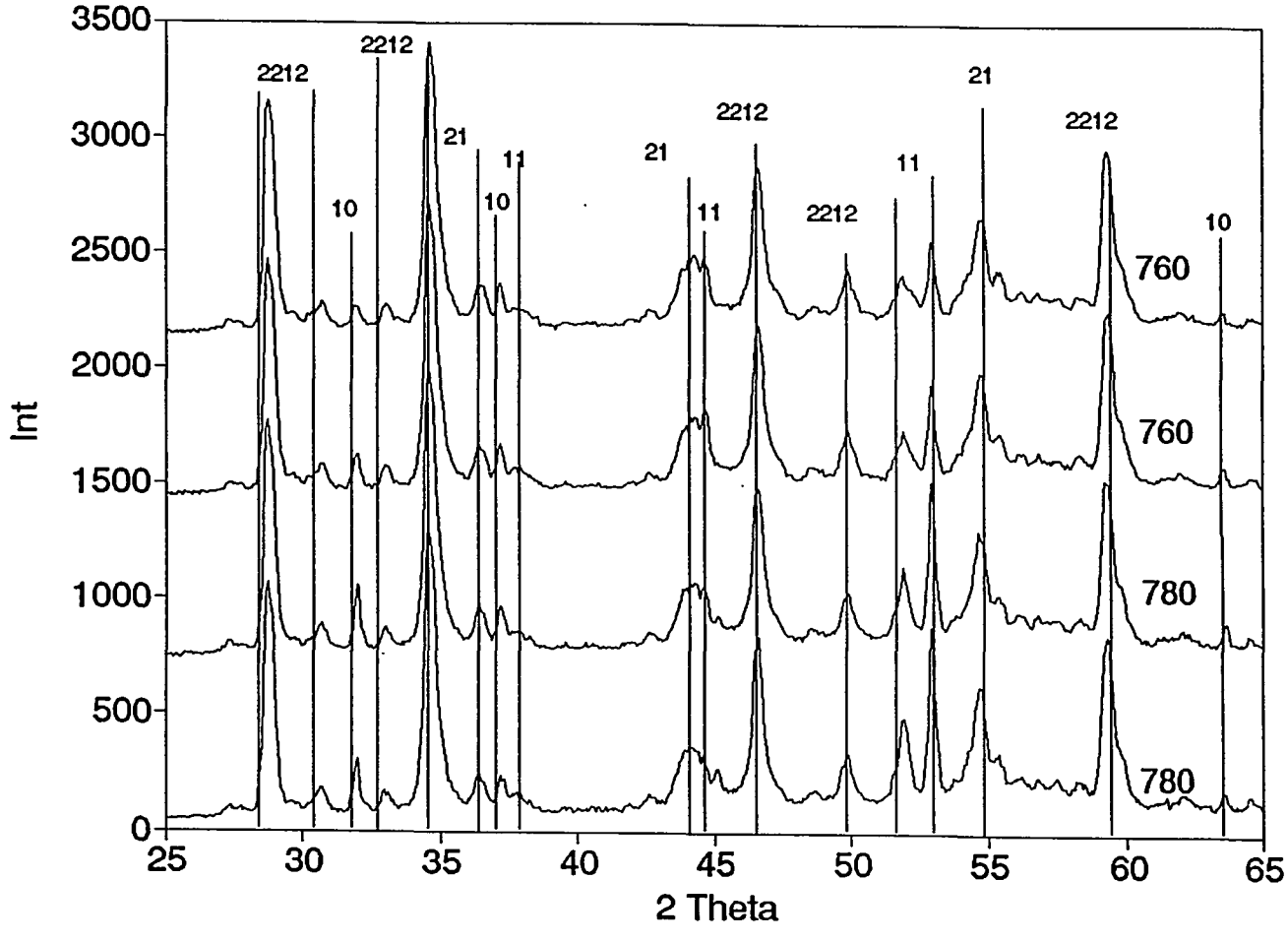
3500
3000
2500
2000
1500
1000
500
0
Int
25
30
35
40
45
50
55
60
65
2 Theta
2212
2212
21
10
10
11
21
11
2212
2212
11
21
2212
10
760
760
780
780

Fig. 3.2 Cont

with a peak at 56.6°. Very small peaks of 11 and 21 phase were also observed at this temperature. The 11 phase had peaks at 44.0° and 51.6° which correspond to the (080) and (200) planes, respectively. The peak that corresponds to 21 phase was the (002) located at 54.4°. When the temperature was lowered to 840°C, the only change in the diffraction pattern observed was a small increase in intensity of the (200) and (002) peaks corresponding to the 11 and 21 phases. At 820°C, the the diffraction patterns showed the growth of the 2212 phase with peaks at 29.0°, 34.2°, 46.2°, and 59.2° which corresponds to the (00,10), (00,12), (00,16), and (00,20) planes. Two more peaks corresponding to the 11 and 21 phases were also observed at this temperature. The (171) peak of 11 and (600) peak of 21 were located at 52.3° and 43.5°, respectively

It is important to notice that while the 2212, 21 and 11 phases have been growing, the intensities of the 10 phase peaks have been decreasing. The 10 phase dissolved back into the melt while the other phases were growing. The intensity of the 56.6° peak did not change

When the temperature is lowered to 800°C, the 2212 phase grows as can be seen by the increase in the intensities of the (00ℓ) peaks.As the temperature is lowered further to 780°C and 760°C, the intensities of the (00ℓ) peaks of 2212 do not

change. At the same time, the intensities of the 11 and 10 peaks decrease. The 21 peaks do decrease, but not to the same extent as 11. The 56.6° peak of the unknown phase is not observed below 800°C. Below 800°C, the phase dissolves back into the melt.

0.02 Atm Po_2 Study

In the 0.02 atm case, there was a major change in the second phase formation when solidifying the melt. The first diffraction scans at 840° (see Fig. 3.3) showed the 10 and the 56.6° peak phases present in the melt. The second scan at this temperature showed the 11 phase, with the (200) peak at 51.6° starting to grow. By 820°C, the intensity of the 11 phase increased sharply. At the same time, the 10 phase peaks started to decrease in intensity. At 800°C, 2212 starts to grow along with the 11 phase as could be seen by the rising intensity of the (00ℓ) peaks. Smaller peaks were observed at 37.7° and 44.0° corresponding to the (131) and (080) planes of 11 phase. The 21 phase also grew out of the melt at 800°C(with a peak at 54.6°, corresponding to (002)) but only in small quantities.

When the temperature was lowered further to 780°C and 760°C, the 2212 phase continued to grow. During the solidification of the melt, when 2212 was growing, the

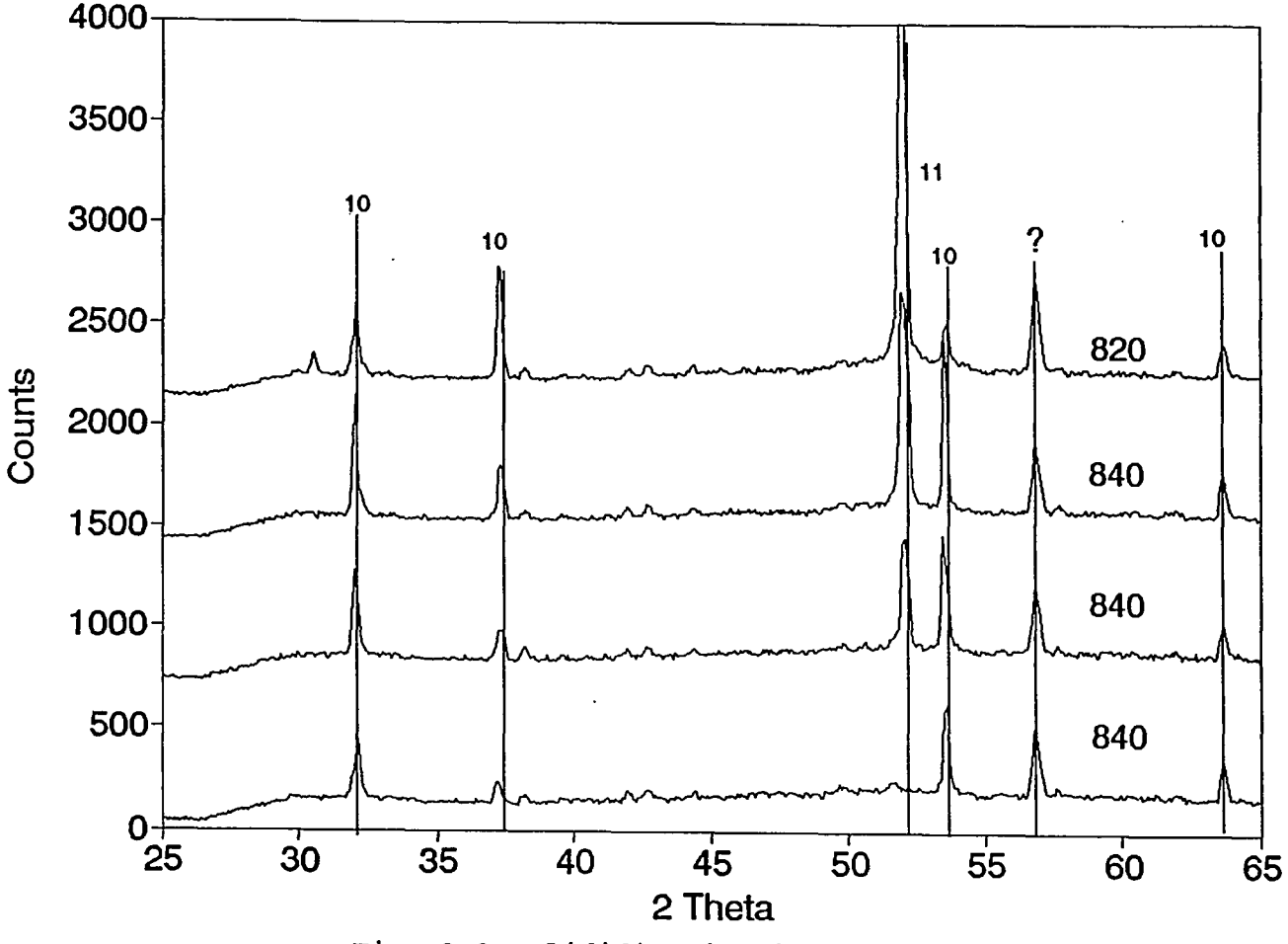

Fig. 3.3 Solidification in 0.02 atm PO2

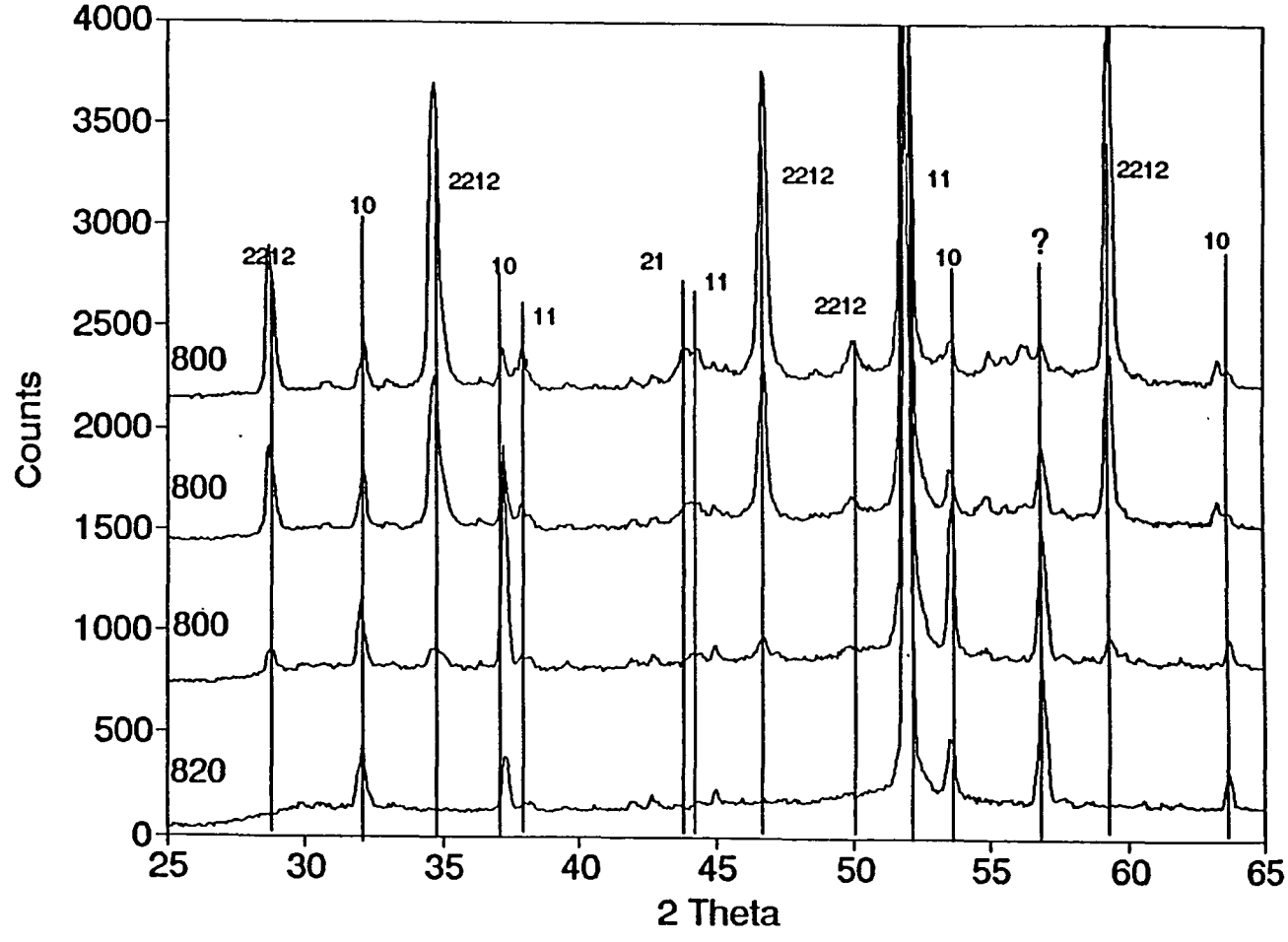
4000
3500
3000
2500
2000
1500
1000
500
0
Counts
25
30
35
40
45
50
55
60
65
2 Theta
800
800
800
820
2212
10
2212
10
11
21
11
2212
2212
11
10
?
2212
10

Fig. 3.3 Cont.

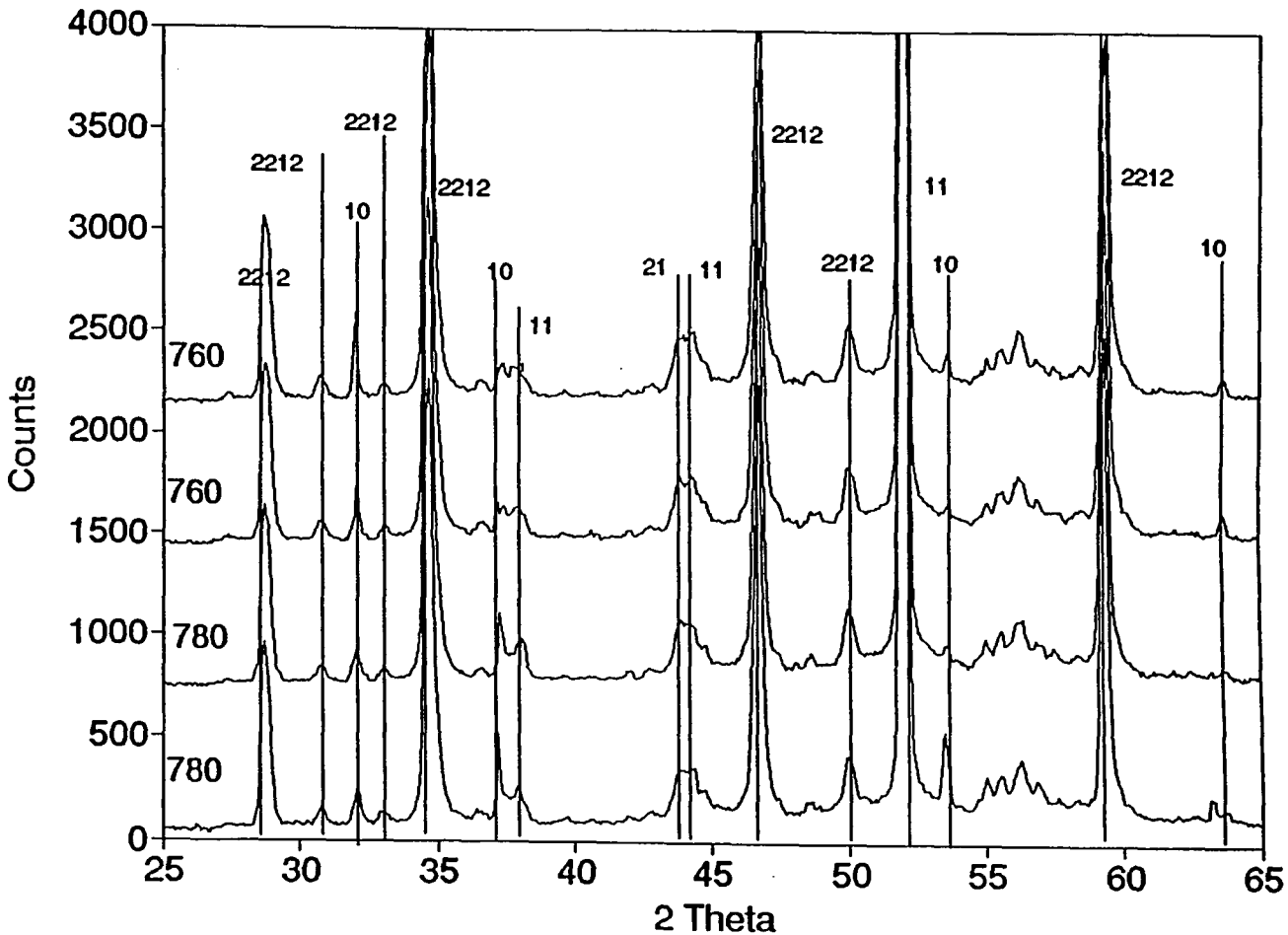
4000
3500
3000
2500
2000
1500
1000
500
0
Counts
25
30
35
40
45
50
55
60
65
2 Theta
760
760
780
780
2212
2212
2212
2212
2212
2212
10
10
10
10
11
11
11
21

Fig. 3.3 Cont.

intensities of the 10 phase peaks became weaker as it dissolved back into the liquid. The 21 phase never formed in large quantities as did the 11 phase when cooled below 800°C. As in the 0.1 atm case, the unknown phase with a peak at 56.6° dissolves back into the melt, below 800°C.

N_2 Atmosphere Study

When studing the solidification of the 2212 melt in a N_2 atmosphere, the first diffraction patterns were taken at 820°C(see Fig. 3.4). At this temperature the major phases present were 10, with peaks at 32.0°, 37.0°, 51.6° and 24X with peaks at 28.4°, 29.7° and 41.4°. Small amounts of 11 and 21 phase were also present with peaks at 52.4° and 53.4°,respectivly. A new phase that had not been observed before in previous studies, grows out of the melt. With peaks at 35.5°, 37.7° and 41.3° the phase has been identified as 23X. The peaks at 28.4° and 29.7° can also correspond to the 23X phase.

As the temperature was lowered to 800°C, the only change in the diffraction patterns was a small increase in the 35.5° and 41.3° peak intensities of the 23X phase while the 41.3° peak of 24X phase decreases in intensity. More peaks of the 23X and 24X phase appeared at 780°C and 760°C. The new peaks were located at 46.0° and 43.1°. These peaks correspond to

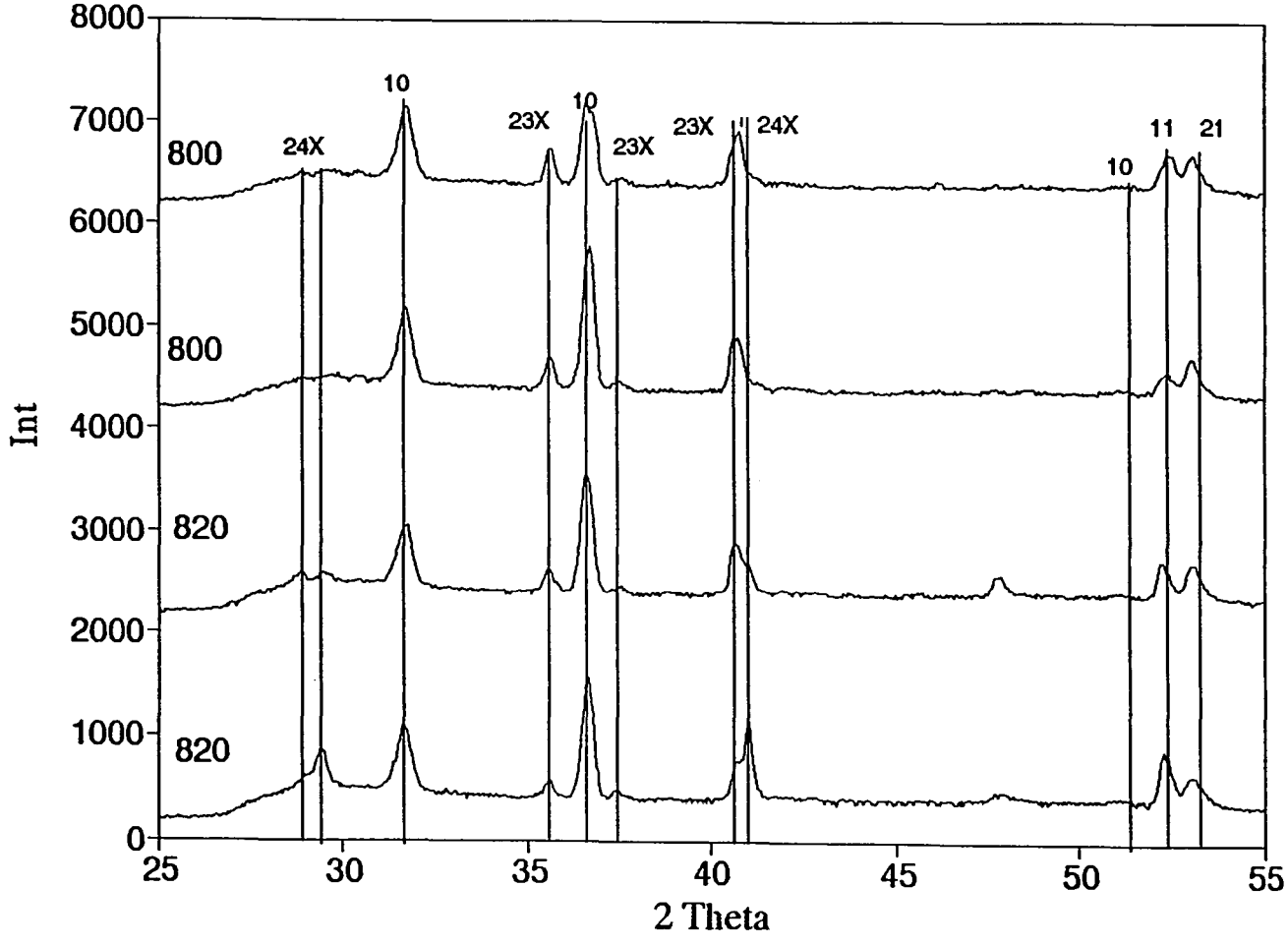

Fig. 3.4 Solidification of 2212 in N2 atmosphere

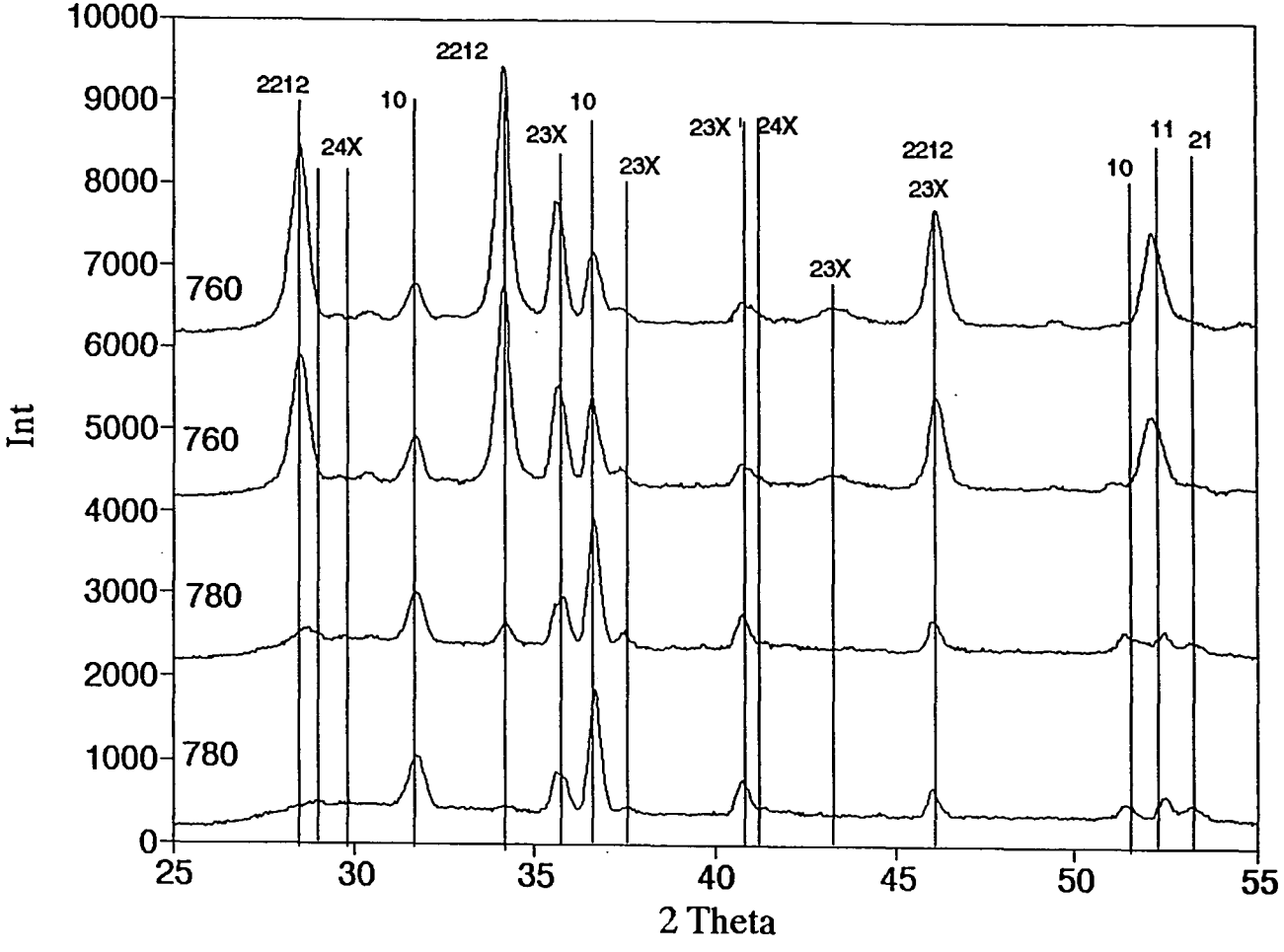
10000
9000
8000
7000
6000
5000
4000
3000
2000
1000
0
Int
760
760
780
780
2212
24X
10
2212
23X
10
23X
23X
24X
23X
2212
23X
10
11
21
25
30
35
40
45
50
55
2 Theta

Fig. 3.4 Cont.

23X and 24X phases, respectivly. Starting at 780°C, 2212 began to grow with the (00,10),(00,12) and (00,16) peaks increasing in intensity. At these temperatures, the 46.0° peak is actually composed of two peaks corresponding to 2212 and 23X phases. Both the 11 and 23X phases increased in phase fraction, while 10 decreased at 760°C.

DISCUSSION

One of the characteristics of the 2212 melt during solidification is the large undercooling. The melt needs to be cooled to 780°-760°C before it solidifies completely. Such a large undercooling of the melt is caused by the slow nucleation and growth kinetics of the various crystalline phases forming from the liquid. Because of the slow growth kinetics, the 2212 melt cannot be considered to be in chemical equilibrium during the solidification process with the cooling rate used in the study.

The solidification of the 2212 melt from 900°C follows a specific formation sequence of Sr-Ca-Cu-O phases. In general, the Sr-Ca-Cu-O phase formation sequence is 21-11-10 as the partial oxygen pressure is lowered. In all of the partial O_2 pressure studies, most of the phases are observed, but the relative phase fraction of each phase varies greatly.

In 0.2 atm of partial oxygen pressure, the 21 phase had grown out of the liquid in large quantities, making it the major second phase, before the first diffraction was taken at 860°C (see Fig. 3.1). A small amount of 11 phase was also present at this temperature. The amount of 21 phase in the melt stayed relatively constant as the temperature was lowered, while 11 phase decreased slightly. At no time

throughout the solidification was 10 phase present.

The 0.1 atm of partial oxygen pressure study showed relatively equal amounts of 11 and 21 phase growing out of the melt at 840°C (see Fig. 3.5). Both phases were present at lower temperatures, but started to dissolve back into the melt at 780°-760°C. Unlike the 0.2 atm case, the 10 phase was present throughout the solidification. The 10 phase began to dissolve into the melt at 840°C.

A significant change occurs at 0.02 atm O_2 partial pressure where the first major second phase was 11 (see Fig. 3.6). The 11 phase first formed at 820°C and grew as the temperature was decreased toward 780°C. Only a small amount of 21 formed at temperatures below 800°C. At 760°C, the 21 phase dissolved back into the melt. The 10 phase was also present during the solidification process, but began to dissolve back into the melt at 800°C.

The major second phase in the pure N_2 solidification was 10 (see Fig. 3.7). Throughout the cooling process, from 820°C to 760°C, the 10 phase was present in large quantities. The 10 phase began to dissolve back into the melt at 770°C. Only at 770°-760°C does 11 phase grow out of the melt.

These observations indicate that the high oxygen partial pressures favor the formation of the 21 phase as a major second phase during the solidification. By lowering the partial O_2 pressure, the formation of 11 and 10 phases

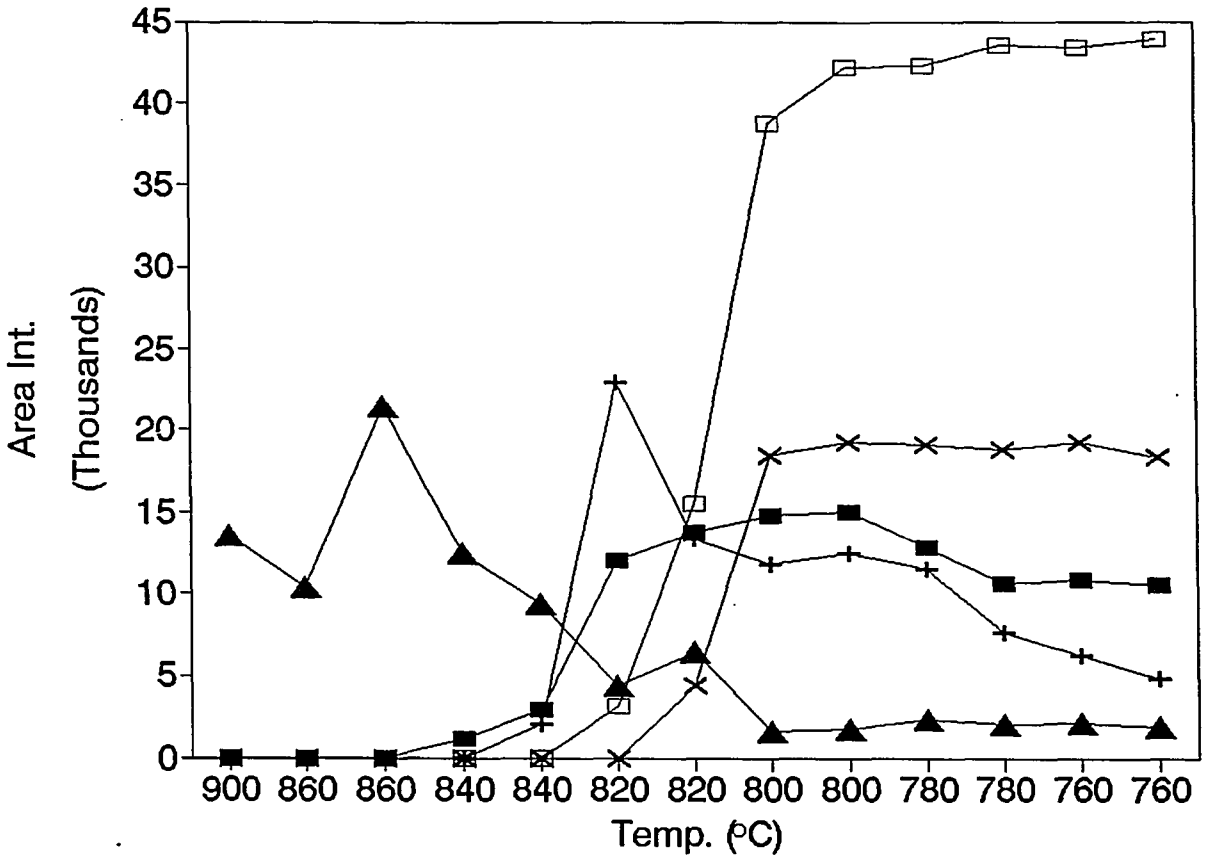

Fig. 3.5 Formation of second phases in 0.1 atm PO2

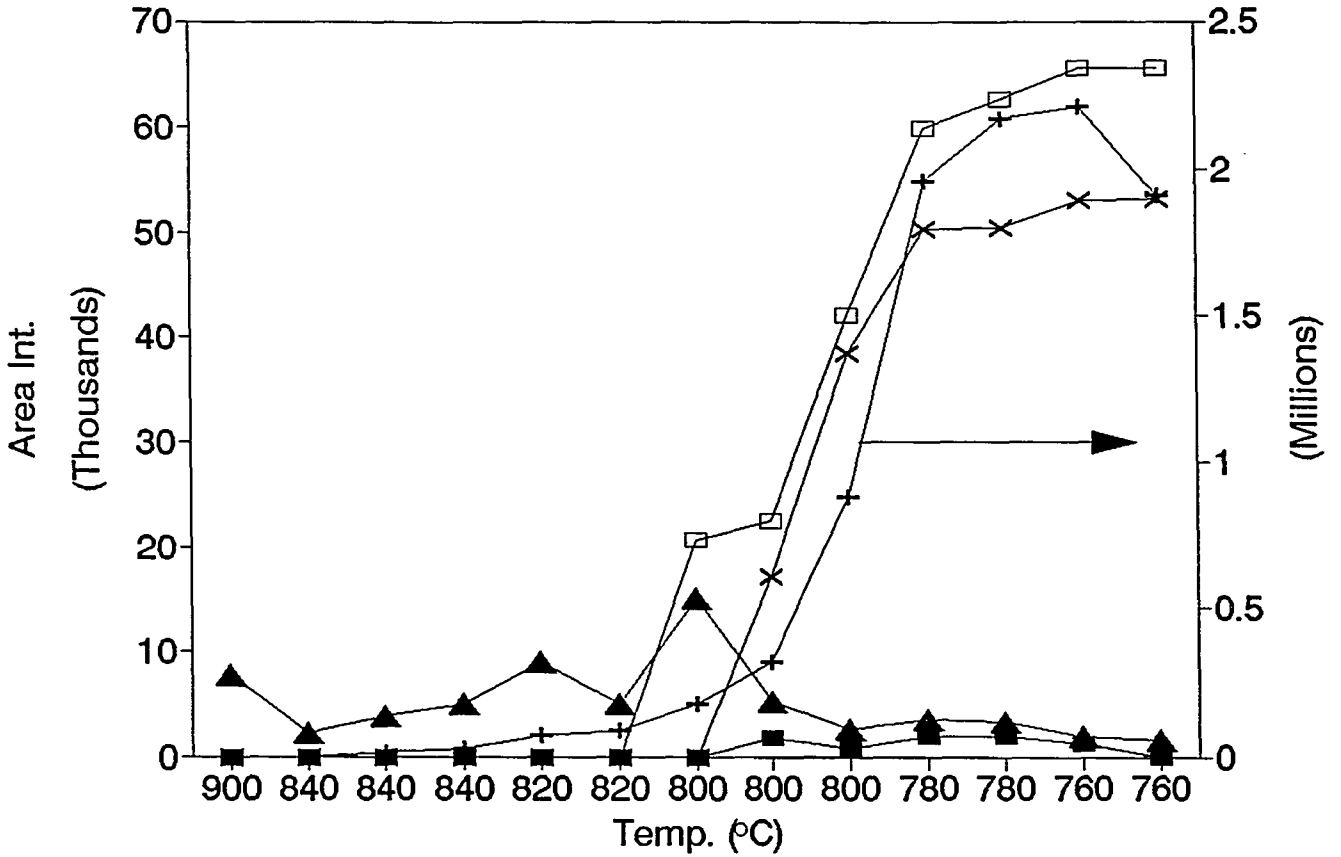

Fig. 3.6 Formation of second Phases in 0.02 atm PO2

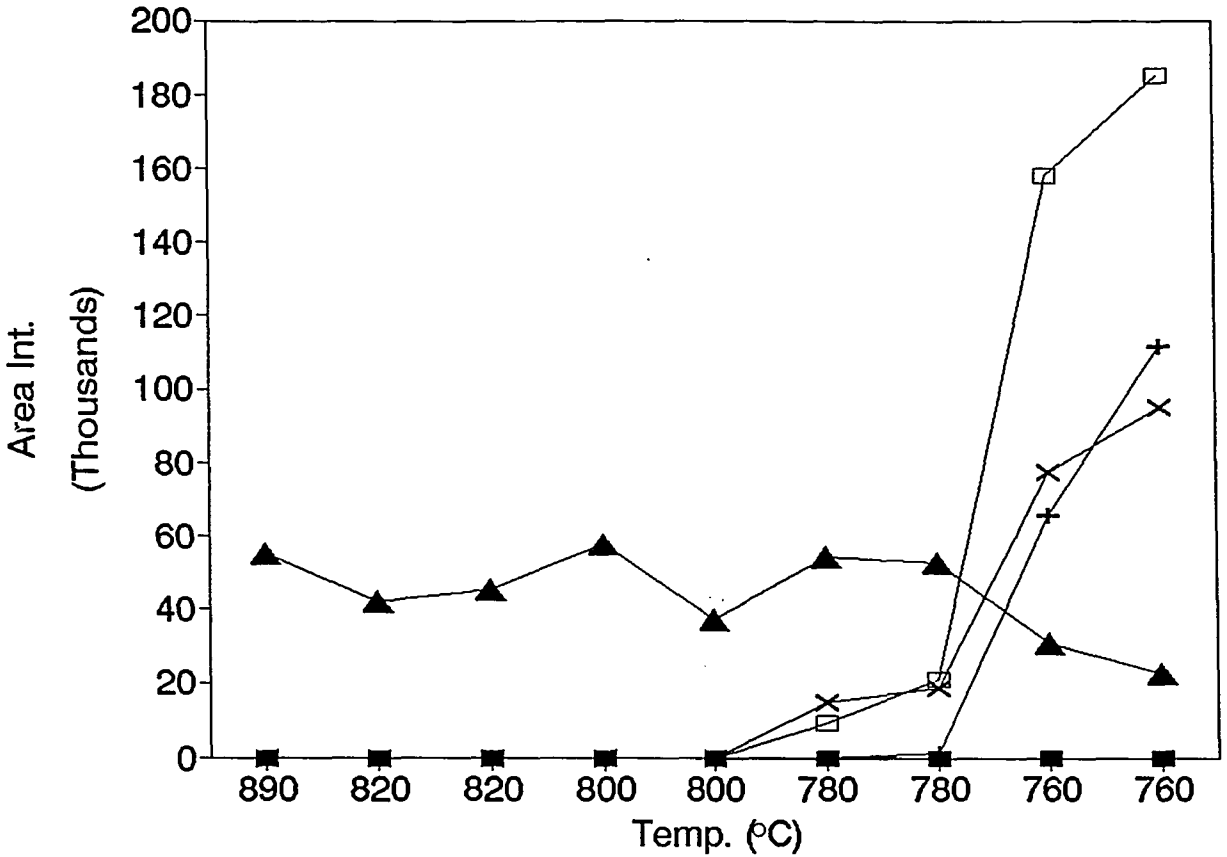

Fig. 3.7 Formation of second phases in N2 atmosphere

as the major second phase becomes preferable. Holesinger[1], using room temperature X-ray diffraction and SEM, also observes the formation of 21 phase during solidification at higher oxygen partial pressures. A correlation can be made between the major second phase formation during the solidification and the phase sequence in the melting of 2212 as a function of partial O_2 pressure. The last Sr-Ca-Cu-O phase to dissolve into the liquid during melting(see Table 2.2 in section 2), will be the major second phase on solidification. As the partial oxygen pressure is lowered, the last cuprate phase to dissolve during the incongruent melting and the major second phase to form on solidification changes from 21 to a mixture of 21 and 11 phases to 11 phase. The formation of 10 phase is also a function of partial O_2 pressure in both the melting and solidification process (see Fig. 3.8). As the partial oxygen pressure is lowered, the temperature at which 10 phase forms in the incongruent melting and its presence in the melt during solidification are also lowered.

The partial oxygen pressure also affects the temperature at which the second phases start to grow out of the melt (see Fig. 3.9). In a partial oxygen pressure of 0.2 atm, most of the 21 phase has grown out of the liquid above 860^{o}C, while in 0.1 atm of partial oxygen pressure it starts to form at 840^{o}C. When the partial oxygen pressure is lowered to

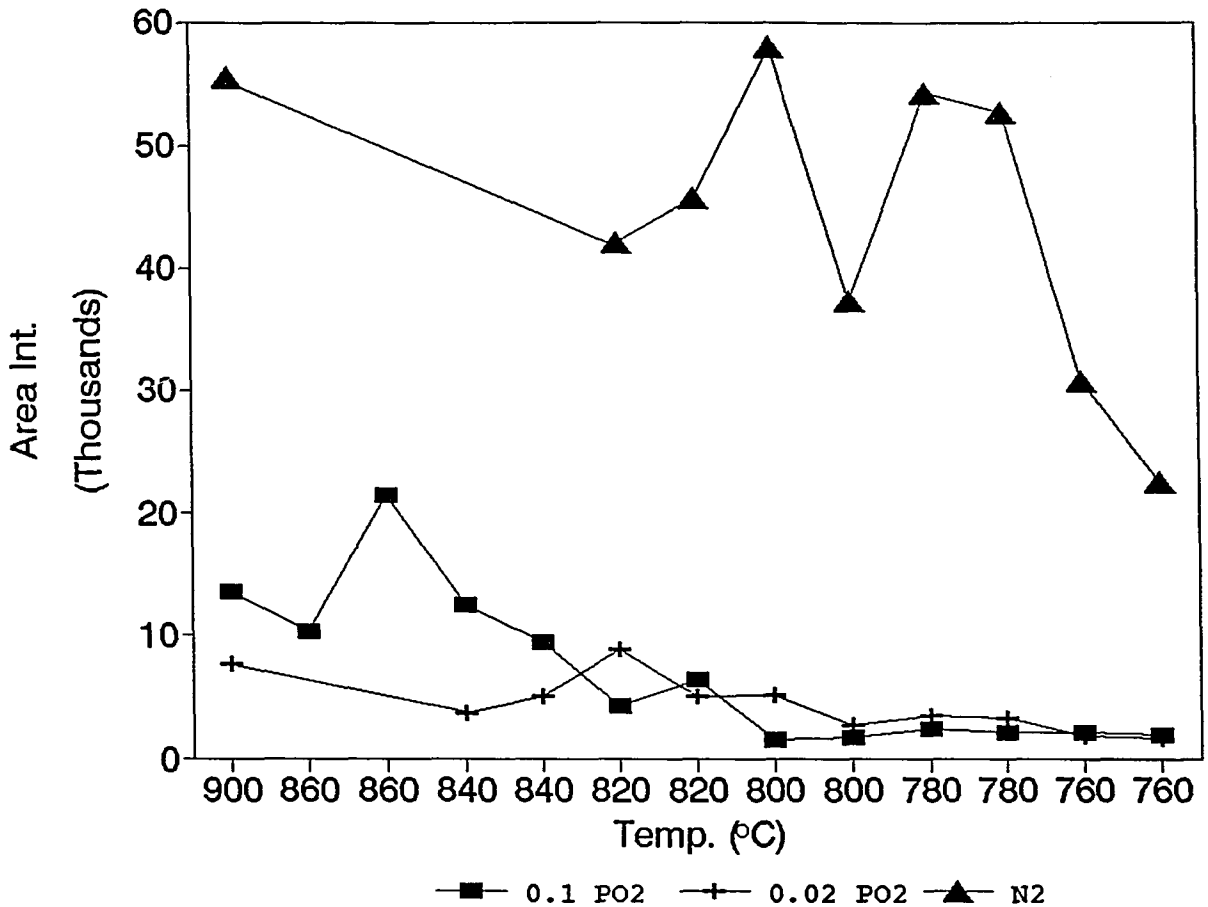

Fig. 3.8 Formation of 10 phase as a function of PO2

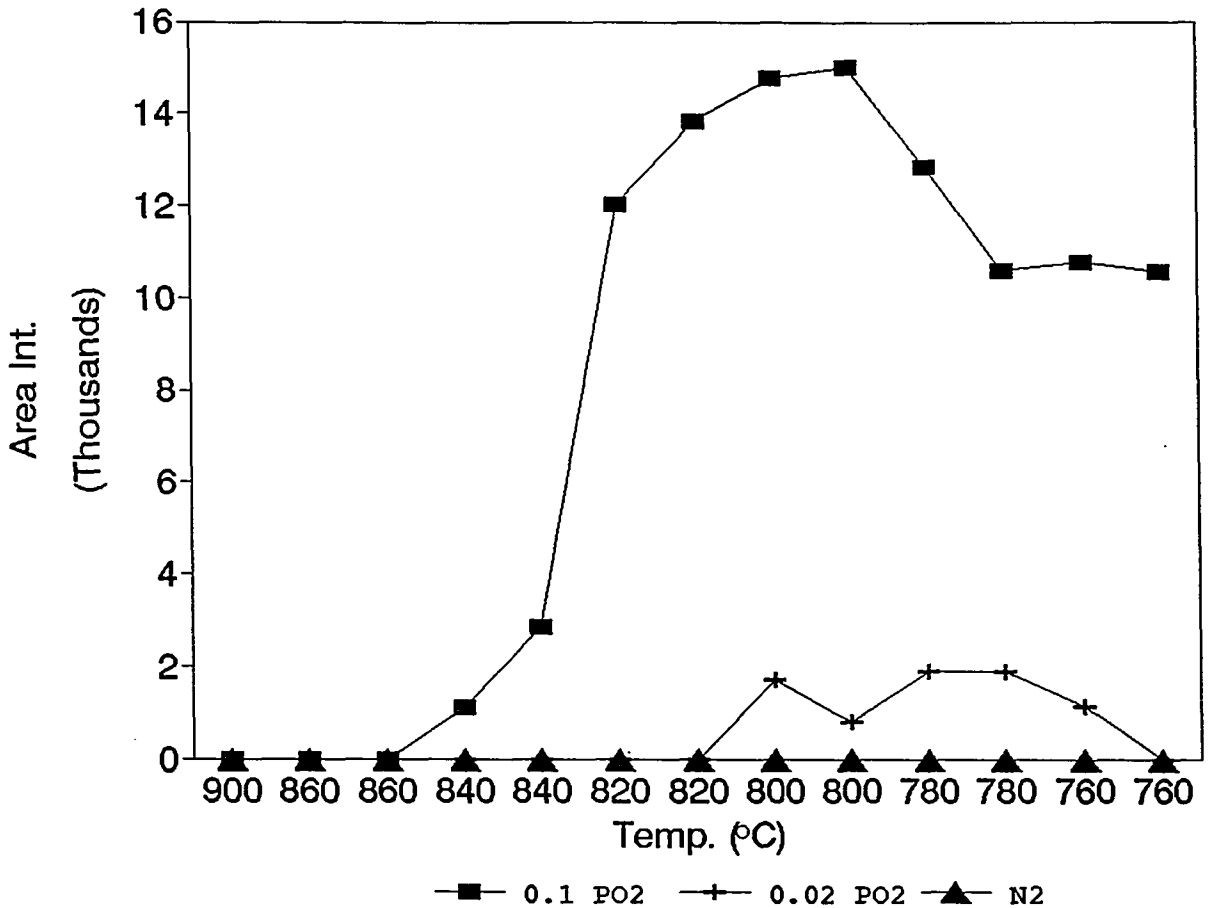

Fig. 3.9 Formation of 21 phase as a function of PO2

0.02 atm, the temperature where 21 begins to form decreases to 800°C. A similar effect occurs with the 11 phase (see Fig. 3.10). In 0.2 atm of partial oxygen pressure, a small amount of 11 phase forms at a temperature above 860°C. When the partial oxygen pressure is lowered to 0.1, 0.02 atm and in N_2, the 11 phase grows out of the liquid at 840°C, 820°C and 770°-760°C respectively.

In all of the partial oxygen pressure studies, except 0.2 atm, the 2212 phase formed out of the melt. Diffraction patterns from the HTPD showed the 2212 phase starting to grow preferentially oriented, with the c-axis perpendicular to the sample holder, on the surface of the sample. The melt was still present when the 2212 was growing, indicating that the location of the phase was on the surface. The location of the initial growth was confirmed by quenching samples. Using room temperature X-ray diffraction and SEM, the 2212 phase was found lying on top of a Bi-rich glass which formed from the melt. Snyder[2] and Maeda[3], using a HTPD, also observed that the initial formation of 2212 occurs on the surface. From the HTPD results, there is no indication of any precursor phase (i.e. 2201) for the formation of 2212.

The formation of 2212 out of the melt is affected by partial O_2 pressure in two ways. The first affect is that the temperature at which 2212 starts to grow decreases as the partial oxygen pressure is lowered (see Fig. 3.11). The

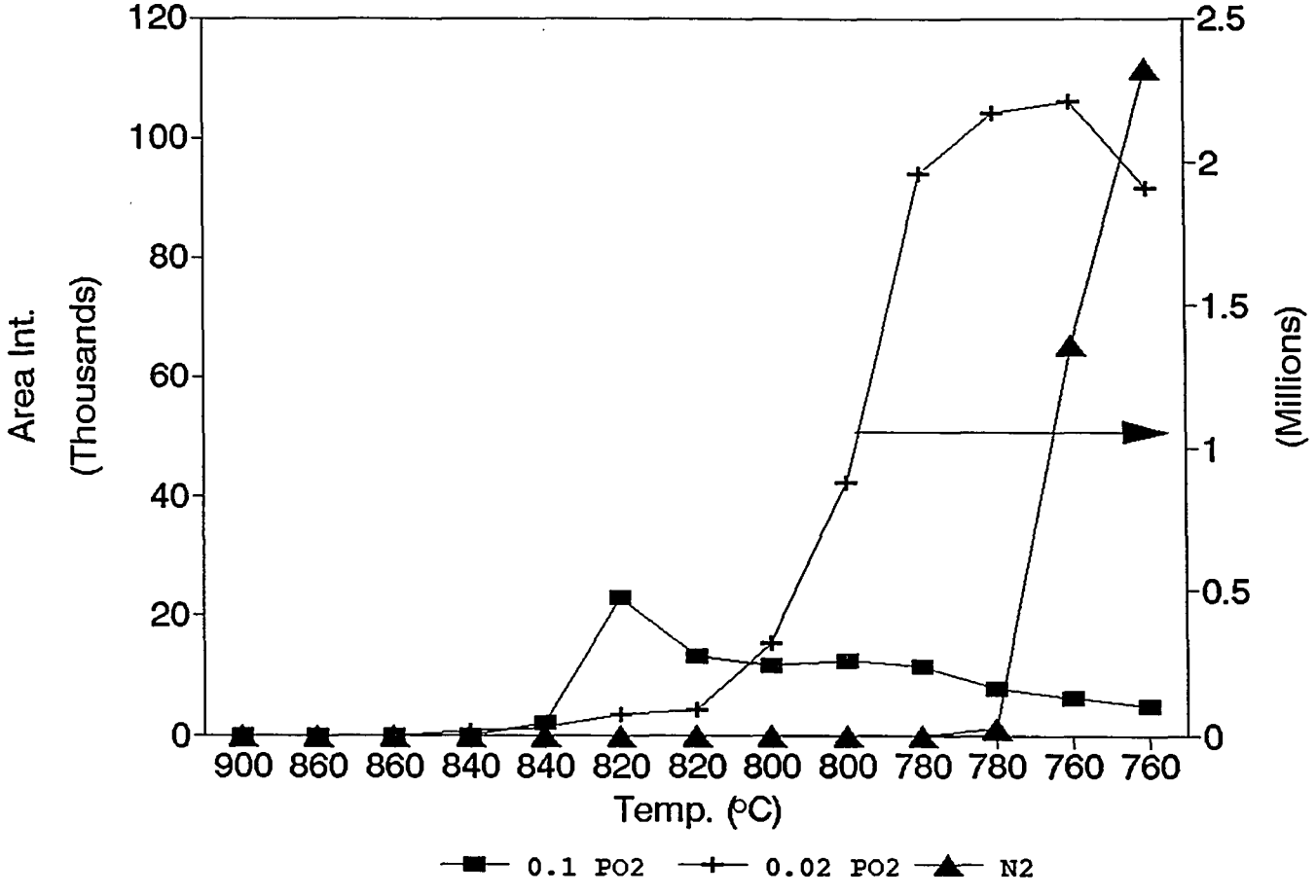

Fig. 3.10 Formation of 11 phase as a function of PO2

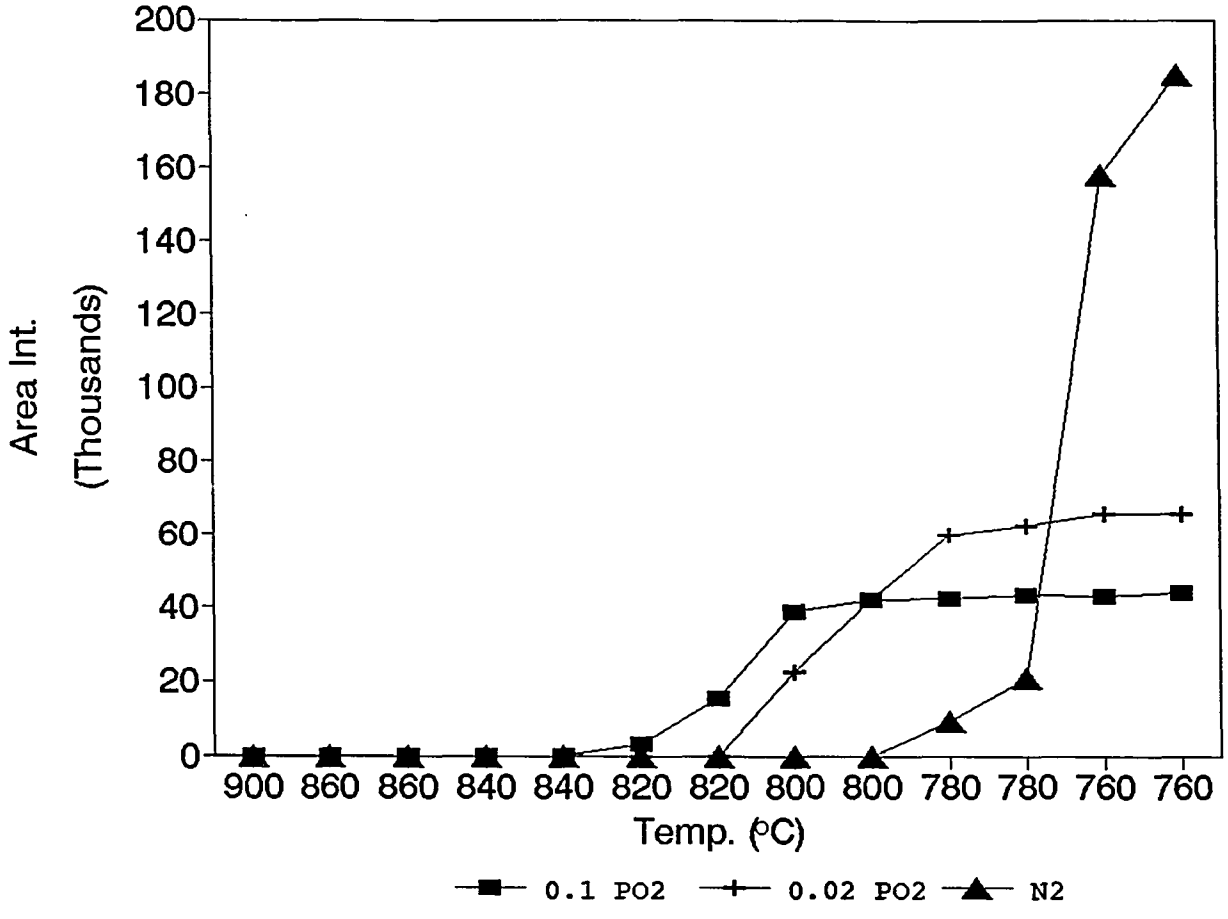

Fig. 3.11 Formation of 2212 phase as a function of PO2

initial formation temperatures of 2212 are 820°C, 800°C and 780°C under partial O_2 pressures of 0.1, 0.02 atm and N_2. The second, indirect, affect is the presence of second phase in the melt before 2212 forms. The presence of certain second phases affects the formation of 2212 significantly. Large amounts of 21 phase inhibit the formation of 2212, as can be seen in the 0.2 atm partial O_2 pressure study. In this case, the sample surface is encrusted with 21 and only 2201 formed underneath it. The formation of 2201 was verified by a room temperature θ-2θ diffractometer. The reason why the 21 phase acts as an inhibitor is because the phase removes a large amount of Ca from the melt. Ming Xu[4] found that the 21 phase has complete solubility of Sr and Ca in the alkaline earth metal sites. From the position of the (002) peak of 21 phase in the HTPD diffraction patterns, the phase has 50-60% Ca in the alkaline earth metal sites. Another problem with the 21 phase in the melt is that the phase will not dissolve back into the melt at lower temperatures to any significant degree. Only by heating the sample for long periods of time will the 21 phase decompose back into the system. In effect, the 21 phase locks the Ca in the system away from the melt. Under such conditions, the 2201 phase will grow out of the melt instead of 2212. The small amount of Ca in the melt is incorporated in the 2201 phase.The 2201 phase has a Ca solubility of 10% on the Sr sites.

In contrast to the 21 phase, the presence of 10 phase promotes the formation of 2212. Even though the 10 phase has 75-80% Ca in the alkaline earth metal sites as determined by the position of the (111) peak, the phase dissolves back into the melt. By doing so, the Ca is released back into the melt. Comparing Figs. 3.8 and 3.11, one notices that the formation of 2212 coincides with the depletion of 10 phase. For the partial oxygen pressures of 0.1, 0.02 atm and N_2, the temperatures of the 2212 formation and 10 depletion are 820°C, 800°C and 780°C, respectively. The reason for the coincidence is that the Ca being released by 10 initiates the growth of 2212. As the temperature is lowered the 10 phase is consumed in the formation of 2212. In the case of 11, the presence of the phase in the melt does not hinder or assist in the formation of 2212. The 11 phase normally contains 10% Ca on the alkaline earth metal site during solidification.

None of the partial oxygen pressure studies showed any presence of copper free phases. In the N_2 atmosphere study, two copper free phases formed out of the melt during solidification. The diffraction peaks of the 24X phase were observed in the first scan taken at 820°C. This phase was present in the melt throughout the solidification study. The other phase, 23X, started to grow out of the melt at 800°C and continued to grow as the sample was cooled to 780°C and 760°C. Vander Sande[5] and Holesinger[1] also observed

copper free phase in the melt at lower partial oxygen pressures. From these observations, the copper free phases form during solidification only at very low partial oxygen pressures ($<10^{-4}$ atm). The presence of these two phases shifted the composition of the melt to be more copper rich than in the other three partial oxygen pressure studies. Because of the higher concentration of copper, both 11 and 21 phases were present in small amounts at 820°C. Only when the sample was cooled to 760°C did the 11 phase grow and 21 phase dissolve back into the melt.

The unidentified phase with a peak at 56.6° is present during the beginning of every solidification study except for the N_2 case. When the sample is cooled to 800°C or lower, the unidentified phase dissolved back into the melt. Because it dissolves at lower temperature, the unidentified phase could not be quenched in for identification by SEM.

GENERAL SUMMARY

The incongruent melting of 2212 follows a phase sequence of 11 → 21 → 10 as the temperature is raised above the melting point. In the phase sequence, a crystalline phase undergoes a copper depletion in composition when the next phase in the sequence forms. All of the second phases that form in the incongruent melting process grow with a preferred orientation with respect to the sample holder, except for the 10 phase.

Changing the partial oxygen pressure affects the phase sequence in two ways. When the partial oxygen pressure is lowered, the melting point of 2212 is also lowered. In 0.02 atm of O_2 and N_2 atmosphere studies, the 2212 phase melts at 850^{o}C and 830^{o}C, respectively. In the studies done in 0.2 and 0.1 atm of partial oxygen pressure, the melting point is 870^{o}C. Lowering the partial oxygen pressure also affects the temperature ranges in which the second phases form. At lower partial oxygen pressures, the 21 and 10 phases form at the melting point. Also, the 21 phase is not present in the melt at higher temperatures as compared to the 0.2 atm partial oxygen case. In lowering the partial oxygen pressure, the 11 and 10 phases become the major crystalline phases present in the melt.

The crystalline phase formation during the solidification of the 2212 melt is dependent on the partial oxygen pressure. In 0.2 atm of partial O_2 pressure, the major second phase forming out of the melt is 21. When the partial O_2 pressure is lowered to 0.02 atm, 11 becomes the major second phase. The 10 phase becomes the major second phase only at very low partial oxygen pressures (N_2 atmosphere).

The temperature at which 2212 starts to grow out of the melt is also a function of partial oxygen pressure. At partial O_2 pressures of 0.1, 0.02 atm and N_2 atmosphere, the 2212 phase begins to form at 820^{o}C, 800^{o}C and 780^{o}C, respectively. The 2212 phase does not form in the 0.2 atm case because of the large amounts of 21 present. The 21 phase inhibits the growth of 2212 by removing a significant amount of Ca from the melt. In effect, the 21 phase acts as a "getter" for Ca. Without any Ca in the melt, the only bismuth cuperate that forms in the melt is 2201.

The formation of Cu free phases (23X and 24X) is observed in 0.02 atm of partial oxygen pressure and N_2 atmosphere studies. only the 24X phase is observed during the incongruent meting process. In the solidification of the melt in a N_2 atmosphere, the 24X phase forms at 830^{o}C. as the temperature is lowered to 820^{o}C, the 24X phase dissolves back into the melt and 23X phase begins to form.

REFERENCES

Introduction

1. J. G. Bednorz and K. A. Muller Z.Phys. 64 (1986) 189

2. M. K. Wu, J. R. Ashborn, C. J. Torng, P. H. Hor, R, L. Meng, L. Gao, Z. J. Huang, Y. Q. Wang and C. W. Chu Phys.Rev.Lett. 58 (1987) 908

3. N. Nucker, H. Romberg, X. Xi and J. Fink Phys.Rev B 39 (1989) 6619

4. H. Maeda, Y. Tanaka, M. Fukutomi and T. Asano Jpn.J.Appl.Phys 27 (1988) 208

5. E. Yanagisawa, T. Morimoto, D. R. Dietderch, H. Kumakura K. togana and H. Maeda Appl.Phys.Lett. 25 (1989) 54

6. K. Togana, H. Kumakura, H. Maeda, E. Yanagisawa, N. Irisawa, J. Shimoyama and T. Morimoto, Jpn.J.Appl. Phys. 28 (1989) 95L

7. J. Kase, N. Irisawa, T. Morimoto, K. Togana, H. Kumakura D. R. Dietdrich, and H. Maeda Appl.Phys.Lett. 10 (1990) 56

8. D. R. Dietderich, B. Ullmann, H. C. Freyhardt, J. Kase, H. Kumakura, K. Togana and H. Maeda Jpn.J.Appl.Phys. 29 (1990) L1100

9. S. T. Misture, D. P. Matheis, R. L. Snyder Physica C (1993), in press

10. I. Matsubara, H. Tanigawa, T. Ogura, H. Yamashita and M. Kinoshita Appl.Phys.Lett. 23 (1990) 57

11. R. D. Ray and E. E. Hellstrom Physica C 172 (1991) 435

12. K. Togana, H. Kumakura, D. R. Dietdrich, H. Maeda, J. Kase, T. Morimoto, B. Ullmann and H. C. Freyhart Proc. ICMC 90, Toical Conf. on HTSC, 9-11 May, Garmisch-Patten Kirchen, FRG (1990)

13. J. Kase, K. Togana, H. Kumakura, D. R. Dietderich, N. Irisawa, T. Morimoto and H.Maeda Jpn.J.Appl.Phys. 29 (1990) L1096

14. J. Kase, T.Morimoto, K.Togana, H. Kumakura, D. R. Dietderich and H. Maeda Proc. Appl. Supercond. Conf., 24-28 Sept., Snowmass, CO. USA (1990)

15. D. R. Dietderich, B. Ullmann, H. C. Freyhardt, J. Kase, H. Kumakura, K. Togana and H. Maeda Jpn.J.Appl.Phys. 29 (1990) L1100

16. Y. Oka, N. Yamamoto, H. Kitaguchi, K. Oda and J. Takada Jpn.J.Appl.Phys. 28 (1989) L213

17. Y. Oka, N. Yamamoto, Y. Tomii, H. Kitaguchi, K. Oda and J. Takada Jpn.J.Appl.Phys. 28 (1989) L213

18. R. D. Ray and E. E. Hellstrom Physica C 175 (1991) 255

19. K. Schulze, P. Majewski, B. Hettich and G. Petzow Zeit.Metall. 11 (1990) 143

20. P. Majewski, H. L. Su, B. Hettich Adv.Mat. 27 (1992) 374

Section Two

1. M. Xu, E. T. Voiles, L. S. Chumbly, A. I. Goldman and D. K. Finnemore J.Mater.Res. 7 (1992) 1283

2. M. Xu private communications (1991)

3. M. Xu, J. Polonka, A. I. Goldman and D. K. Finnemore Appl.Supercond. 1 (1993) 53

4. E. E. Hellstrom, private communications (1992)

5. L. M. Rubin, T. P. Orlando and J. B. Vander Sande Appl.Phys.Lett. 16 (1992) 61

6. K. Schulze, P. Majewski, B. Hettich and G. Petzow Zeits.Metall. 11 (1990) 143

7. R. D. Ray and E. E. Hellstrom Physica C 172 (1991) 435

8. P. Majewski, H. L. Su, B. Hettich Adv.Mater. 27 (1992) 374

Section Three

1. Holesinger, Ph.D. dissertation, Iowa State University (1993)

2. S. T. Misture, D. P. Matheis, R. L. Snyder Physica C (1993), in press

3. K. Togano, H. Kumakura, D. R. Dietderich, H. Maeda, J. Kasey, T. Morimoto, B. Ullmann and H. C. Freyhardt Proc. ICMC.90 Topical Conf on HTSC, 9-11 May, Garmisch-Parten Kirchen, FRG (1990)

4. M. Xu, E. T. Voiles, L. S. Chumbley, A. I. Goldman and D. K. Finnemore J.Mater.Res. 7 (1992) 1283

5. L. M. Rubin, T. P. Orlando and J. B. Vander Sande Appl.Phys.Lett. 16 (1992) 61

ACKNOWLEDGMENTS

I would like to thank H. F. Franzen, A. I. Goldman and D. K. Finnemore for their guidance, encouragement and enthusiasm throughout this work. Special thanks to Dr. Ming Xu, who carried out the SEM work presented here. The friendship and help from friends and group members are also greatly appreciated.

I am indebted to my mother, who raised me through many difficult years and stood behind me.

I want to dedicate this dissertation to professor Gray Kolks, who was my undergraduate advisor and mentor. He started and guided my interest in the wonderful and exciting field of solid state materials chemistry.

This work was performed at Ames Laboratory with the U.S. Department of Energy under contract No. W-7405-ENG-82. This work was supported by the DOE, the Office of Basic Energy Sciences.